STUK

STUK-**YTO**-TR 150   January 1999

The properties of and transport phenomena in oxide films on iron, nickel, chromium and their alloys in aqueous environments

T. Laitinen, M. Bojinov, I. Betova, K. Mäkelä, T. Saario
VTT Manufacturing Technology

In STUK this study was supervised by **Seija Suksi**

**STUK • SÄTEILYTURVAKESKUS • STRÅLSÄKERHETSCENTRALEN
RADIATION AND NUCLEAR SAFETY AUTHORITY**

The conclusions presented in the STUK report series are those of the authors
and do not necessarily represent the official position of STUK.

ABSTRACT

The construction materials used in coolant systems in nuclear power plants become covered with oxide films as a result of exposure to the aqueous environment. The susceptibility of the materials to different forms of corrosion, as well as the extent of the incorporation of radioactive species on the surfaces of the primary circuit, are greatly influenced by the physical and chemical properties of these oxide films. The composition and characteristics of the oxide films in turn depend on the applied water chemistry. This work was undertaken in order to collect and evaluate the present views on the structure and behaviour of oxide films formed on iron- and nickel-based materials in aqueous environments. This survey should serve to recognise the areas in which more understanding and research effort is needed.

The review begins with a discussion on the bulk oxides of iron, nickel and chromium, as well as their mixed oxides. In addition to bulk oxides, the structure and properties of oxide films forming on pure iron, nickel and chromium and on iron- and nickel-based engineering alloys are considered. General approaches to model the structure and growth of oxide films on metals are discussed in detail. The specific features of the oxide structures, properties and growth at high temperatures are presented with special focus on the relevance of existing models. Finally, the role of oxide films in localised corrosion, oxide breakdown, pitting, stress corrosion cracking and related phenomena is considered.

The films formed on the surfaces of iron- and nickel-based alloys in high-temperature aqueous environments generally comprise two layers, i.e. the so-called duplex structure. The inner part is normally enriched in chromium and has a more compact structure, while the outer part is enriched in iron and has a cracked or porous structure. The information collected clearly indicates the effect of the chemical environment on the properties of oxide films growing on metal surfaces. In addition, the films are to a large extent influenced by the kinetic factors determining their growth rate and steady state thickness. Thus a thermodynamic consideration of the film is not sufficient to model and predict its growth and dissolution. Instead, kinetic models based on in situ experimental data are required.

The kinetic models presented in the literature for both ambient and high-temperature aqueous oxidation of metals lack a correlation between the structure of the oxide films and their electronic and ionic properties. Also, a quantitative treatment and thus the capability to predict material behaviour in varying conditions is lacking. A comprehensive understanding of the correlation between applied water chemistry, the behaviour of oxide films and optimum performance of the plant is thus also lacking.

The situation calls for more experimental work combined with comprehensive modelling of the behaviour of both the compact and the porous part of the oxide film formed on a metal surface. This will make it possible to recognise the rate-limiting steps of the processes in the film, and thus to influence the rate of activity incorporation and different corrosion phenomena related to transport of species in the film.

TIIVISTELMÄ

Ydinvoimalaitosten jäähdytysvesipiirien putkistoissa käytettävien rakennemateriaalien pinnoille syntyy veden hapettavan vaikutuksen vuoksi hapettumakerros eli oksidifilmi. Oksidifilmien fysikaaliset ja kemialliset ominaisuudet vaikuttavat materiaalien korroosiokestävyyteen ja myös radioaktiivisuuden kerääntymiseen putkistojen pinnoille. Oksidifilmien koostumus ja ominaisuudet taas riippuvat metallin koostumuksesta ja laitoksen käyttämästä vesikemiasta. Tämän kirjallisuustyön tarkoitus oli koota ja arvioida kirjallisuudessa esitetyt näkemykset rauta- ja nikkelipohjaisen seosten rakenteesta ja käyttäytymisestä vesiliuoksissa. Tavoitteena oli tunnistaa alueet, joilla tarvitaan lisäymmärrystä ja tutkimuspanosta.

Katsauksen alussa käsitellään raudan, nikkelin ja kromin bulkkioksideja ja niiden sekaoksideja. Bulkkioksidien lisäksi käsitellään raudan, nikkelin, kromin ja rauta- sekä nikkelipohjaisten seosten pinnalle syntyvien oksidifilmien rakenteita ja ominaisuuksia. Filmien rakenteen ja kasvun mallinnuksessa käytettyjä lähestymistapoja käsitellään yksityiskohtaisesti. Oksidirakenteiden, oksidien ominaisuuksien ja niiden kasvun erityispiirteitä korkealämpötilavedessä käsitellään kirjallisuudessa esitettyjen mallien relevanttiuden kannalta. Lopuksi paneudutaan oksidifilmien osuuteen paikallisessa, piste- ja jännityskorroosiossa.

Rauta- ja nikkelipohjaisten seosten pinnoille korkealämpötilavedessä muodostuvissa filmeissä on tyypillisesti kaksi kerrosta, eli niillä on kaksoisrakenne. Sisempi osa on yleensä tiiviimpi ja siihen on rikastunut kromia, kun taas ulompi osa on huokoinen, se voi olla halkeillut ja siihen on rikastunut rautaa. Kirjallisuuden perusteella on selvää, että kemiallinen ympäristö vaikuttaa metallipinnoille kasvavien oksidifilmien ominaisuuksiin. Lisäksi kineettiset tekijät määräävät filmien kasvunopeuden ja paksuuden stationaaritilassa. Tämän vuoksi filmien käyttäytymistä ei voi mallintaa ja ennustaa pelkästään termodynaamisen tarkastelun perusteella, vaan lisäksi tarvitaan kokeellisiin in situ-mittaustuloksiin perustuvaa kineettistä mallintamista.

Kirjallisuudessa esitetyissä metallien huoneenlämpötila- ja korkealämpötilahapettumisen malleissa ei ole pystytty ottamaan riittävästi huomioon oksidifilmien rakenteen eikä niiden elektronisten ja ionisten ominaisuuksien vaikutusta. Lisäksi mallit eivät ole kvantitatiivisia, joten niiden avulla ei voi ennustaa materiaalien käyttäytymistä erilaisissa olosuhteissa. Tämän vuoksi käytetyn vesikemian, oksidifilmien käyttäytymisen ja laitosten optimisuorituksen välisiä korrelaatioita ei vielä tunneta.

Tehdyn kirjalisuustutkimuksen perusteella on ilmeistä, että metallien pinnalle muodostuvan oksidifilmin käyttäytymisen ymmärtäminen vaatii sekä sisemmän, tiiviin että ulomman, huokoisen kerroksen mallinnusta kokeellisten tulosten pohjalta. Tämä mahdollistaa filmissä tapahtuvien prosessien nopeutta rajoittavien vaiheiden tunnistamisen ja siten aktiivisuuden kerääntymiseen ja eri korroosiotapahtumiin liittyvien ilmiöiden nopeuteen vaikuttamisen.

CONTENTS

ACKNOWLEDGEMENTS

1 INTRODUCTION

The engineering alloys used as construction materials in power plants and in process industry become covered by oxide films as a result of exposure to aqueous environments. The properties of oxide films influence the susceptibility to corrosion phenomena taking place on material surfaces, i.e. on uniform attack as well as on localised corrosion or stress corrosion cracking. In addition, oxide films may have a great influence on susceptibility to other harmful phenomena, such as the incorporation of active species into the primary circuit materials in nuclear power plants. This may result in increased occupational doses of radiation for the maintenance personnel. Minimising such risks calls for a better understanding of the electrochemical behaviour of metal oxides in aqueous environments.

The nature and the properties of metal oxide films depend strongly on the environment to which the material is exposed. From a thermodynamic point of view, the stability of different oxides is influenced by the temperature, pH, potential and type and concentration of dissolved ions in the solution. An oxide film on a metal, however, cannot be considered as a system in thermodynamic equilibrium, but its properties and composition are to a great extent affected by the kinetic factors determining its growth rate and stationary state thickness. This often leads to the formation of a film consisting of two or more sublayers, or of a film, the composition and stoichiometry of which change gradually with distance from the film/environment interface.

The aim of this report is to give an introduction to the fundamental concepts concerning the properties and structure of oxide films in aqueous environments as well as the transport phenomena leading to the growth of the films and incorporation of new species into the film. To begin with, bulk oxides of metals with focus on iron, nickel and chromium oxides as well as their mixed oxides are discussed, in order to define the necessary concepts and to review the general properties of oxide phases (chapter 2). The structure and properties of oxide films formed on pure iron, nickel and chromium and on iron- and nickel-based engineering alloys are considered (chapters 3 and 4). Chapter 5 deals with general approaches to model the structure and growth of oxide films on metals, with comments on the relevancy of the models in the case of iron, nickel, chromium and their alloys. Special attention is focused to extend the current understanding on oxide films to cover the structure, properties and growth of films at elevated temperatures which are relevant in several practical applications (chapters 6 and 7). Finally, the role of oxide films in phenomena related to localised corrosion (oxide breakdown, pitting, stress corrosion cracking) is the topic for chapters 8 and 9.

The role of oxide films in activity build-up and in stress corrosion cracking in nuclear power plants, as well as the influence of modified water chemistries, is discussed in another review [1].

2 STRUCTURE AND PROPERTIES OF BULK OXIDES OF METALS

2.1 Oxide structures

2.1.1 Classification of structures

Several metal oxides are essentially ionic compounds. Their structure is often based on close-packing of the oxygen ions, which are considerably bigger than the metal cations.

Hexagonal closest packing (hcp) refers to a structure in which O^{2-} layers comprising an array of contiguous equilateral triangles are stacked in such a way that the hexagonal symmetry of each layer is retained by the entire stack. This requires that the spheres of layers 3, 5, etc. are directly above those of layer 1, and that the spheres of layers 4, 6, etc. are directly above those of layer 2, which results in an ABABAB... pattern [2 p.102]. On the other hand, cubic closest packing (ccp) refers to a structure in which a cubic arrangement is produced instead of the hexagonal pattern. This requires that the spheres of the 4th layer are directly above those of the 1st layer, those of the 5th layer directly above those of the 2nd layer and so on. This can be described as an ABCABC... pattern [2 p.102].

Two kinds of sites can be recognised between two layers of a close-packed structure of O^{2-} ions: octahedral and tetrahedral (see Fig. 1). It is these
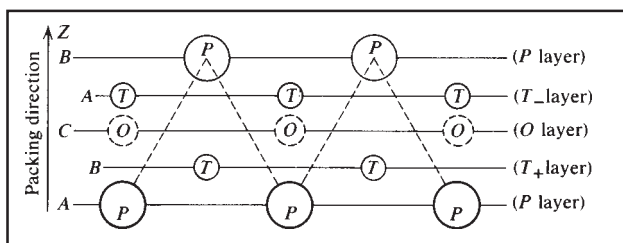
Fig. 1. Construction of the basic close-packed unit: P = packing atom, i.e. oxygen in the case of metal oxides; O = octahedral cation site; T = tetrahedral cation site; A, B, C = the three relative packing positions [3 p. 201].

sets of sites that are occupied by the cations in metal oxides [2 p.103,3 p.201], and for the sake of clarity they are called cation sites from now on in this report.

Some metal oxides have the NaCl structure, which refers to a cubic closest packing of anions, with metal ions occupying octahedral sites in every close-packed layer [2 p.103]. One of the most important metal oxide structures is the corundum (α-Al_2O_3) structure, which in turn refers to a hcp array of O^{2-} ions with 2/3's of the octahedral cation sites occupied, but not in a layered fashion [2 p.104].

Many metal oxides contain two or more different kinds of metal ions. They usually adopt one of the three basic structures, the spinel, the ilmenite or the perovskite structure, the names of which originate from the first or most important compound found to have that structure. Ilmenite is the mineral $FeTiO_3$, and its structure is closely related to the corundum structure except that the cations are of two kinds. Perovskite is the mineral $CaTiO_3$, and its structure is based on a ccp array of O^{2-} ions together with large cations which are comparable in size with the O^{2-} ions. The smaller cations lie in the octahedral sites formed entirely by the O^{2-} ions [2 p.104]. Spinel is the mineral $MgAl_2O_4$, and its structure is based on a ccp array of oxide ions, with Mg^{2+} ions in a set of tetrahedral sites and Al^{3+} ions in a set of octahedral sites. Each unit cell of a spinel contains eight formula units of $MeMe^*_2O_4$, in which Me and Me^* refer to lower- and higher-valence cations (commonly bi- and trivalent). Accordingly, the unit cell contains 32 O^{2-} ions (32c-positions) as well as 64 tetrahedral and 32 octahedral cation sites, of which eight tetrahedral sites (8a) and sixteen octahedral sites (16d) are occupied by lower and higher-valence cations, respectively. This low occupation suggests a high mobility of cations in the lattice. The

theoretical unit cell dimension based on the closest packing principle is equal to 0.8 nm, while experimentally determined values for spinels range from 0.80 to 0.89 nm [4,5]. A scheme of the structure of a spinel is shown in Fig. 2.

Spinels can be classified as normal, inverse and intermediate, depending on the location of Me and Me* ions in the tetrahedral and octahedral sites. Higher-valence cations tend to prefer the octahedral sites [2 p.104]. When all the eight Me cations exist in the tetrahedral sites and all the sixteen higher-valence Me* cations in the octahedral sites, a normal spinel structure prevails. In an inverse spinel eight higher-valence Me* ions are located in the tetrahedral sites, and the remaining eight Me* ions and the eight lower-valence Me ions occupy the sixteen octahedral sites in a statistically disordered manner (see Fig. 3).
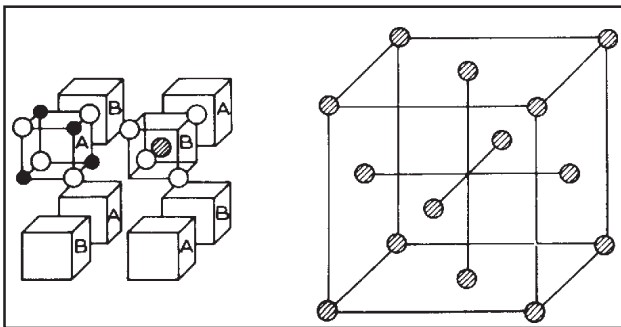
Fig. 2. *The structure of spinel, $MgAl_2O_4$. The structure contains four MgO_4 tetrahedra(B) and four Al_4O_4 cubes (A) arranged as shown in the eight octants of a face-centred cube of Mg atoms (right). The unit cell contains 32 oxygen atoms arranged as in cubic close-packing with 8 Mg in tetrahedral spaces and 16 Al in octahedral spaces [23 p.197].*
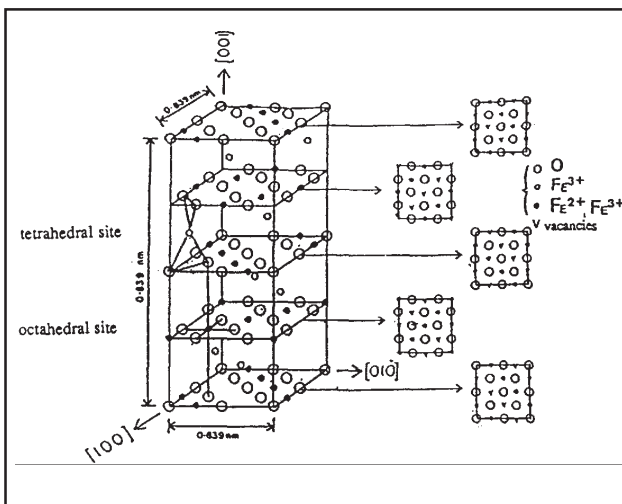
Fig. 3. *The structure of an inverse spinel, Fe_3O_4 [6].*

In intermediate spinels the Me and Me* cations are arranged in a disordered manner both in tetrahedral and octahedral sites. There also exist spinels which contain only trivalent ions and vacant lattice sites [4].

As discussed by Harding [7] and Lister [8], three terms contribute to the stability of an ion in an octahedral or tetrahedral site: crystal field stabilisation energy (CFSE), the Madelung term and the short range term. The Madelung term characterises the contribution of the geometrical structure to the electrostatic energy, while the short range term describes the quantum mechanical repulsion energy. However, the estimation of the crystal field stabilisation energy of the cation alone can be considered a good indication of whether the ion will sit in an octahedral or tetrahedral site, and it can be used to predict the structure of the spinel. The stability of different cations in spinel structures is discussed in more detail in another report [1].

2.1.2 Oxides and oxyhydroxides of Fe, Ni and Cr

Iron can form a sequence of oxides: FeO, Fe_3O_4 (magnetite, $FeO \cdot Fe_2O_3$), γ-Fe_2O_3 (maghemite) and α-Fe_2O_3 (hematite). α-Fe_2O_3 possesses a corundum structure, i.e. hcp array of oxide ions with Fe^{3+} occupying 2/3's of the octahedral sites [2p.104,9], while FeO, Fe_3O_4 and γ-Fe_2O_3 are structurally very closely related having a close packed cubic sublattice of O^{2-} ions [5,10,11]. FeO has the NaCl structure [12 p.105], while Fe_3O_4 and γ-Fe_2O_3 belong to inverse spinels, and their cubic sublattice is face centred [5,10]. The unit cell lengths for bulk crystalline Fe_3O_4 and γ-Fe_2O_3 are both about 0.84 nm [13].

In Fe_3O_4 (magnetite) eight of the octahedral and the eight tetrahedral sites are filled by Fe^{3+} ions and the remaining eight octahedral sites are filled by Fe^{2+} ions. This inverse spinel structure is due to the fact that Fe^{2+} has six 3d electrons and thus has a higher CFSE for octahedral than for tetrahedral co-ordination. Fe^{3+} has zero CFSE for both octahedral and tetrahedral co-ordination, and therefore has no site preference [10]. In γ-Fe_2O_3 (maghemite), the 24 cation sites in the unit cell are occupied at random by 21 1/3 Fe^{3+} ions. [5,10]. The relatively high mobility of the iron ions leads

to an easy interconvertibility between γ-Fe_2O_3 and Fe_3O_4 [5].

γ-FeOOH is based on a cubic close-packed sublattice of O^{2-} ions, as also FeO, Fe_3O_4 and γ-Fe_2O_3 [11]. According to Davenport and Sansone [10], oxyhydroxides γ-FeOOH (lepidocrocite) and α-FeOOH (goethite) are composed of double bands of $FeO_3(OH)_3$ octahedra. In α-FeOOH these are linked by corner-sharing to form tunnels (big enough only for protons), whereas in γ-FeOOH the double bands share edges to form zig-zag layers that are connected to each other by hydrogen bonds. Only half the octahedral sites are filled in these two structures [10]. According to Keddam and Pallotta [14], the structure of the α–FeOOH lattice characterised by two FeO layers between OH planes allows water molecules and small ions to be intercalated resulting in a material of a highly flexible composition.

Tomlinson [15] has pointed out that the existence of a series of iron oxides and oxyhydroxides based on a cubic close-packed array of oxygen ions leads to a peculiar feature: Starting with FeO, which accommodates 32 O^{2-} ions and 32 Fe^{2+} ions in a cubic edge of 0.86 nm, iron ions can be gradually moved from the structure (and protons added when necessary) to give in turn Fe_3O_4 , γ-Fe_2O_3 and γ-FeOOH without any change in the structural arrangement of the oxygen ions. The structure is controlled by the close-packed oxygen framework through which highly mobile protons and relatively mobile iron ions can move.

NiO has the NaCl structure [12 p.100]. This means that it is based on a close-packed cubic sublattice of oxygen ions in which the metal ions are the faster moving species determining the oxidation rates [9,12 p.100].

α-Cr_2O_3 has the corundum structure [2 p.392,12 p.114]. Two types of distances between nearest neighbour oxygen ions in the planes constituting the lattice can be found in the structure: 2.62 and 2.98 Å [16]. Cr_2O_3 has also been reported to have a hexagonal lattice presenting a spinel type of structure with a unit cell dimension of 8.37 Å [17].

Concerning mixed oxides of Fe, Ni and Cr, Fe and Cr form a continuous series of spinels from Fe_3O_4 ($FeO \cdot Fe_2O_3$, magnetite) to $FeCr_2O_4$ ($FeO \cdot Cr_2O_3$, ferric chromite). Ni can also be incorporated up to a composition of $Ni(Fe,Cr)_2O_4$. [9],

i.e. Ni can replace divalent ions in the structure while Fe(III) cannot be replaced [18]. In the absence of chromium, a $NiFe_2O_4$ ($NiO \cdot Fe_2O_3$, nickel ferrite) spinel can be formed. According to Tarasevich and Efremov [4], ferrites are inverse spinels as magnetite, while chromites are normal spinels. This agrees with the view of Lister [8], who has predicted that Cr(III) and Ni(II) will be particularly stable in octahedral sites. A recent characterisation of $Me_xCo_{1-x}Fe_2O_4$ spinels using XPS can be found in the report by Allen and Hallam [19], who discussed the distribution of different cations between the surface and the bulk of spinel oxides.

2.2 Defects in oxides

Even synthetic bulk oxides are never perfect at temperatures above absolute zero but contain imperfections or defects in their structure. In spite of the often low concentration of defects, many important properties of solids, e.g. the electrical resistance and the mechanical strength, are governed by the presence of defects in the lattice [20 p.36]. The defects found in oxide lattices can be classified as point defects, line defects and plane (or planar) defects [12 p.33,21 p.119,22]. The presence of defects is connected with the disorder of the crystal, i.e. with its entropy. Therefore, more point defects are likely to be present at higher temperatures [18 p.36].

Point defects can be either cation or anion vacancies, cation or anion interstitials or substitutionals in the lattice. The point defects found in oxide lattices can be classified as stoichiometric or non-stoichiometric defects, depending on whether or not they influence the stoichiometric composition of the oxide [23 p.204].

The formation of cation and oxygen vacancies without changing the stoichiometric composition can be discussed in terms of the Schottky reaction [12 p.43] (Fig. 4), which is written below using the Kröger-Vink notation [12 p.34]:

$$\text{null} = V_M^{x-} + V_O^{2+} \qquad (2\text{-}1)$$

Since the reaction involves a pair of charged species, both the stoichiometry and electric neutrality are maintained.

A Frenkel defect is due to the displacement of a cation or anion to an interstitial position, thereby leaving a vacant lattice site behind. Again, the

stoichiometry of the compound does not change. Frenkel defects are most likely to exist in crystals in which the cation and anion differ greatly in size, so that the smaller ion can fit into the interstitial sites [3 p.230]. The formation of metal interstitials can be expressed using the Frenkel reaction. [12 p.44] (see Fig. 5):

$$M_M = M_i^{x+} + V_M^{x-} \qquad (2\text{-}2)$$
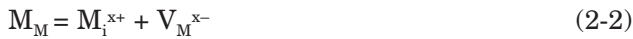
In any particular type of compound, there is usually one type of defect which is dominant. Schottky defects are associated with compounds in which balance of coulombic forces is critical. Frenkel defects are likely to occur in covalent crystals, where molecular polarisation decreases the effects of charge dislocation [3 p.231,23 p.204].
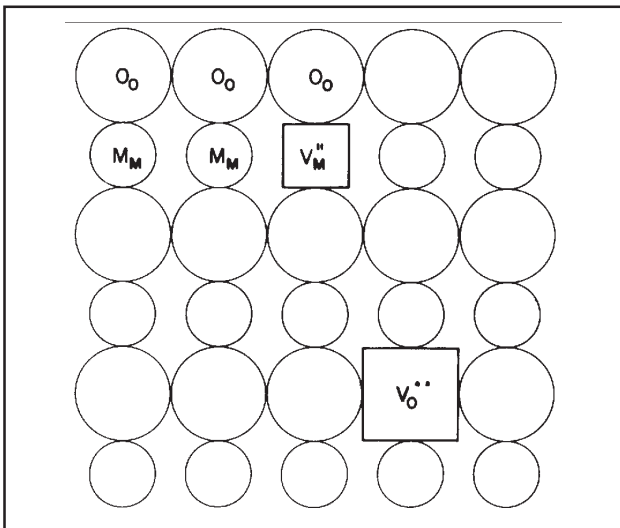
Fig. 4. Schematic illustration of Schottky disorder in an oxide MO [12 p.43].
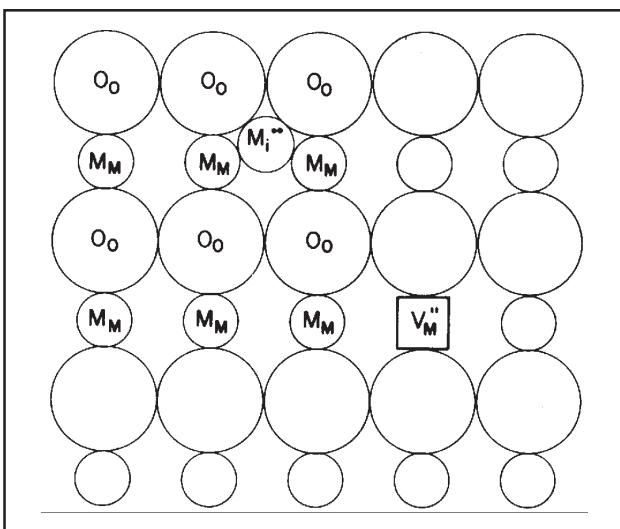
Fig. 5. Schematic illustration of Frenkel disorder in an oxide MO [12 p.44].

Non-stoichiometric point defects, i.e. defects which change the stoichiometric composition of the oxide, can be formed by three different ways: substitutional incorporation, interstitial incorporation and subtraction, of which the latter one produces vacancies in the lattice [23 p.206].

Of the oxides of most interest in this survey, Fe_3O_4 may be cation deficient or have cation excess, depending on the partial pressure of oxygen. The oxygen sublattice remains fixed because its defects have higher energy. The cation deficiency has been observed to increase with decreasing temperature [12 p.111,22]. However, also Fe_3O_4 formed as a result of oxidation of steel in oxygen free water at high temperatures (200...350 °C) has shown deficiency of Fe compared to stoichiometric magnetite [15]. Because of the structural similarity between Fe_3O_4 and $\gamma\text{-}Fe_2O_3$ (see above), it can be assumed that also the latter exhibits cation deficiency. On the other hand, the non-stoichiometry of $\alpha\text{-}Fe_2O_3$ is small, and according to Kofstad it has not been possible to determine the predominant defects with sufficient accuracy [12 p.113]. Atkinson [22] has commented that oxygen vacancies seem to be the dominant defects in Fe_2O_3.

Robertson [11] has given an illustrative description of how Fe_3O_4 can be transformed to $\gamma\text{-}Fe_2O_3$ or to FeO: The cation deficiency is due to missing Fe^{2+} ions at octahedral sites. Overall charge neutrality is maintained by creating two holes per vacancy, which is equivalent to converting two Fe^{2+} ions to Fe^{3+} ions. This process will eventually convert the Fe_3O_4 lattice to a $\gamma\text{-}Fe_2O_3$ lattice. In the case of cation excess in Fe_3O_4, extra Fe^{2+} ions occupy vacant octahedral cation sites. Charge neutrality requires that these are compensated by two electrons or the conversion of two Fe^{3+} ions to Fe^{2+} ions. This process ultimately generates the FeO lattice. Vacancies can also be compensated by protons in Fe_3O_4. As only its Fe^{2+} ions can be removed, two protons are needed to compensate for a cation vacancy. The protons convert O^{2-} ions to OH^- groups, and finally, a $\gamma\text{-}FeOOH$ lattice is generated.

NiO has been found to deviate from stoichiometric composition because of a small amount of cation vacancies [12 p.100,24]. Also Cr_2O_3 has been explained to be cation deficient at high oxygen pressures, but cation excess has been suggested at low oxygen pressures [22,25].

The existence of point defects facilitates the movement of metal and/or oxygen ions. For instance, metal or oxygen ions can jump from their position to a vacancy and occupy it, leaving a new vacancy behind. This is how they can move through the whole film. The role of point defects becomes more pronounced in the case of metal oxide films (see chapter 2.5), whose composition may be far from that corresponding to ideal stoichiometry.

Point defects present in high concentrations (i.e. mole fractions greater than 10^{-3}–10^{-2}) may associate or cluster and thus form larger units or aggregates. In certain structures point defects may also form extended defects such as shear planes, which is an example of a planar defect [12 p.33]. Stacking faults, internal surfaces (i.e. grain boundaries), external surfaces, twin boundaries and different types of dislocations belong to line or planar defects. They may offer preferential pathways for the transport of species in the film. [12 p.33,20,22] A comprehensive discussion on line and plane defects is beyond the scope of this survey, but it can be found for instance in [20 p.36].

2.3 Electronic properties of oxides

The total conductivity of metal oxides consists of both electronic and ionic contributions. Ionic conduction calls for defects in the structure of the oxide, as already indicated in chapter 2.2. The existence of defects not only gives rise to ionic conductivity but also influences the electronic conductivity of the oxide. This is due to the fact that the whole film must be electroneutral in steady state conditions. The formation of defects changes the local charge distribution in the oxide, and this has to be compensated by means of electrons and/or electron holes.

To classify solids on the basis of their conductivity, an approach based on the band structure of the material is useful. The ground state energy levels of valence electrons in atoms comprising a solid form a valence energy band. The band corresponding to the energy level immediately above the free atom valence level (i.e. the first excited state) is called the conduction band, and it may or may not be occupied. The level below which all states are occupied and above which all states are empty (at absolute zero) is called the Fermi energy level. The band structure, including the band widths of the conduction and valence bands and the band gap between the conduction and valence band, is to a great extent determined by the crystallographic structure of the oxide. On the other hand, the level up to which the bands are filled, i.e. the Fermi level, is determined by the elements which form the oxide, their oxidation states and also by the applied potential [21 p.54].

Solids, in which the valence band is full and separated from the conduction band by a definite energy gap, are either insulators or semiconductors. A typical value for the band gap of a semiconductor is of the order of 1...2 eV, while higher values lead to insulating behaviour. Solids, in which the valence band is either partially filled or overlapping a partially filled conduction band, are metals. This is illustrated in Fig. 6 [21 p.76].
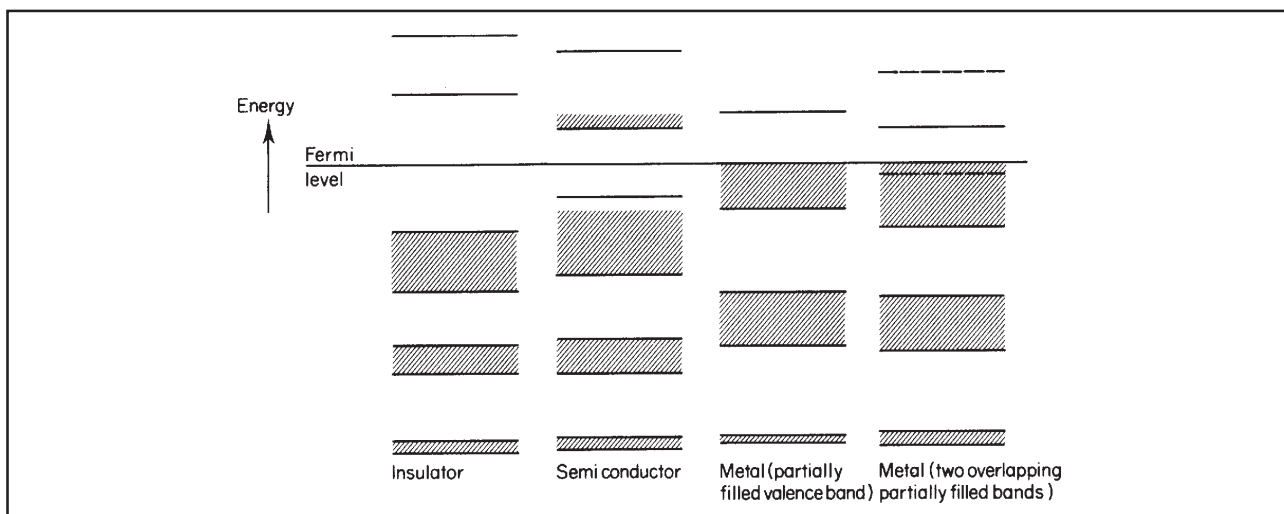
When the electronic current in a semiconduc-

Fig. 6. Energy band scheme for various classes of material [21 p.76].

tive solid is mainly carried by electrons, the solid is called an n-type semiconductor. It contains electron donors, and the Fermi level is situated close to the conduction band edge. On the other hand, conductivity due to positively charged electron holes is called p-type conductivity. A p-type semiconductor contains electron acceptors, and the Fermi level is situated close to the valence band edge.

Fe_3O_4 exhibits almost metallic conductivity. Davenport and Sansone [10] and Gerischer [5] have suggested that the high conductivity of magnetite can be attributed to the continuous exchange of electrons between Fe^{2+} and Fe^{3+} in the octahedral sites. As reviewed by Gerischer [5], the band structure of Fe_3O_4 has been analysed thoroughly, and the results of the analysis are in accordance with its metallic conductivity.

α- and γ-Fe_2O_3 behave as n-type semiconductors with a band gap of ca 1.8…2.1 eV [26,27 p.187,28,29,30] and a specific resistance of $10^{10}…10^{11}$ Ωcm [26,29]. It can be assumed that due to the similarity in structures, analogous electronic energy bands are found in γ-Fe_2O_3 as in Fe_3O_4. The electron density in these bands will be somewhat lower than in the case of Fe_3O_4 because of the lower Fe concentration in the unit cell [5]. Kennedy and Frese [31] have explained their capacitance and photocurrent measurements on polycrystalline α-Fe_2O_3 samples in terms of two donor levels, one situated very close to the conduction band (shallow level) and another at about 0.6 eV below the conduction band (deep level). They ascribed the deep level to the presence of Fe^{2+} species. Dielectric constants varying from 80 to 120 have been reported for α-Fe_2O_3 [31].

Due to its defect structure (see chapter 2.2), NiO exhibits p-type semiconductivity [12 p.101,24]. For the same reasons (see chapter 2.2) Cr_2O_3 is generally close to an insulator. It exhibits n-type behaviour in low oxygen pressures, which correspond to low potentials in aqueous solutions. p-type behaviour has been observed in high oxygen pressures, which correspond to high potentials in aqueous environments [12 p.115,25].

2.4 Solubilities of oxides

The dissolution of an oxide can be either isovalent, oxidative or reductive. The first one is a chemical reaction, while the two latter ones are electrochemical reactions, i.e. they necessarily involve electron transfer. The solubility of an oxide can be estimated solely on the basis of chemical equilibrium only if no electron transfer in involved. If the dissolution proceeds via an electrochemical route, assessing the equilibrium solubility requires data on both the pH of the solution and the potential difference between the oxide and the electrolyte solution. The exact composition of the solution, for instance the presence of complexing agents or colloids [32], also contributes in both cases.

As discussed below in chapter 2.5, a growing oxide film on a metal is a dynamic system. The outer layer of a growing film may in some cases be assumed to be in chemical equilibrium with the solution to which it is exposed. Simple thermodynamic solubility calculations may give valuable information concerning the behaviour of this outer oxide film. All estimations of the equilibrium solubility of different oxide phases per se must always be based on the use of (synthetic) bulk oxides representing only the outer part of the film.

The chemical solubility of an oxide can be estimated either by means of experimental measurements or by thermodynamic equilibrium calculations. The chemical solubilities of oxides found in power plant conditions, i.e. at high temperature aqueous environments, have been determined or reviewed e.g. by Berry and Diegle [33], Sweeton and Baes Jr. [34], Rosenberg [18,35], Tanner and Rosenberg [36], Kunig and Sandler [37], Kang et al. [38], Bergmann et al. (for magnetite and nickel ferrite) [39] and Polley et al. (for magnetite and nickel ferrite) [40]. According to Tanner and Rosenberg [36], the solubilities of at least Fe_3O_4 and NiO are well known up to 300 °C.

In general, the solubilities of oxide phases found in oxide films formed on construction materials in power plants are relatively low in high temperature water [33]. The only possible oxides of iron, nickel or chromium that would be highly soluble are the ferrous hydroxides [41,42]. However, they are not stable at higher temperatures but are rapidly transformed to Fe_3O_4 above 100 °C.

The solubility of Fe_3O_4 should be proportional to $[H_2]^{1/3}$, and this dependence has experimentally been demonstrated to be obeyed over a range of hydrogen levels from $4.5 \cdot 10^{-4}$ to $6.0 \cdot 10^{-3}$ mol/kg (10…134 cc/kg) [41,42]. Some data point to almost

similar solubility of Fe_3O_4 and $NiFe_2O_4$ [18]. However, $NiFe_2O_4$ has also been suggested to be the least soluble of the Ni-Fe compounds found in reactor coolant conditions, and it is probably the predominant phase when enough Ni is present [35]. $NiFe_2O_4$ can be reduced to Ni and Fe_3O_4 due to the presence of hydrogen [7,43]. According to Lambert et al. [44], the solubilities of both synthetic magnetite Fe_3O_4 and synthetic nickel ferrite $Ni_{0.65}Fe_{2.35}O_4$ are at minimum at temperatures around 300 °C in conditions corresponding to the coolant in a pressurised water type nuclear reactor. This value of the minimum depends on pH and the hydrogen content of the solution. Suitable coolant conditions guarantee a positive temperature coefficient of solubility for magnetite, and a minimum solubility also for nickel ferrite at a slightly higher pH [8].

Lister [8], Kang and Sejvar [45], Ashmore [43] and Rosenberg [18] have reported that chromites are extremely insoluble and prevent corrosion, at least as long as the reducing conditions are maintained. However, Cr(III) can be oxidised and dissolved under oxidising conditions.

Exact thermodynamic calculations on the stability and solubility of oxide phases at high temperatures are complicated by the lack of reliable thermodynamic data for aqueous species at high temperatures. These calculations require knowledge of the temperature dependence of ionic entropies (which is equivalent to knowing the temperature dependence of ionic heat capacities). The stability of oxides of iron, nickel, chromium etc. have usually been reported in terms of the pH-potential (Pourbaix) diagrams [46,47,48,49,50,refs. in 51] established utilising the Criss and Cobble's Entropy Correspondence Principle (described briefly e.g. in [50]). Unfortunately, this commonly used Criss-Cobble method assumes a linear dependence of the ionic entropy of aqueous species on temperature even at temperatures above 150 °C, which is not realistic and is likely to lead to partly erroneous results [51].

Recently, calculations and input data based on a more appropriate extrapolation (revised Helgeson-Kirkham-Flowers, i.e. HKF model, which allows uncharged species to be handled) have been published [51,52,53,54,55,56]. This has facilitated the estimation of the thermodynamic stability of

oxides of iron (taking into account experimental data on the solubility of Fe_3O_4), chromium, nickel and zinc at high temperatures. The most interesting results show that $Fe(OH)_2$ is not stable above 85 °C, and iron seems to dissolve in a significant potential range between the immunity and passivity areas at all temperatures in high purity water (molalities 10^{-8}). Cr_2O_3 was found to be the only stable solid chromium compound in aqueous solutions at 25...300 °C (molalities 10^{-6} and 10^{-8}), with the exception of 10^{-8} molal solutions at T > 150 °C under which conditions no solid chromium compound was found to be stable. Concerning nickel, $NiH_{0.5}$, β-$Ni(OH)_2$/NiO and the β- and γ-NiOOH were found to be possible stable compounds.

2.5 Correlations between bulk oxides and oxide films on metals

As indicated in the introduction, the properties of the oxide films on metal surfaces formed as a result of oxidation of the substrate metal greatly determine the performance of the material. The film can be formed either at open circuit or under anodic polarisation. In this report no distinction is made between the films formed by anodic oxidation (anodic films) and oxidation under open circuit conditions. If the film prevents further oxidation of the metal, it is called a passive film. If the passive film is thin or a good electronic conductor, a redox reaction can occur on its surface in spite of the established passive state with respect to metal oxidation. On the other hand, a poor electronic conduction does not guarantee passivation of the metal.

The discussion in chapters 2.1...2.4 was focused on the properties of (synthetic) bulk oxides in thermodynamic equilibrium with the environment, with no concentration or stoichiometry gradients within the phase. Considering oxide films formed on metals, the system as a whole cannot be discussed in terms of thermodynamic equilibrium. For instance, the concentrations of dissolved species on the oxide surface most probably exceed the concentrations in the bulk electrolyte because of continuous oxidation. A thermodynamic equilibrium in an oxidative environment can be achieved only when all of the metal has been transformed

to an oxide, and the solution has been saturated with ions dissolving from or through the oxide. However, the film growing on a metal may reach a steady state, in which the formation and dissolution rates are equal. Also, the prevailing situation in some part of the system (for instance at the film/solution interface) can be approximated to be in equilibrium, if the processes there are much faster than in other parts of the system. But in all cases the metal/film/electrolyte system as a whole is a dynamic system, most often under mass transport, charge transfer or other kinetic control.

Accordingly, the properties and structure of oxide films on metals are likely to differ from those of bulk oxides under thermodynamic equilibrium. An illustrative presentation of different possible morphologies of passive films can be found e.g. in the review given by Sato [57]. Oxide films very often consist of two or more sublayers, differing either in chemical composition or physical properties such as porosity. For instance, a duplex film consisting of a dense and a porous part can arise whenever the volume of an oxide exceeds that of its parent metal. Another possibility to form a duplex film is a localised dissolution process at the originally dense film/electrolyte interface. As an alternative to a duplex film, the composition and stoichiometry of the film and hence its physical properties may change gradually with distance from the film/environment interface. In addition, the low thickness of several oxide films may result in lack of well-defined periodicity normal to the surface. Oxide films

contain more defects than stoichiometric bulk oxide phases, and they may be more or less hydrated and even amorphous or glassy. As discussed above in chapter 2.2, the growth of oxide films proceeds in most cases by means of transport via defects in the oxide structure, while an oxide film without any defects can actually grow only by means of deposition from the solution. The electronic properties of oxide films may change as a function of distance from the film interfaces and as a function of potential, which may complicate quantitative determination of their properties. If the models and concepts developed for crystalline bulk semiconductors are applied to oxide films on metals, they have to be modified to take into account the localised energy states and other factors related to the nature of thin films.

In spite of the differences between bulk oxides of metals and oxide films formed on metals, the discussion on bulk oxides presented above can be used as a basis for the understanding of the behaviour of oxide films. A special case are thick and crystalline oxide films (forming for instance at high temperatures), the outer part of which may be completely identical to synthetic bulk oxide phases. In addition, studies on thin synthetic oxide films are likely to be helpful in separating the oxide film properties from the behaviour of the underlying metal or alloy, which otherwise is not a straightforward task [58].

The rest of this report is focused on understanding the properties and behaviour of oxide films formed on metal surfaces.

3 STRUCTURE OF OXIDE FILMS ON METALS

In the following text it is essential to distinguish between the concepts referring to different types and parts of the oxide film on a metal. A bi-layer film is defined as a compact film consisting of two layers with different compositions. On the other hand, a duplex film refers to a film which contains two parts differing in their physical properties (most commonly porosity or degree of hydration). The latter can be formed at sufficiently long oxidation times whenever the volume of the oxide exceeds that of its parent metal, or also when a the film is formed via a mechanism involving deposition from the solution. Even a film consisting of three parts (layers) may be formed (see e.g. Asakura et al. [59]), if both these preconditions are fulfilled.

Chapter 3.1 focuses on compact oxide films on iron, nickel and chromium, while films on iron- and nickel-based alloys are considered in chapters 3.2 and 3.3.

3.1 Films formed on pure iron, nickel and chromium

3.1.1 Films on iron

Iron exposed to an aqueous environment at ambient temperatures (i.e. below 100 °C) becomes covered with a thin film, the thickness of which is of the order of 5 nm [13,60,61]. This is roughly equal to 20 atomic layers. The film is compact and contains Fe, O and maybe protons [15,61], in the form of oxides, hydroxides or oxyhydroxides. The structural similarity of several oxidation products of iron, as outlined e.g. by Gerischer [5], Robertson [9] and Tomlinson [15] and as discussed in chapter 2.1.2, probably leads to easy and/or gradual changes in the composition of different parts of the film.

Experimental observations have led to slightly different views on the detailed structure of the anodic film on iron. A scheme of the several suggested structures is given in Fig. 7 [62,63]. The main controversial questions are:

- whether the film has a bi-layer (sandwich) or a single film structure; i.e. whether different oxidation products can be distinguished in the film
- whether the film is partly dehydrated or not
- whether the film is amorphous or crystalline

On the basis of the number of distinguishable layers, Rahner has summarised the existing views as follows [64]:

a) a bi-layer (sandwich) film on the basis of the scheme Fe / Fe_3O_4 / γ-Fe_2O_3 with variable stoichiometry in the different parts [62,65,66], (the inner layer may even be described as γ-Fe_2O_3 with a gradient of incorporated Fe^{2+} of increasing concentration towards the metal surface [61]

b) a single layer film on the basis of the scheme Fe / Fe_2O_3 - FeOOH, with a wide stoichiometry range of the Fe(III)oxy-hydroxide [67,68,69,70]

Supporting evidence for both the bilayer and the single layer concept has been presented on the basis of the structural features of the oxidation products of iron. Davenport and Sansone [10] have pointed out that the proposed bi-layer type Fe_3O_4/ γ-Fe_2O_3 structure has a special appeal: it would

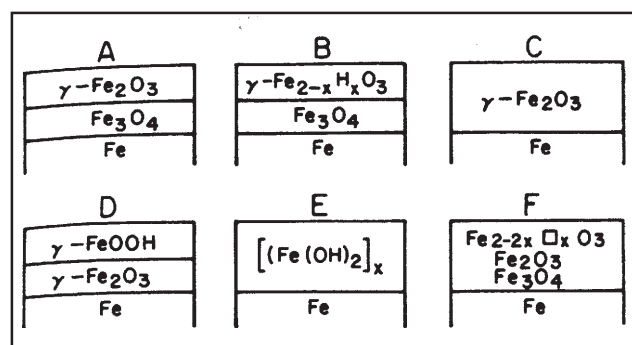**Fig. 7.** *Suggested structures for the passive film on iron: A) a bi-layer Fe_3O_4 / γ-Fe_2O_3; B) a bi-layer with H in outer layer; C) a single layer γ-Fe_2O_3; D) a hydrated layer γ-Fe_2O_3 / γ-FeOOH; E) polymeric layered $[Fe(OH)_2]_x$; F) non-stoichiometric cation deficient γ-Fe_2O_3 with varying number of protons [62,63].*

allow the passive film to have a continuous array of close-packed oxide ions in which the main outer layer has cation sites filled only with Fe(III) to give Fe_2O_3 with an inner layer containing some Fe(II) (i.e. approaching magnetite) at the metal/film interface. These two structures are distinct among the oxides and oxyhydroxides in containing some tetrahedrally co-ordinated iron. The structures of all the other possible products have only octahedral co-ordination. However, Cahan and Chen [69] and Kuroda et al. [70] ended up in proposing the single layer concept because of the same facts: Based on the similarity of the structures of γ-Fe_2O_3 and Fe_3O_4, they considered it possible that the structure of the whole passive film could consist of a continuous array of oxide ions with a gradient in average valence and occupancy of cation sites. An overlayer may also be formed under some conditions, such as re-precipitation from the solution.

Unfortunately, it has been relatively difficult to find conclusive experimental support to either of these two types of film structures. This is mainly due to the fact that the results of any structural analysis of a film thinner than 5 nm must almost always be considered only speculative. The existence of different layers containing different oxidation products of iron in the film, i.e. the bi-layer concept, has been supported by cathodic reduction experiments combined with rotating ring disk detection [64], with SIMS studies in [18]O enriched borate buffer solution [61] and with recent in situ XANES studies [10,74], as well as by surface analytical studies using such techniques as AES, XPS, SIMS, Mössbauer, RHEED, X-ray analysis, EELS and TEM [75]. On the other hand, modulation spectroscopic measurements [76] have lent support to the single layer concept. The contradictory results may be due to variations in the conditions under which the film was formed, to different ways of polarisation during film formation, uncertainties in potential control, influence of the removal of the sample from the solution, exposure to air and the electron beam in ex situ analyses etc. [10,70]. Schmuki et al. [73] showed in a very illustrative way by means of XANES that a finding of two reduction steps during galvanostatic reduction experiments, which have been widely used to study the passive films on iron, does not necessarily mean that a bi-layer film was

originally present on the surface. Bardwell et al. [61] even pointed out that galvanostatic reduction curves alone can be and have been used as a proof for both single layer and bi-layer models.

The most recent XANES results [77] show that the composition of the passive film on iron can be described as a mixed-oxidation-state iron oxide, containing both Fe^{3+} and Fe^{2+}. The oxide contains mainly Fe^{3+} ions, and the proportion of Fe^{2+} ions varies between 0 to 10% at +0.4 V vs. MSE (E $\cong$ 1.04 V vs. SHE) and 14 to 20% at –0.8 V vs. MSE (E $\cong$ –0.16 V vs. SHE). This view seems to approach the concept of a single layer film. It is also close to the transition layer concept introduced by Sato et al. [71,72]. They suggested the structure Fe/mixed Fe(II)-Fe(III) oxide - FeOOH to prevail at low potentials and the structure Fe/Fe_2O_3 - FeOOH to exist at high potentials in neutral solutions. It can be concluded that there probably is no big discrepancy between the bi-layer and the single layer concepts.

In addition to the question whether the film on iron is a bi-layer or a single one, also the degree of hydration and the possible amorphous or crystalline nature of the film are subject to some uncertainty. The presence of hydrated disordered γ-FeOOH overlayers has often been proposed for room temperature films and has been observed also for high-temperature passive films by Mössbauer spectroscopy [11]. Although the ex situ SIMS measurements by Graham [75] have pointed to crystalline nature and absence of hydroxyl ions within passive films on iron, Oblonsky and Devine [78] have demonstrated by means of in situ SERS that the passive film in borate buffer contains an amorphous $Fe(OH)_2$-like product, in addition to amorphous Fe_3O_4 or γ-Fe_2O_3. The hydrated part of the layer has been proposed to almost disappear in the acidic pH range [71,72]. It has been suggested [10,79] that factors such as the reoxidation of dissolved ferrous species to form disordered hydrated structures or other difficulties or differences in experimental conditions may give rise to contradictory observations concerning the presence of a hydrated overlayer.

Recent ex situ STM examinations [79] of sputtered thin films of pure iron in borate buffer solutions (pH 8.4) showed long-range crystalline order on the film surfaces, with the same triangular lattice of spacing 0.30 ± 0.01 nm appearing on

all the crystallites studied. In situ STM examination at intermediate potentials after passivating at high potentials showed the same lattice on a large number of areas, which means that the orientation in the oxide is indifferent to the orientation of the substrate. The structure is consistent with the $Fe_3O_4/\gamma\text{-}Fe_2O_3$ structure of the passive film, and the results appear to refute the suggestion that the film is a highly disordered or amorphous material. The results of Ryan et al. [79] agree with the observations of Davenport and Sansone [10], according to which only compounds with iron in mixed co-ordination (i.e. Fe_3O_4 and $\gamma\text{-}Fe_2O_3$) or hypothetical structures with distorted co-ordination polyhedra but no hydrated compounds could be possible. A further proof for the crystalline nature was given by Toney et al. [80]: Using in situ and ex situ XRD analysis, they determined the structure of the passive oxide film formed on Fe(110) and Fe(001) at +0.4 V vs. MSE ($E \cong 1.04$ V vs. SHE) in borate buffer (pH = 8.4) to be based on Fe_3O_4. The film was found to be nanocrystalline with a small crystallite size and to be oriented with the substrate. The nanocrystallinity points to better mechanical properties (hardness, ductility) than those of bulk solids.

3.1.2 Films on nickel

Passivity of nickel can be readily achieved in a wide variety of solutions over a large range of pH. Ex situ analyses have shown that the passive film on nickel is entirely NiO of thickness 0.9-1.2 nm (i.e. only approximately three atomic layers), and it is not affected by air exposure. Electron diffraction studies on Ni(111) have shown that the epitaxy of the NiO film is maintained during polarisation in the passive potential region, but is lost in the oxygen evolution region where a porous, sponge-type oxide is formed [75].

According to the data reviewed by Itagaki et al. [81], the composition of the passive film formed on nickel varies slightly as a function of pH: In alkaline solutions the passive film has been reported to consist of divalent oxide NiO, while in borate buffer solutions with pH 8.42 the film contains NiO and also Ni_2O_3 at high positive potentials. In 1 M sulphuric acid solutions NiO can be oxidised to NiOOH.

Recent in situ SERS investigations by Oblon-sky and Devine [78,83] have indicated the presence of amorphous $Ni(OH)_2$ and some NiO at –0.1 V vs. SCE (E = about +0.140 V vs. SHE) in borate buffer solutions, while at +0.1 V vs. SCE (E = about +0.34 V vs. SHE) NiO was not observed. At +0.9 V vs. SCE (E = about +1.14 V vs. SHE, the transpassive region) it was speculated that the species responsible for the Raman scattering resembles NiOOH. Upon returning from the transpassive region to +0.1 V vs. SCE (E = about +0.34 V vs. SHE), the original $Ni(OH)_2$ film did not reform, but instead, a film containing a mixture of $Ni(OH)_2$, NiO and some unidentified species formed [78,83]. The results of earlier in situ Laser Raman spectroscopic studies on Ni in 0.05 M NaOH at about +0.6 V vs. Hg/HgO (E = about +0.7 V vs. SHE) were explained by the presence of hydrated Ni_2O_3 [84].

The in situ STM results obtained by Yau et al. [85] are in fairly good agreement with the Raman results discussed above. Yau et al. found out that a well-ordered rhombic structure of the film on Ni prevails at low potentials (–0.7…–0.5 V vs. SHE), while at higher potentials (E > +0.18 V vs. SHE) a quasi-hexagonal structure corresponding to either $\beta\text{-}Ni(OH)_2$ or to NiO was observed. Also Marcus and Maurice [86] employed in situ STM and were able to describe the structure of passive films formed on nickel as crystalline with steps, kinks and point defects. However, no evidence of the hydroxide outer part was obtained, which was considered likely to be caused by a certain tunnelling mechanism during the STM measurement.

The in situ AFM experiments of Kowal et al. [87] have led to the conclusion that the oxidation of a $Ni(OH)_2$ film formed in 1 M KOH is associated with removal of protons from the film.

3.1.3 Films on chromium

Using SERS, Oblonsky and Devine [78] came to the conclusion that the passive film on chromium at –0.1 V vs. SCE (E = +0.14 V vs. SHE) in borate buffer solutions consists of $Cr(OH)_3$ and another substance that may resemble $Cr(OH)_2$, CrOOH, or a previously unidentified species that has no bulk analogy. A review on the different views on the composition of the film on chromium can be found in [88]: The presence of small amounts of Cr(VI) in the film has been established at high potentials.

Cr(VI) is incorporated into the oxide, or is tenaciously adsorbed on the surface. The formation and reduction of Cr(VI) was found to be reversible. The electronic conductivity of the passive film on chromium was observed to increase both at potentials close to the region in which active dissolution proceeds and close to the region where transpassive dissolution takes place [88].

The most recent model points to an insulating nature of the Cr_2O_3 film, which may also contain some water. Its properties are influenced by changes in the stoichiometry close to the metal/film and film/environment interfaces [89].

3.2 Films formed on steels

3.2.1 Films on carbon steels

The films formed on carbon steel can be considered closely similar to those formed on pure iron. During long polarisation, duplex films consisting of a dense and a porous part can be formed [9,11].

3.2.2 Films on stainless steels

The films formed on stainless steels in ambient conditions have steady state thicknesses in the range 1...3 nm, and the thickness decreases with decreasing pH and increasing Cr content [90,91,92,93,94,95]. The film seems to reach the steady state thickness during the first hour of polarisation [90,91]. Oblonsky and Devine [78] have detected amorphous $Fe(OH)_2$ and Fe_3O_4 or γ-Fe_2O_3, $Ni(OH)_2$, NiO, $Cr(OH)_3$ and the $Cr(OH)_2$-like species in the passive film on AISI 308 stainless steel in borate buffer solutions. Chromium has been described to influence the structure of anodic films on stainless steels by occupying octahedral and tetrahedral sites in a unit cell of spinel structures [98]. The presence of Cr(VI) in the oxide film on a Fe-26%Cr alloy at high potentials close to the transpassive region has also been confirmed [96]. Molybdenum content in the passive film formed on Mo-containing stainless steel is low. This element is present as Mo(IV) at low passive potentials and as Mo(VI) at higher potentials [97].

According to Hakiki et al. [97], the oxide film formed on stainless steel has a bi-layer type structure both in neutral and acidic solutions. The inner layer is composed of chromium(III)oxide with some oxidised iron. The existence of divalent chromium at low passivation potentials has also been suggested [93,94]. The outer layer consists mainly of iron oxides and hydroxides at the film/electrolyte interface. The hydroxide part may comprise at least one third of the whole film [97]. The outermost parts of the passive film formed on iron, carbon steel and stainless steels can be regarded as very similar, at least in neutral and slightly acidic solutions [17,97]. This outer Fe-rich layer is more influenced by the external conditions both in thickness and stoichiometry. The overall degree of hydration of the film decreases with potential but the fraction of FeOOH increases. This implies the existence of two different hydrated products, $Fe(OH)_2$ and FeOOH, predominating at low and high potentials respectively [17].

However, the observation that the various constituents of the passive film on AISI 308 stainless steel were concurrently reduced during cathodic polarisation [78] is inconsistent with the view that passive films on stainless steels are composed of discrete layers. This shows that it is still uncertain, as in the case of pure iron, whether the possible oxidation products are present as separate phases or whether the film has a gradually changing composition. The latter view is supported by the observation that the stoichiometry of the oxides on stainless steels changes with the time as the film grows [17].

It is generally accepted that Cr_2O_3 based products form barrier layers and are responsible for the superior corrosion resistance of stainless steels. A barrier layer refers to a continuous layer which can prevent current flow (i.e. metal dissolution) and thus support a high electric field within the film. The low solubility and high stability of Cr_2O_3 based products thus reduce the passive current and increase the size of the passive region on the pH-potential diagram. Cr_2O_3 based barrier layers tend to be formed on Cr-containing iron based alloys if the Cr content of the alloy exceeds 12...15%. This transformation threshold to more passive steel is probably independent of temperature. The formation of the Cr_2O_3 based barrier layer at the metal/film interface can be attributed to the slow dissolution of iron through the film already during the first 30 hours of oxidation. During this period the thickness and the chromi-

um content of the inner oxide layer increases, while the total film thickness is unchanged already after the first hour of oxidation. It has also been suggested that some dehydration of the film takes place simultaneously [9,17,76,90,91,92,97,99,100].

According to the percolation theory approach, the crucial factor in forming a passivating oxide film is the degree of connectivity of Cr atoms through the three-dimensional lattice: the Cr atoms must be close enough together in the lattice structure so that adsorbed oxygen anions can bridge what is to become oxidised chromium [101]. With too small a content, no continuous film of Cr(III) oxide may form and dissolution will continue until Fe(III) oxide forms at sufficiently high potentials [100]. The passive film is assumed to initially consist of disordered CrOOH that may undergo structural relaxation [101], i.e. transient phenomena in the structure of the film, which may be equal to the dehydration suggested by Yang et al. [90]. The ex situ STM results of Ryan et al. [101] on sputter-deposited microcrystalline Fe-Cr alloys seem to support the validity of the percolation model. Calinski and Strehblow [100] did not observe any special change in the film composition when exceeding the magic 12% Cr content of the alloys in their ISS studies exhibiting excellent monolayer sensitivity when compared e.g. with XPS.

Graham [75] has cast a doubt upon all ex situ analyses of oxide films on steels by stating that films on Fe-Cr alloys change on removal from solution, the extent of change increasing with increased chromium content in the alloy. This makes the conclusions of the disordered structure of passive films on stainless steels drawn e.g. on the basis of electron diffraction studies uncertain. As an interesting curiosity he commented that the tendency of the films to change may reflect their ability to adapt to changing environmental conditions (a rigid Fe_3O_4/γ-Fe_2O_3 layer formed on pure iron would break down under a drastic change of environmental conditions, rather than subtly rearrange itself to respond to changing conditions).

Recent in situ STM examinations on Fe-Cr alloys polarised in 0.01 M H_2SO_4 solutions at +0.4 V vs. SCE (E = +0.64 V vs. SHE) have shown that highly crystalline films are formed on alloys with Cr contents as low as 13.8% [102]. At higher Cr contents, only short range order was observed, probably because of the thinner film. Both these in situ and earlier ex situ experiments [101] have shown that the orientation in the oxide was indifferent to the orientation of the substrate.

3.3 Films formed on nickel-based alloys

The passive films formed on Ni-20%Cr alloys in 1 M NaOH and 0.5 M H_2SO_4 during short polarisation times (ranging from only 10 ms to 1000 s) have been observed to possess a bi-layer structure on the basis of XPS investigations [103]. The film consisted of an outer hydroxide part and an inner oxide part, and the maximum thickness was about 6 nm in NaOH and 3.5 nm in H_2SO_4. Ni was found to be enriched at the metal surface beneath the passive film compared to the metal bulk composition. This refers to selective oxidation of other constituents.

Ni formed the major part of the outer hydroxide layer in 1M NaOH, especially at positive potentials and for long passivation times, except for the very high potentials close to the transpassive region. An oxide layer consisting of mainly Cr_2O_3 and NiO was found to exist in the transpassive potential range, where also some Cr(VI) was found in the layer. In acidic electrolytes, both the hydroxide and the oxide part of the passive film contained only Cr(III) ions with minor contributions of Ni(II) and Cr(VI) in the transpassive range [103].

4 ELECTRONIC PROPERTIES OF OXIDE FILMS ON METALS

As discussed in chapter 2.5, the properties of oxide films on metals often change more or less gradually as a function of distance from the film interfaces. This is true also for the electronic properties of the films. However, it is reasonable to use the electronic properties of (synthetic) bulk oxides reviewed in chapter 2.3 as a starting point when evaluating the electronic properties of films growing on metals. The electronic properties of passive films may in some cases be directly correlated with the susceptibility to corrosion: a low bandgap energy should lead to poorer resistance to corrosion [104]. In addition, the presence of a donor level close to the conduction band or an acceptor level close to the valence band are associated with doping of the oxide, and this may also lead to poorer resistance to corrosion. The doping densities reported for passive films are generally of the order of $10^{19} \ldots 10^{20} \, cm^{-3}$, which are high values compared with the doping densities of $10^{16} \, cm^{-3}$ reported for classical semiconductors such as Si, Ge [97]. Metallic conduction is approached when the doping density is close to $10^{21} \, cm^{-3}$.

4.1 Films formed on pure iron, nickel and chromium

Kruger [63] has pointed out that the electronic conductivity of the passive film on iron has been a major controversial issue in the studies reported in the literature: both good electronic conductivity and almost insulating behaviour have been proposed.

The inner Fe_3O_4 part of the oxide film on iron can be presumed to be an almost metallic conductor [97], and it should not contribute significantly to the electronic behaviour of the oxide film as a whole. Lorang et al. [17] associated the electronic properties of the passive films on iron (and also on stainless steel) with the Fe^{2+} content in Fe_2O_3 in the passive film. These ions are supposed to be donor species, and their amount decreases with potential. Accordingly, mainly n-type semiconducting properties have been associated with the γ-Fe_2O_3 layer [97]. However, a γ-Fe_2O_3 layer has also been reported to behave as an insulator or even like a p-type semiconductor [105].

At pH 8.4, a band-gap energy E_g = 1.6 eV, a dielectric constant ε = 12 and a donor concentration of about $10^{20} \, cm^{-3}$ have been ascribed to the γ-Fe_2O_3 layer [105]. Also slightly higher values for the donor concentration [106,107] and for the

band gap have been reported, mainly on the basis of photocurrent measurements [13, 97, 106, 108, 109]. A direct bandgap of 3.0 eV has also been reported by Trefz et al. [110]. The band gap energy has been observed to be independent of the pH in the range 4.8–13 [106]. Gerischer [5] has commented that the energy distance between the highest filled band and the conduction band in Fe_2O_3 cannot be as large as photocurrent spectra have suggested. Instead, the existence of energy bands at a distance of approximately 1.2 eV form the conduction band could be possible. Similar ideas were also suggested by Azumi et al. [111]. The existence of such bands could explain the results of Noda et al. [112], according to which the major part of the film is well conductive and only a minor part of the applied potential is consumed as a potential drop within the film.

In the chemi-conductor concept introduced by Cahan and Chen [67,68,69] and discussed in more detail in chapter 5.4.2, the oxide film on iron was regarded as a trivalent iron oxy-hydroxide film, capable of existing over a wide range of stoichiometry. From the ellipsometric data, the principal gap between filled bands was estimated to be above 5.5 eV. It is worth commenting that this does not correspond to the concept of a band gap in a semiconductor sense. However, a close simi-

larity between the spectroscopic ellipsometric results of Chen and Cahan [67] and photocurrent spectroscopic measurements have been demonstrated by Abrantes and Peter [106]. They extrapolated both the ellipsometric and the photocurrent spectra to an indirect optical gap energy of ca 1.9 eV. Moreover, Cahan and Chen reported localised d-states to exist within the gap. They explained that in a highly disordered passive film the energies of these d-states can be spread significantly around the mean values to form a "non-stoichiometry band" which could increase the conductivity e.g. by means of a local hopping mechanism. Thus the passive film is neither a semiconductor nor an insulator, but a combination of both. This model approaches the ideas presented by Gerischer and Azumi et al. and discussed above.

Further discussion on the electronic properties of oxide films on iron can be found in chapter 5.4.1 titled Semiconductor models for the passive film on iron.

Band gap energies ranging from 1.8 eV to 3.5 eV have been attributed to the anodic film on nickel [108,113,114]. Stimming [108] regarded the values 2.2 eV and 3.4 eV as the most reliable. Sunseri et al. [114] reported band gap values of 3.0...3.5 eV for Ni(II) oxide and 2.5...2.6 eV for Ni(III) oxide. This is in agreement with the suggestion of Bernard et al. [82]. They stated that the incorporation of Ni(III) increases the conductivity of the divalent film.

The electronic properties of the oxide films on chromium have been recently reviewed and investigated by Bojinov et al, and the results can be found in references 88 and 89.

4.2 Films formed on steels

Hakiki et al. [97] commented critically the fact that when the semiconducting properties of passive films formed on stainless steels have been considered, the electronic structure of the inner Cr rich layer has not been taken into account.

On the basis of Mott-Schottky analysis (see e.g. [27]), Hakiki et al. [97] stated that the films on AISI 304 stainless steel and Fe-Cr alloys (Cr content: 0...30%) in a boric acid + borate buffer solution of pH 9.2 behave as a p-type semiconductor below a certain potential (–0.5 V vs. SCE, i.e.

–0.26 V vs. SHE) and as an n-type semiconductor above that potential. They attributed the p-type behaviour to the inner Cr_2O_3 film and the n-type behaviour to the outer part of the film and explained how the different parts of the film control the electronic current during polarisation at high and low potentials. They ascribed the critical potential to a common value of the flatband potential. This, however, seems a bit confusing, because Cr_2O_3 and Fe_2O_3 are not known to have the same values for the flatband potential. Acceptor and donor densities were observed to decrease with increasing formation potential of the film, which is in good agreement with the films formed at lower potentials being more disordered. The donor density was independent of the Cr content of the alloy, while the acceptor density increased with decreasing Cr content approaching quasi-metallic conductor properties for pure iron.

A more detailed analysis of Hakiki and Da Cunha Belo [98] indicated that the capacitance behaviour of the passive films formed on ferritic Fe-17%Cr alloys is related to the contributions of a shallow ionised donor level very close to the conduction band and a deep donor level at about 0.4 eV below the conduction band. The latter is not ionised under flatband conditions but becomes ionised in the space charge layer (see chapter 5.4.10) under polarisation. Photoeffects observed for subbandgap photon energies revealed that this deep donor level behaves like a trapping electronic state situated in the space-charge zone of the passive film. Finally, capacitance and photoelectrochemical results revealed the great influence of the electric field. This is related to the development of the space charge region at the film-electrolyte interface. The addition of Mo was found to decrease the donor density of the deep level.

4.3 Films formed on nickel-based alloys

Only few investigations on the electronic properties of films formed on nickel-based alloys can be found in the literature. Jabs et al. [103] have suggested that the semiconductor properties of the passive film on Ni-20%Cr alloy change with increasing potential as a result of accumulation of Ni(III) ions in the film.

5 APPROACHES TO MODEL OXIDE FILM STRUCTURE AND OXIDE GROWTH

In this chapter, experimentally observed growth laws for oxide films on metals are first reviewed briefly (chapter 5.1). Subsequently, theoretical approaches to model both the structure and the growth of oxide films are discussed. The growth of an oxide film may be controlled by transport through the film (see chapter 5.2) or reactions at film interfaces (see chapter 5.3). Even if the film has a duplex structure, i.e. if it consists of a compact inner layer and a porous outer layer, it is usually justified to assume that the transport through the compact part is slower than the transport in the more porous part (see e.g. [9,11]). Therefore, the main focus is in the growth processes of non-porous oxide films containing only point defects. The role of one- and two-dimensional defects as well as of the outer porous oxide layer will be commented in later chapters when considered relevant. A comprehensive discussion on the ionic transport in porous oxide films is beyond the scope of this report.

Although iron- and nickel-based alloys are the most interesting materials from the viewpoint of this report, not only models related strictly to these materials and their constituents but also models for the growth of oxide films on metals in general were found necessary to describe (chapter 5.4). Verifying their validity and applicability remains partly a future task. Chapters 5.5 and 5.6 form a link between theoretical models and experimentally measurable film growth rates discussed in chapter 5.1.

5.1 Growth laws for oxide films

The growth of an oxide film may follow different types of relationships between thickness and time during different stages of the growth. The various rate laws observed experimentally can be classified as follows (see e.g. [115,116,117,118]):

i) Linear growth: $L = k\,t$ (5-1)

ii) Logarithmic growth: $L = A + B \ln t$ (5-2)

iii) Inverse logarithmic growth: $L^{-1} = C - D \ln t$ (5-3)

iv) Parabolic growth: $L = (2k't)^{1/2}$ (5-4)

v) Cubic growth: $L = (2k''t)^{1/3}$ (5-5)

A challenge for theoretical models of film growth is to be able to predict the observed growth behaviours in a quantitative way.

5.2 Factors affecting transport through oxide films

The growth of an oxide film proceeds either at the metal/film interface or at the film/solution interface. When the growth occurs solely via deposition of species present originally in the solution, no ionic transport through the film is required. In all the other cases transport of ionic species through the film is necessary to make film growth and other related phenomena possible.

The type of the moving species depends on the composition and structure of the oxide. Either cation or anion species may dominate, or they can in some cases exhibit comparable transport rates. Transport of oxygen species from the film/solution interface (equivalent to transport of oxygen vacancies from the metal/film interface) through the film results in film growth at the metal/film interface (for details, see Fig. 12 in chapter 5.4.8). On the other hand, transport of cation species from the metal/film interface (equivalent to transport of metal vacancies from the film/solution interface) can contribute not only to film growth directly at the film/solution interface but also to dissolution of metal ions to the electrolyte and successive deposition on the existing oxide surface.

The transport rate of species through oxide films is determined by their mobility in the film and the driving force, which may be electric field resulting in migration of species and/or concentration gradient resulting in diffusion of species. The mobility of a specific species is greatly influenced by the medium in which the transport takes place, i.e. by the oxide structure. As discussed above, the

film may consist of different layers exhibiting different chemical and physical properties. Accordingly, the mobilities of the species as well as the driving forces may be different in the different parts of the film. To be able to model and predict the transport rate of species through the whole film, it is essential to identify the rate-determining processes in all the different layers of the film (and also at the interfaces). If several parallel processes are possible in the same layer, the fastest one determines the transport rate in that layer. On the other hand, the transport rate through the whole film is controlled by the transport through the part of the film in which the transport rate is the slowest.

Field assisted defect transport can be described using the following general equation [119] (written in this case for the transport of oxygen vacancies), in which the first term describes generalised diffusion and the second term corresponds to non-linear migration:

$$J_O(x) = -D_O \frac{dc_O(x)}{dx} \cosh\left[\frac{zFaE(x)}{RT}\right]$$
$$-\frac{D_O}{a} c_O(x) \sinh\left[\frac{zFaE(x)}{RT}\right] \qquad (5\text{-}6)$$

The solution of this equation under a homogeneous field approximation (field $E(x)$ = constant) results in:

$$J_O = \frac{\frac{D_O}{a} \sinh\frac{zFaE}{RT}\left\{c_O(0)\exp\left[-\frac{L}{a}\tanh\frac{zFaE}{RT}\right] - c_O(L)\right\}}{\left\{1 - \exp\left[-\frac{L}{a}\tanh\frac{zFaE}{RT}\right]\right\}} \qquad (5\text{-}7)$$

In the case of a poorly conducting semiconductor oxide or of an insulating film (band gap > 2...3 eV), the redox reactions on the surface of the film may be suppressed and a very high electric field may result (field strength $\geq 10^6$ Vcm^{-1}). In this case, the mechanism of the ionic transport must be discussed in terms of high field ionic migration, i.e. the current is exponentially proportional to the electric field within the film. In the high-field limit (i.e. $zFaE/RT \gg 1$), the resulting transport equation is:

$$J_O = \frac{D_O}{2a} \exp\frac{zFaE}{RT}\left\{c_O(0)\exp\left[-\frac{L}{a}\right] - c_O(L)\right\} \qquad (5\text{-}8)$$

For films growing via oxygen vacancy motion, the film growth current density can be expressed as $i = -2FJ_O$. In the high-field limit, concentration gradients in the film are usually neglected when compared to the migration term $c_o(L) \gg c_o(0)\exp(-L/a)$ and the growth current is given by the approximate expression (high-field migration equation):

$$i = \left(\frac{zFD_O c_O(L)}{2a}\right)\exp\left(\frac{zFaE}{RT}\right) \qquad (5\text{-}9)$$

However, if the gradient of the electric potential extends only over one part of the film, diffusion in other parts of the film in series with the one containing the potential gradient may control the overall transport rate. This is likely to happen in the case of thick films (e.g. d > 100 nm).

Under low-field conditions, i.e. when $zFaE/RT \ll 1$, the approximation $\sinh(zFaE/RT) = 2zFaE/RT$ can be used. Thus the rate of diffusion may be comparable to that of low-field migration. In this case the transport of species through the film can be modelled in terms of the linear gradient of the electrochemical potential. The electrochemical potential of the species includes the contributions of both the chemical potential of the species and the electrostatic potential (see also chapter 5.4.6). The overall transport is in terms of the Nernst-Planck equation which stems from equation (5-6) in the low-field limit:

$$J_O(x) = -D_O \frac{dc_O(x)}{dx} - \frac{D_O}{a} c_O(x)\left[\frac{zFaE(x)}{RT}\right] \qquad (5\text{-}10)$$

Integrating this in the homogeneous field approximation gives the vacancy flux vs. the field relation in the form

$$J_O = \frac{\left\{c_O(0)\exp\left[-\frac{zFEL}{RT}\right] - c_O(L)\right\}}{1 - \exp\left[-\frac{zFEL}{RT}\right]} \frac{zFD_O E}{RT} \qquad (5\text{-}11)$$

5.3 Reactions at the film interfaces

Macdonald et al. [116,120] have given an illustrative presentation on the reactions occurring in the metal/film/electrolyte system, and their presentation is utilised in this report. By means of the Kröger-Vink notation [12 p.34], the total reactions can be summarised as follows (the model of Macdonald et al. for the anodic film is presented in more detail in chapter 5.4.8 below; see also Fig. 12):

film growth: $m + \left(\dfrac{x}{2}\right)H_2O = MO_{\frac{x}{2}} + xH^+ + xe^-$ (5-12)
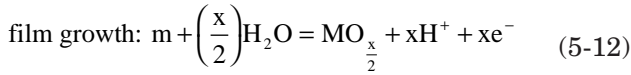
(isovalent) dissolution of the film:

$$MO_{\frac{x}{2}} + xH^+ = M_{aq}^{x+} + \left(\dfrac{x}{2}\right)H_2O \qquad (5\text{-}13)$$
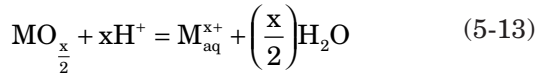
When the oxygen species (or oxygen vacancies) are considerably more mobile than cation defects, equation (5-12) is the sum of the generation of oxygen vacancies at the metal/film interface:

$$m = M_M + \left(\dfrac{x}{2}\right)V_O^{2+} + xe^- \qquad (5\text{-}14)$$

and the annihilation of the vacancies at the film/ solution interface:

$$V_O^{2+} + H_2O = O_O + 2H^+ \qquad (5\text{-}15)$$

When the cation vacancies are considerably more mobile than oxygen vacancies, equation (5-12) is the sum of the generation of cation vacancies at the film/solution interface:

$$H_2O = V_M^{x-} + O_O + xH^+ \qquad (5\text{-}16)$$

and the annihilation of the vacancies at the metal/ film interface

$$m + V_M^{x-} = M_M + xe^- \ (+\text{vacancy in the metal}) \qquad (5\text{-}17)$$
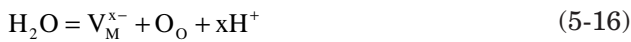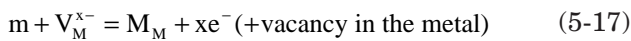
In the latter case metal dissolution through the film can occur as follows:

$$m + V_M^{x-} \qquad\qquad = M_M + xe^- \qquad (5\text{-}18)$$

$$\underline{\qquad M_M \qquad\quad = M_{aq}^{x+} + V_M^{x-} \qquad (5\text{-}19)}$$

$$\text{total: } m \qquad\qquad = M_{aq}^{x+} + xe^- \qquad (5\text{-}20)$$
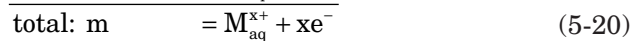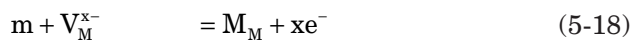
If cation interstitials act as major ionic defects,

metal dissolution through the film is also possible. In that case a slightly modified set of equations can be used to describe the process.

If a reaction such as injection of defects at one of the interfaces is the rate limiting step of the whole growth, an exponential equation is likely to describe the dependence of the current on potential.

5.4 Summary of models for oxide films and transport phenomena

This chapter summarises briefly the various models presented for the energy band structure, chemical structure and for the growth of oxide films. Material-specific models discussed here are all related to iron-based or nickel-based alloys and their constituents, while kinetic models for oxide growth are presented also on a more general level.

Fromhold Jr [121] has defined that in anodic oxidation the parent metal in a solution is made the anode by means of an externally applied potential source. Thus it becomes positively charged, which leads to an electric field driving the ionic species through the oxide to enable more oxide to grow. In this report no distinction is made between the models developed for anodic oxidation and oxidation under open circuit conditions.

5.4.1 Semiconductor models for the passive film on iron

Stimming and Schultze [105] have derived a semiconductor model for a bi-layer type anodic film on iron on the basis of capacitance measurements (see Fig. 8). They explained the electrochemical
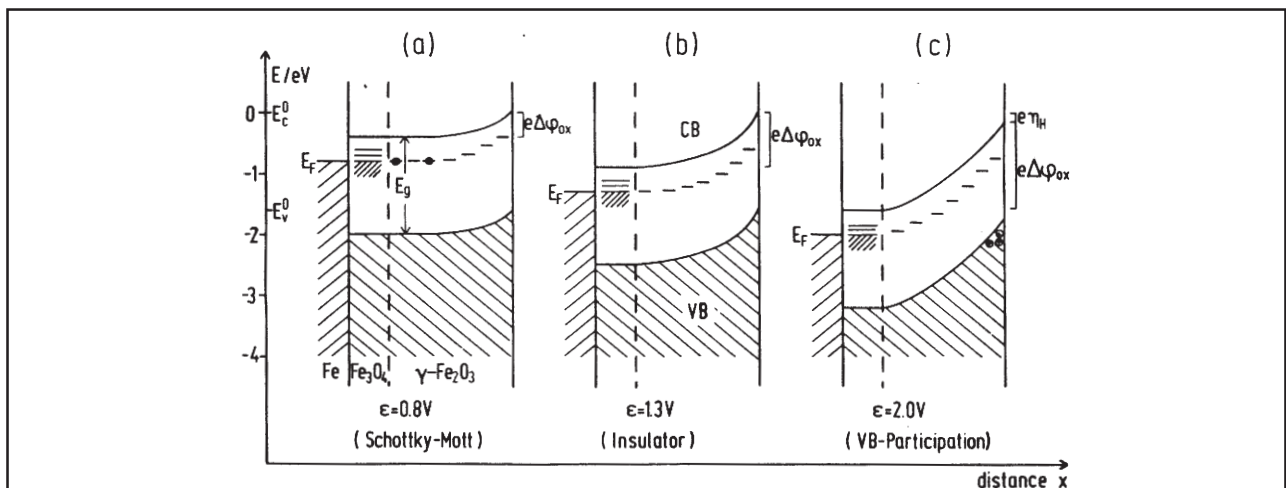
Fig. 8. *Band structure model for a bi-layer type anodic film on iron at different potentials [105].*

reactions occurring on passive iron by means of an energy band diagram constructed for a film composed of a thin (< 1…2 nm) Fe_3O_4 layer covered by a Fe_2O_3 layer of about 2…3 nm, and by making a strict distinction between electron transfer (etr) and ion transfer reactions (itr). Due to the high conductivity of the Fe_3O_4 layer, its role in the band scheme was not considered significant. Etr's were explained to take place via the conduction band at low potentials and via the valence band at very high potentials. At intermediate potentials the outer layer becomes an insulator.

The total potential drop $\Delta\phi_{total}$ (i.e. the applied potential E) was divided into the drop in the oxide $\Delta\phi_F$, the drop in the Helmholtz layer at the oxide surface $\Delta\phi_{F/S}$ and to all other potential drops $\Delta\phi_{other}$ which can be regarded as constant:

$$E = \Delta\phi_{total} = \Delta\phi_F + \Delta\phi_{F/S} + \Delta\phi_{other} \qquad (5\text{-}21)$$

Under steady state conditions in the passive state, $\Delta\phi_{F/S}$ depends only on pH but not on E. This means that any change in the applied potential causes a change of $\Delta\phi_F$ and of the steady state film thickness. The potential drop $\Delta\phi_F$ was explained to be equivalent to the band bending in the oxide.

Gerischer [5] has presented a similar band diagram to that proposed by Stimming and Schultze [105], but for a film with a continuous change in composition. This refers to a Fe_xO_4 layer with a continuous transition from x = 3 to x = 2.67. The latter value corresponds to Fe_2O_3 (Fig. 9).

This picture does not represent a chemical equilibrium situation, but electronic equilibrium (E_F = constant) is assumed. To account for the different conductivities of Fe_3O_4 and Fe_2O_3, the electronic states of the conduction band for Fe_3O_4 must have a position well above the Fermi level in Fe_2O_3. Gerischer was able to explain the onset potentials for activation in acid solutions as well as for water oxidation using this approach.

5.4.2 Chemi-conductor model for the passive film on iron

Cahan and Chen [67,68,69] introduced the chemi-conductor model for the passive oxide film on iron in order to describe the film more adequately than the early semiconductor models did. Instead of a semiconductor with relatively well-defined band-gaps and fixed dopants, the chemi-conductor was defined as a single phase insulator whose stoichiometry can be varied by oxidative and/or reductive valence state changes (Fig. 10). These non-stoichiometries were explained to be able to modify the local electronic (and/or ionic) conductivity of the film. This is equivalent to a variable doping with defects rather than with foreign species. The film on iron in borate buffer solution was assumed to consist of a trivalent iron compound like Fe-OOH with stoichiometry varying continuously

Fig. 9. *Course of the energy bands in the passive film on iron with a continuous change in film composition [5].*

Fig. 10. *A schematic presentation of the chemi-conductor model for the passive film on iron at high positive potentials [69].*

with thickness and electrode potential, because the authors had not found reliable evidence for the existence of a separate Fe_3O_4 layer in the film.

The transport of material through the film was stated to be responsible for the growth. Fe^{2+} species, protons, oxygen deficiencies and Fe^{4+} species were mentioned as possible defects, and it seems to be implicitly assumed that the transport of mainly iron ions contributes to film growth.

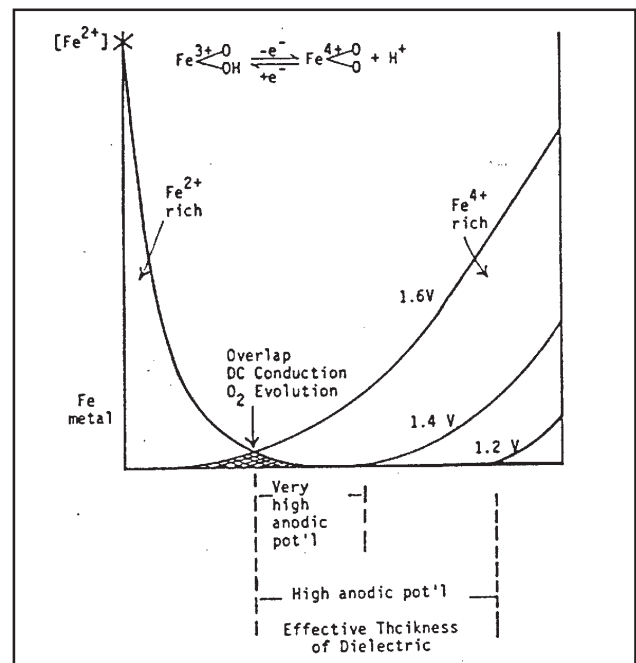The model assumes that the excess concentration of divalent iron species leading to higher conductivity at the inner interface is fixed as a result of the equilibrium of the reaction $FeOOH + H^+ + e \rightarrow Fe(OH)_2$. The potential dependence of the excess concentration was for some reason neglected. Charge neutrality was explained to be maintained by the balancing effect of protons coming from the film/electrolyte interface. A linear gradient of the chemical potential of divalent iron corresponding to an exponential concentration gradient was said to be established (Fig. 10). The profile of divalent species extends the closer to the film/electrolyte interface, the lower the applied potential is. At sufficiently low potentials the profile was described to reach the film/electrolyte interface leading to the dissolution of the film.

Cahan and Chen explained that protons are removed from the film at high potentials, and only a very thin layer of excess divalent iron next to the metal surface exists, while the outer part of the film approaches stoichiometric composition. Under these conditions the film behaves as an insulator. Cahan and Chen suggested that further removal of protons may finally induce tetravalent iron species into the film. The incorporation of tetravalent iron species is equivalent to the formation of vacancies of Fe(III), i.e. V_{Fe}^{3-} or to hydroxyl radicals [122]. As a result, an exponential concentration gradient of tetravalent iron species was described to extend towards the film bulk increasing the conductivity in that part of the film. The concentration of tetravalent iron at the outer surface is exponentially dependent on the potential drop across the outer interface and is thus not fixed at a constant value. At sufficiently high potentials, a significant concentration of tetravalent iron may reach the region enriched in divalent iron close to the inner interface. This was described to cause an overlap of more conductive regions enriched in divalent and tetravalent spe-

cies and to create a possibility for dc conduction through the whole film making oxygen evolution possible.

In the absence of redox couples, the film thickness will be limited by the resistance of the film. In the presence of a redox couple, which can alter the relative concentrations of the iron species (Fe^{2+}, Fe^{3+}, Fe^{4+}), defects are injected into the oxide film. This causes corresponding changes in the film conductivity.

The IMPS and EIS results of Peat and Peter [122] have lent some support to the chemiconductor model. They found out that the photocurrent response of passive iron is to a great extent determined by the life-time of holes captured in the non-stoichiometric layer close to the film/solution interface. This confirms the existence of high-valence intermediate species in this layer. According to Rahner [64], a considerable uncertainty exists as to the nature of the high-valence iron species assumed to be present at higher potentials. Some authors consider the possibility of the formation of peroxide and superoxide ions at the film/solution interface resulting in the formation of a monolayer of the film with a higher valence state.

5.4.3 Behaviour of the hydrated layer on iron at the film/solution interface

Keddam et al. [123] have made an attempt to establish a connection between the passive oxide film on iron, anions in the solution and some basic properties of iron oxides especially in their colloidal state in an acidic medium. The resulting model describes the passive film on iron as a film consisting of two layers: an inner γ-Fe_2O_3 region which is nearly independent on the solution composition and in which the electric potential drop is located, and an outer transition region composed of α–FeOOH. An important role was ascribed to this outer layer, which was suggested to accommodate the composition effects. Anions were stated to penetrate this layer, contributing to its properties. The response of the passive current density to changes in the electrolyte composition or hydrodynamic conditions (increase of the passive current on iron with increasing rotation rate of the iron electrode) was explained to be caused by the hydrodynamic and transport properties of the ou-

ter transition region.

This model assumes simultaneously main potential drop, high-field migration and good electronic conductivity of the inner layer. This is reasonable, if the electronic conductivity is high and the ionic conductivity low in the inner layer. On the other hand, the outer layer exhibits low electronic conductivity and high ionic conductivity. Especially the role of the outermost part of the oxide film on iron certainly deserves more attention.

5.4.4 Bipolar duplex membrane model for the films on stainless steels

Clayton and Lu [124] have also discussed the role of the outer hydrated oxide layer in film growth. They promoted the idea that the passive films formed on stainless steels appear to follow the behaviour expected of a bipolar duplex membrane. A bi-layer film consisting of a chromium-rich inner part and an outer part containing more iron was used as a starting point. It was suggested that the whole film is originally anion selective but that the presence of CrO_4^{2-} species (and also MoO_4^{2-} species) converts the outer hydrated oxides to cation selective phases. As a result of the existing electric field the deprotonation reaction $Cr(OH)_3 = CrOOH + O^{2-} + 2H^+$ is enhanced. Protons can be transported towards the solution through the cation selective layer, while the remaining O^{2-} ions pass through the anion selective layer towards the metal/film interface where they react with the metal substrate.

5.4.5 Early models for the growth kinetics of passive films

Early models for the growth of anodic oxide films, including also the pioneering concepts presented by C. Wagner, have been reviewed for instance by Kruger [63], Chao et al. [116], Fromhold Jr. [119,121], Vermilyea [125] and Battaglia and Newman [126], and the brief summary given below is mainly based on their reports.

Many early approaches were based on transport under high electric field, and the rate of transport was suggested to be exponentially dependent on the electric field. In the high-field conduction models it is usually assumed that:

- the structure of the film is independent of thickness and potential
- the space charge (see chapter 5.4.10) within the film is negligible
- the potential drops within the film, at the metal/film interface and at the film/ environment interface remain constant

Verwey assumed in his model that the growth of oxide films is limited by the rate of transport of cation species. The transport was described in terms of a high-field migration mechanism, in which the transport rate is exponentially dependent on the local electric field. The concept of a local field refers to the possibility of variation of the electric field strength with time and position. The transport was described as "hopping", which means random jumps of defects promoted by the thermal vibrational motion of the oxide at temperature T. Cabrera and Mott agreed with Verwey on the assumption that ionic transport is dominated by high-field cation migration. However, the rate limiting step for film growth was argued to be the reaction at the metal/film interface, i.e. the injection of metal cations into the film. Fehlner and Mott, on the other hand, suggested that transport of anions is responsible for film growth and that the rate limiting step is the reaction at the film/solution interface. It has also been suggested that the electric-field-dependent formation of interstitials in the oxide film controls the rate of processes occurring in the film.

The predictions of the early high-field models did not agree well with experimental results. Attempts to explain the differences between experiments and predictions of the model have led to considerations including the influence of space charge, dielectric relaxations (dielectric transient phenomena) or structural changes in the oxide. These aspects are discussed in chapters 5.4.9 and 5.4.10.

Another approach has been the so called place-exchange mechanism. In this model it is postulated that a layer of oxygen is adsorbed onto the surface which then exchanges places with underlying metal atoms. A new layer of oxygen is then adsorbed, followed by the simultaneous rotation of the two metal-oxygen pairs. The repetition of this process results in the growth of the oxide film [116,121,126]. From a physical point of view, it

seems unlikely that the place-exchange model can be used to describe the formation of films thicker than one or two monolayers.

5.4.6 Model of Vetter for general kinetics of passive films

Vetter [60] has discussed in detail the general kinetics of the formation of passive films with regard to the processes at the metal/film and film/solution interfaces and the potential gradient within the film. He assumed the film growth to be due to high-field (10^6–10^7 V/cm) migration of ions, and divided the total ionic current into two parts: the dissolution current i_d due to the reaction Me^{z+} (film) => Me^{z+} (aq), and the part i_L responsible for the growth or removal of the film. Stationary state was defined as a situation in which $i_L = 0$. This situation requires that the ionic current flowing through the film must be equal to the ionic charge transfer current at the film/solution interface. Vetter also commented that if cation migration dominates, film growth proceeds at the film/solution interface, while anion migration leads to film growth at the metal/film interface.

Vetter assumed that an electronic equilibrium exists, i.e. that E_F is constant (see also chapter 5.4.1), from the metal throughout the film. This means that the electrochemical potential of electrons is constant throughout the system. According to Vetter, this assumption can be made, if the electronic conductivity is sufficiently high, i.e. at least of the order of 10^{-10} $\Omega^{-1}cm^{-1}$. The electrochemical potential of electrons η_e, which can be identified as the Fermi level E_F of the electrons in the film, can be expressed as:

$$\eta_e = \mu_e - F\phi \qquad (5-22)$$

This assumption made it possible to determine the distribution of the electric potential and the composition $n(x)$ of a metal oxide MeO_n as a function of the distance x. The electric field strength was shown to be a function of the oxide composition $n(x)$ and the total ionic current density, which has the same value for all distances x. The results of the derivation showed that when a certain current is applied, the oxide composition $n(x)$ at any value x in the layer is uniquely determined, because the electric potential in the film is uniquely determined.

Vetter first discussed the case, in which the potential drop at the inner interface was fixed by a thermodynamic equilibrium between the metal and the film, while at the outer interface it was fixed by the reaction:

$$H_2O(aq) = O^{2-} (ox) + 2H^+(aq) \qquad (5-23)$$
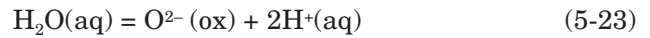
He presented potential profiles in which the overall trend was decreasing from the inner interface towards the outer interface, but in which a stepwise increase of potential from the metal to the film was depicted at the interface. This is illustrated in Fig. 11. The latter feature is not straightforward but rather confusing, and certainly deserves re-evaluation. A similar kind of stepwise potential increase at the metal/film interface was shown also for the cases in which potentiostatic or galvanostatic polarisation was applied.

Vetter already suggested that a finite time is required for the defects to achieve new steady state concentrations after potential or current perturbations. This feature is discussed also in chapter 5.4.7, and analytical expression to take the required relaxations into account are presented in chapter 5.4.12.
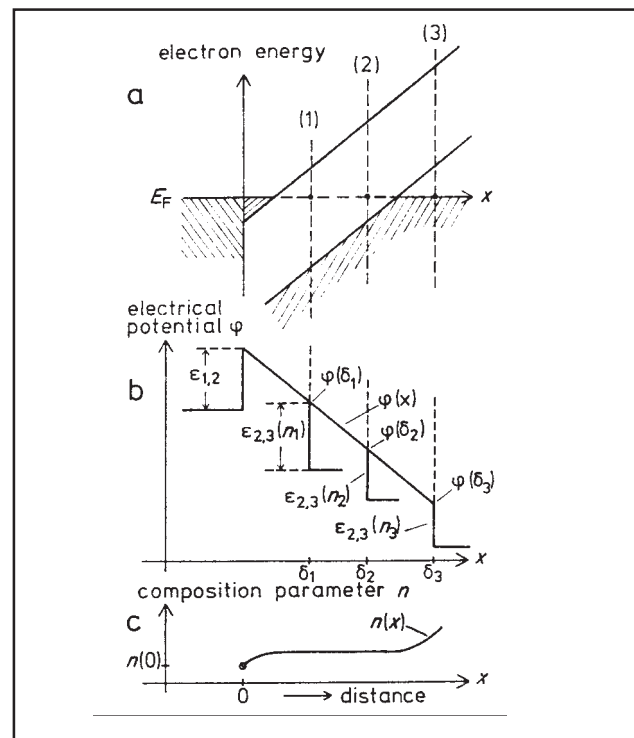
Fig. 11. Distribution of a) the electronic energy band edges, b) of the electric potential denoted with $\varphi(x)$ and c) of the composition parameter $n(x)$ as a function of the distance co-ordinate x for different layer thicknesses δ_1, δ_2 and δ_3. E_F = Fermi level. A schematic presentation, arbitrary signs of the potential jumps $\varepsilon_{1,2}$ and $\varepsilon_{2,3}$ [58].

5.4.7 Vetter-Kirchheim model for film growth on iron

Kirchheim and co-workers [127,128,129] have explained the processes occurring in the passive film on iron in acid and neutral solutions using a model which is to a great extent based on the concepts presented by Vetter [60] and the results reported by Vetter and Gorn [130]. The combined models of Kirchheim and Vetter and Gorn are called the Vetter-Kirchheim model in this report.

The model assumes the transport through the film to be assisted by a strong electric field, in accordance with several earlier models discussed e.g. in chapters 5.4.5 and 5.4.6. The nature of the moving species was not exactly defined, but instead the transport was suggested to occur either by a cation- or an anion-vacancy (or the corresponding interstitial) mechanism. For the sake of simplicity only the case in which iron ions are transported through the film by a vacancy mechanism was discussed. The growth kinetics of the film was described in terms of the corrosion reaction:

$$Fe^{3+}(\text{oxide}) \rightarrow Fe^{3+} (\text{electrolyte}) \qquad (5\text{-}24)$$

and the film formation reaction

$$H_2O\,(\text{aq}) \rightarrow O^{2-}(\text{oxide}) + 2H^+(\text{aq}) \qquad (5\text{-}25)$$

both taking place at the oxide/electrolyte interface.
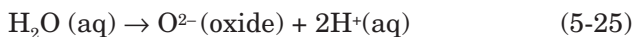
Similar assumptions were made also by Gabrielli et al. [131,132] in their work to clarify the passivation mechanism of iron using the electrochemical quartz crystal microbalance under ac regime. When iron ions originating from the metal/film interface reach the film/solution interface, they were described to be either dissolved or used for film formation leaving a vacancy in the film. If oxygen ions had a greater diffusivity, the processes taking place in the film could be described as oxygen ion migration towards the metal/oxide interface and film growth at that interface by oxidation of the metal substrate and creation of anion vacancies.

Advantages of the Vetter-Kirchheim model are that it couples the current densities through the film with those through the film/solution interface, and that it takes into account the possibility of relaxation effects, i.e. the possibility of transient phenomena in the film. By changing the current through the passive film the system was proposed to react in two ways: the electric field in the oxide is changed, or the concentration of the mobile defects is changed, and a relaxation time may be required to distribute changes in defect concentration within the film after perturbations. This means that during the formation of passive films or during instationary periods the fluxes of moving species are expected to have divergencies at the metal/film and film/solution interfaces and within the film. This gives rise to enrichment or depletion of some of the species. These are caused by the different mechanisms of transport, i.e. high-field transport within the film or charge transfer reactions at the film/electrolyte interface. Both Kirchheim [127] and Gabrielli et al. [131,132] discussed the instationary behaviour assuming that the concentration of mobile Fe^{3+} (or iron ion vacancies) is the one responding to current or potential perturbations with a finite rate and thus causing the relaxation effects.

5.4.8 Point Defect Model (PDM) for anodic barrier films

D.D. Macdonald et al. presented in 1981 the so-called Point Defect Model (PDM) [116] (reviewed in [120] and in [133]) to describe the growth and transport phenomena of barrier type oxide films. As mentioned already in chapter 3.2.2, a barrier film refers to a continuous film which can prevent current flow and thus support a high electric field. This model has been used to explain the breakdown of anodic films due to interaction between the composition of the solution and the oxide film, and later further developed to include also finite-rate interfacial kinetics [134]. At the moment the PDM model is very widely used. It has also been able to explain the effect of alloying elements on the resistance to film breakdown (the so-called solute-vacancy interaction model, SVIM, [135]).

The PDM model emphasises the role of mobile charged point defects in conducting the current through the film. Point defects are assumed to be present in the form of cation and anion vacancies due to the preponderance of the Schottky reaction. As a result of jumps from a vacancy to another, ionic species can be transported through the film.

The equations presented by Macdonald et al. for the total reactions occurring in the system and

for the reactions at the metal/film and film/solution interfaces have been given already in chapter 5.3. A scheme of the processes is shown in Fig. 12.

The main assumptions of the model are summarised below:

- Oxygen vacancies injected at the metal/film interface and annihilated at the film/solution interface contribute to film growth.
- Metal vacancies injected into the film at the film/solution interface and annihilated at the metal/film interface contribute to metal dissolution through the film.
- The transport of ions through the film can be described using a Nernst-Planck equation.
- The electric field within the oxide is its structural characteristic and is independent both on film thickness and applied potential.
- The applied potential is distributed as interfacial and bulk potential drops ($E = \Delta\phi_{M/F} + EL + \Delta\phi_{F/S}$), and the potential drop at the film/solution interface is proportional to the applied potential and the pH of the solution: $\Delta\phi_{F/S} = \alpha E + \beta pH + \Delta\phi_{F/S}^0$.

The model has been developed to a quantitative level. It successfully accounts for the observed linear dependence of the oxide film thickness on potential and the exponential dependence of the steady state current on potential found experimentally for many systems.

Unfortunately, several features of the model require further re-evaluation and limit its use.
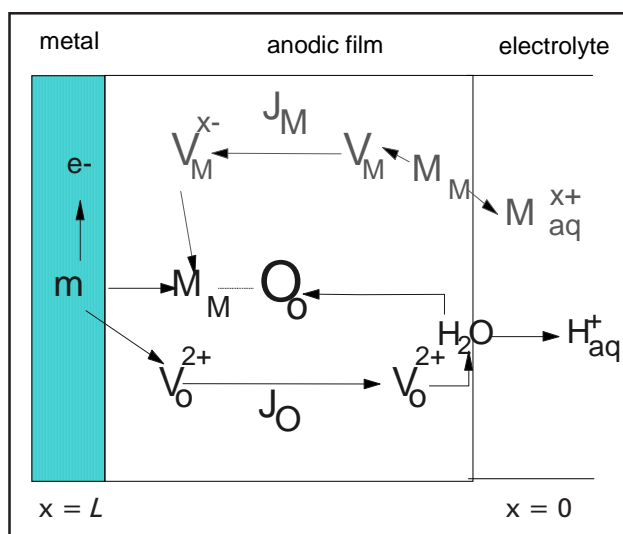
Fig. 12. *A scheme of the defects and processes taking place in an anodic barrier film according to the Point Defect Model [120].*

The major weaknesses or uncertainties are listed below:

- The Nernst-Planck equation for the transport of the oxygen and metal vacancies through the film is based on a linear dependence on electric field strength. However, in several anodic films the dependence of the flux on the field strength is exponential due to high-field assisted migration of defects.
- The concept of the independence of the electric field on applied potential and film thickness is not straightforward, although its influence on quantitative results is probably rather insignificant.
- The validity of the model in its refined form [136,137], representing the anodic layer as a combination of semiconductor and insulator layers, is still to be proved for thicker anodic films.
- The model states explicitly as an assumption that the film is electronically conductive, but seems to be valid mainly for electronically insulating and wide band-gap semiconducting films so far.
- The model does not include the influence of space charge layers (see chapter 5.4.10) in the film, i.e. the fact that there may be a part in the oxide layer in which a potential gradient does not exist and another part within which a potential gradient exists.
- The model postulates an instantaneous build up of the potential drops at the interfaces upon alteration or modulation of the applied potential—no relaxation of the charge carrier concentration is taken into account.

5.4.9 Influence of structural changes and dielectric relaxation in the film

As already indicated in chapter 5.4.5, several attempts have been required and made to improve the classical high-field conduction model to account for a range of experimentally observed phenomena. In this chapter we discuss two partly related approaches, which take into account possible changes in the film structure caused by the motion of defects.

Dignam [138,139] has introduced the dielectric relaxation model. In his derivation he used the local field concept, which was already used also by

Verwey (see chapter 5.4.5). This includes that the driving force for high-field transport is a local field E_{local} instead of a homogeneous overall field. The distribution of the electric field strength through an inhomogeneous growing film where all the free charges are confined to the interfaces can be given by the following form of the Poisson equation [138,139]:

div (K E) = 0 (5-26)

where   K = εε$_o$

The equation is written for zero space charge (see chapter 5.4.10), but it allows for variation of the dielectric constant with position.

If the film is amorphous, microscopic regions of low mean density will correspond to regions of low mean K and hence high mean E. For the case of ionic conduction, lattice or network dissociations are likely to be favoured at these microscopic regions. In the simplest form, the local field in these regions can be given by:

$$E_{local} = E\left[1 + \gamma_{local}\left(\frac{K}{K_{local}} - 1\right)\right]$$ (5-27)

Within the frames of this concept, all the high-field conduction equations relevant to anodic oxide film formation can be written as follows:

$$i = AL^g exp\left[-\frac{W(E_{local})}{kT}\right]$$ (5-28)

where

$$W(E_{local}) \approx W_e - \mu^{\neq}E_{local}\left[1 - d_2\left(\frac{\mu^{\neq}E_{local}}{W_e}\right)\right]$$

(5-29)

According to Dignam, there is considerable evidence that the field responsible for film growth is a local one varying proportionally to KE. Dignam represents the local field by

$$E_{local} = w(KE) = w(E + P)$$ (5-30)

Differentiating with respect to time yields:

$$\frac{1}{w}\frac{dE_{local}}{dt} = K_1\frac{dE}{dt} + \frac{dP}{dt}$$ (5-31)

The relaxation rate of the polarisation is represented by:

$$\frac{dP}{dt} = iS(\chi_s E - P)$$ (5-32)

Dignam explained that on passing through the amorphous oxide the ionic defects bring about structural changes in their wake. This is the origin for the relaxation rate of the form of equation (5-32). The constant S is thus the interaction cross-sectional area for a moving defect divided by its charge (capture cross section). Dignam postulated that a possible consequence of the amorphous film structure is the introduction of conduction transients as a result of a dependence of film structure on growth rate and time.

Dignam's model is in a way a particular case of the so-called structural change model presented by Young and Smith [140]. In the structural change model the transient behaviour of the growing oxide film is associated with time dependent structural changes leading to a time dependence in one or more of the kinetic parameters in equation (5-28). In the model of Young and Smith, structural changes are supposed to give rise to changes in the constant A ∝ N, where n is the concentration of the ionic current carriers. The rate of change of this concentration in the transient regime was given by:

$$\frac{dN}{dt} \propto iN[B'E - lnN]$$ (5-33)

Exactly the same kinetic expressions can be obtained by postulating that the structural changes give rise to changes in the zero field activation energy W_e:

$$\frac{dW_e}{dt} \propto i\left[(W_e^o - B''E) - W_e\right]$$ (5-34)

The model of Young and Smith does not assume change of field strength as a result of structural changes, while in the dielectric polarisation model of Dignam the structural changes give rise to polarisation changes and subsequent changes in E_{local}. Dignam suggests that the motion of mobile defects involves in a formal sense the breaking of certain bonds and formation of others with accompanying changes in the structure. By analogy to solid state chemical kinetics it can be assumed that during ion transport through amorphous films the bond rearrangement or reaction rate will be proportional to the number of defect hops per unit volume per unit time, i.e. proportional to the film growth current density. Dignam explains that the polarisation process associated with equation (5-32) corresponds to a fairly long-range structu-

ral rearrangement in an extremely viscous fluid.

To summarise, the models of Dignam [138,139] and Young and Smith [140] regard the film as a continuous fluid-like (gel-like) medium in which motion of defects leads to long-term persisting structural changes (structural relaxations). The defects in this liquid-like structure (vitreous solid) are assumed to be created by transport during growth, and they are likely to be subsequently annihilated after a certain period of time at steady state. However, the present state of understanding describes the structure of anodic passive films on iron- and nickel-based materials as thin nano-crystalline solid films and not as liquid-like. Although the lattice is disordered and current in it is transported via defect motion, the lattice certainly exists. This is evidently at odds with the concepts of the structural change models, and thus the physics underlying these models seems to be unrealistic for the passive films formed on these engineering materials. This is reflected in the fact that in recent years there has not been a single attempt to apply the models of Dignam and Young and Smith to anodic passive films on iron- and nickel-based alloys.

5.4.10 Influence of space charge on oxide film growth

A space charge region is a region resulting from the transfer of charged species in or out of an oxide film. The space charge can be in the form of immobile charged impurities or immobile trapped carriers, or it can be in the form of mobile ions in the bulk of the film [138].

The influence of ionic space charge on film growth kinetics has been discussed e.g. by Fromhold [119], König and Schultze [117], Lohrengel [142,143] and Kanazirski et al. [144].

The electric field in the anodic film is influenced by the extra charge in the space charge region. The local electric field is assumed to be a result of the superposition of the space charge field, governed by the amount of charge carriers according to the Poisson equation, and the overall dielectric field given by the potential difference between the metal/oxide and oxide/electrolyte interfaces. This can be presented as follows [117]:

$$\boldsymbol{E}(\mathrm{x})_{ox} = \boldsymbol{E}(\mathrm{x})_{sc} + \boldsymbol{E}_{diel} \qquad (5\text{-}35)$$

where

$$\frac{\delta \boldsymbol{E}(\mathrm{x})_{sc}}{\delta \mathrm{x}} = \frac{z e N}{\varepsilon \varepsilon_o} \qquad (5\text{-}36)$$

The rate determining step of the growth is assumed to be the field assisted transport, governed by the average field within the layer, i.e. by

$$\boldsymbol{E}_{ox}^{\sim} = \mathrm{L}^{-1} \int_0^{\mathrm{L}} \boldsymbol{E}_{ox}^x \mathrm{dx} \qquad (5\text{-}37)$$

If the carrier concentration (both mobile and immobile) in the space charge region is small, the effect of the space charge field is insignificant and the kinetics is not modified. A large carrier concentration, on the contrary, may create a local field which compensates the dielectric field near the inner or the outer interface of the film. As long as the film thickness is greater than the width of the space charge layer in which the field is compensated, the field assisted transport mechanism controlled by the dielectric part contributes. In the extreme case where the compensating effect of the space charge extends over the whole film thickness, a transition to diffusion controlled film growth may take place [117].

Lohrengel [142,143] has given an explanation to the formation of space charge and to its influence on the early stages of film growth. In his model, both cationic defects emitted at one interface and anionic defects emitted at the other interface were assumed to be responsible for film growth. Close to the interfaces these defects were explained to form an intermediate localised space charge that migrates towards the opposite interface. This space charge influences the local field in the film. Because both the injection and the migration occur with a finite rate, the total charge density of mobile defects was considered to vary greatly during the early stages of oxide film growth. The growth rate was explained to increase slowly until the charge carriers meet the opposite interface, and further oxide growth becomes possible. At this stage the overlapping positive and negative space charges start to compensate each other, and the local field strength in those regions becomes equal to the mean field strength. On the other hand, the local field strength is smaller close to the interfaces, because of the compensating effect of mobile defects, the final concentration of which was found to be

extremely high (ca. 1000 C cm^{-3} or 10^{22} cm^{-3}). Accordingly, the velocity of the defects depends on the position within the oxide: they migrate slowly close to the interface after being emitted, accelerate in the central part and then slow down again. This was explained to cause an accumulation at the opposite interface, and thus a good compensation of the excess charge. The ideas of Lohrengel furnish a bridge between space charge based and surface (or interface) charge assisted high-field migration models. The latter are discussed in chapter 5.4.12.

The ideas of König and Schultze [117] and Lohrengel [142,143] seem capable of explaining the non-steady state film growth on a range of metals (initial stages of potentiostatic oxidation). Both model approaches, however, do not take into account the possible influence of space charge on the kinetics in steady state conditions (e.g. galvanostatic oxidation). A space charge approach to this situation was proposed by Kanazirski et al. [144]. The main assumptions in this approach were as follows:

- Positive charge carriers (metal interstitials or oxygen vacancies) generated at the metal/film interface are responsible for film growth.
- Negative charge carriers (metal vacancies) generated at the film/electrolyte interface form a background space charge (q).
- The negative space charge enhances the transport of positive defects thus increasing the rate of film growth. Thus a continuous decrease of the mean electric field strength in the film under galvanostatic conditions (constant growth rate) is expected. The magnitude of the space charge increases with film thickness reaching a constant value after a definite period of time.
- A mean defect concentration c_0 is defined as the concentration of defects at the reaction plane where film growth proceeds via the reaction of defect annihilation. This quantity depends on the growth rate (current density).
- The interfacial potential drops are neglected vs. the potential drop within the film, and the film formation is assumed to proceed with a 100% efficiency.

The growth current density could be related to the field strength by the equation

$$i = A\exp\left[B\left(\frac{E}{L} + \frac{q}{\varepsilon\varepsilon_o}\right)\right] \tag{5-38}$$

The background space charge q was calculated following the general theory of Fromhold [119]:

$$q = \left(\frac{\varepsilon\varepsilon_o}{B}\right)\ln\left(1 + \frac{L}{x_{sc}}\right) \tag{5-39}$$

where x is the so-called space charge screening parameter

$$x_{sc} = \frac{\varepsilon\varepsilon_o RT}{c_o a(zF)^2} \tag{5-40}$$

The dependence of the potential on film thickness was evaluated on the basis of equations (5-38) and (5-39):

$$E = \left(\frac{L}{B}\right)\ln\left\{\frac{i}{\left[A\left(1 + \frac{L}{x_{sc}}\right)\right]}\right\} \tag{5-41}$$

Due to assuming 100% film growth efficiency, the film thickness can be evaluated using Faraday's law:

$$L = \left(\frac{V_m}{nF}\right)Q \tag{5-42}$$

Inserting (5-42) in (5-41), the dependence of potential on the quantity of charge under galvanostatic conditions can be obtained:

$$E = \left(\frac{V_m}{nFB}\right)Q \cdot \ln\left\{\frac{i}{\left[A\left(1 + \left(\frac{V_m}{nF}\right)\frac{Q}{x_{sc}}\right)\right]}\right\} \tag{5-43}$$

As a result of fitting experimental data for galvanostatic oxidation to equation (5-43) it was found that A increases and x decreases with increasing current density. The value of x was found to reach very small values at high current densities, i.e. in that case most of the background space charge was located in a region close to the film/solution interface. As in the case of the models of König and Schultze and Lohrengel (see above), a bridge between the space charge assisted model and the surface charge assisted high field migration model

(chapter 5.4.12) is furnished. During potentiostatic oxidation following the galvanostatic oxidation, it was assumed that the background space charge gradually dissipates and finally constant field growth occurs.

In spite of the progress afforded by the space charge-based approaches discussed above, they do not give a comprehensive explanation of the behaviour of anodic barrier films. At least the following critical comments concerning space-charge based models can be given:

- All the models usually neglect the role of the interfacial reactions and interfacial potential drops in the process of film growth. This is certainly an oversimplification and makes the validity of such an approach doubtful, especially regarding the growth of thin passive films.

- Most of the models implicitly assume that both positive and negative defects move through the growing film, but usually only the formation of a space charge of single sign is considered. This can certainly not be the case especially during the transient period of oxide film growth. Even if recognised by some authors, the possibility of taking into account two overlapping ionic space charges with a different migration velocity was almost not exploited in the literature.

- The effect of space charge formation on the structure of the oxide films was only mentioned but never explored in detail. This is a major weak point of the available space charge modified models, because the structures of anodic oxides have a paramount influence on their growth and dissolution and thus on the corrosion resistance of the underlying metals.

- None of the space charge modified models considers the possibility of coupling between the ionic and electronic conduction within the oxide and at the interfaces with the substrate and electrolyte. This precludes the possibility to use these models to evaluate the possible behaviour of the metal/anodic oxide system in solutions containing redox couples and thus demonstrates their limited feasibility to predict corrosion behaviour in complex aqueous environments.

5.4.11 Model of Battaglia and Newman

Battaglia and Newman [126] have given a short but rather covering review of models presented by the year 1992 to explain film growth rates. They criticised the reviewed theories because only one mechanism at a time was considered such that an analytical expression for film growth could be derived. Accordingly to literature cited in [126], none of the models is completely consistent with the experimentally observed temperature and potential dependencies. Battaglia and Newman believe that several phenomena may simultaneously play a significant role in oxide growth, and the predominant mechanism is a function of the system being examined and the stage to which growth has transpired. Starting with the framework of Macdonald's point-defect model, they presented a comprehensive general model that includes any number of species that may react homogeneously and heterogeneously, and includes both high-field and low-field transport. The model also includes the effects due to the variations in the adjacent solution phase and can be used to explain film growth and dissolution.

At its present stage the model has been used to explain why the passivation of iron does not take place not until 200 mV above the potential where the formation of an oxide is thermodynamically possible. An estimated value of $2 \cdot 10^{-16}$ cm^2/s for the diffusion coefficient of Fe^{3+} was also given.

5.4.12 Surface charge assisted (SCA) high field migration model

The surface charge assisted (SCA) high-field migration model for anodic film growth suggested first by de Wit, Wijenberg and Crevecoeur [145] has been recently modified and improved by Bojinov et al. [146,147,148]. The defect nature of the film and the reactions taking place in the film have been adopted from the Point Defect Model (see chapter 5.4.8), but the concept of accumulation of defects creating surface charges at the metal/film and film/electrolyte interfaces has been added in order to account for the response of metal/oxide film/solution systems to perturbations in the current or potential.

In the derivation given below, the equations refer to systems in which Schottky defects (cation and anion vacancies) are dominating and in which film growth occurs at the metal/film interface (see Fig. 13). The SCA high field migration model can also be applied to systems in which interstitials are the main charge carriers and/or film growth proceeds at the film/solution interface.

The model assumes that barrier film growth is governed by a high-field migration of point defects, i.e.:

$$i = A \exp\{B\boldsymbol{E}_L\}, \tag{5-44}$$

The high rate of injection of oxygen vacancies at the metal/film interface results in the formation of an n-type semiconductive interfacial region with a thickness $L_{M/F}$, and the corresponding injection of metal vacancies at the film/solution interface causes the formation of a corresponding p-type semiconductive interfacial region with a thickness $L_{F/S}$. Both thicknesses are assumed to be small in comparison to the overall film thickness L, which can in fact be already very low. This treatment implies that the anodic film has a highly-doped n-type/insulator/p-type structure (n-i-p structure); see also Fig. 14.

The total field strength in the system is given by:

$$\boldsymbol{E}_L = \frac{\left(\Delta\phi_{M|F} + \boldsymbol{E}L + \Delta\phi_{F|S}\right)}{L} = \frac{\mathrm{E}}{L} \tag{5-45}$$

The interfacial potential drops obey the Poisson equation:

$$\Delta\phi_{\mathrm{F|S}} = \left(\frac{2\mathrm{eN_{AC}}}{\varepsilon\varepsilon_o}\right)\mathrm{L}_{\mathrm{F|S}}^2 \tag{5-46 a}$$

$$\Delta\phi_{\mathrm{M|F}} = \left(\frac{2\mathrm{eN_D}}{\varepsilon\varepsilon_o}\right)\mathrm{L}_{\mathrm{M|F}}^2 - \boldsymbol{E}L \tag{5-46 b}$$

In analogy to the PDM, the steady state values of the interfacial drops are given by:

$$\Delta\phi_{\mathrm{M|F,s}} = (1-\alpha)\mathrm{E} - \boldsymbol{E}L \tag{5-47 a}$$

$$\Delta\phi_{\mathrm{F|S,s}} = \alpha\mathrm{E} \tag{5-47 b}$$

Following a perturbation, both donor and acceptor densities will change with time at a finite rate until a new steady state is established. Thus surface charges at both interfaces will influence the transport of the charge carriers whose transport results in film growth. If film growth proceeds via transport of positive carriers (oxygen vacancies), the potential drop caused by the finite rate of (i.e. delayed) accumulation of positively charged vacancies at the metal/film interface will retard this transport in the transient regime, i.e. equation (5-44) is to be rewritten in the form

$$i = A\exp\left\{\left(\frac{\mathrm{B}}{L}\right)\left[\alpha\mathrm{E} - \frac{\mathrm{zeN_D}}{\varepsilon\varepsilon_0\mathrm{L}_{\mathrm{M|F}}^2}\right]\right\} \tag{5-48 a}$$
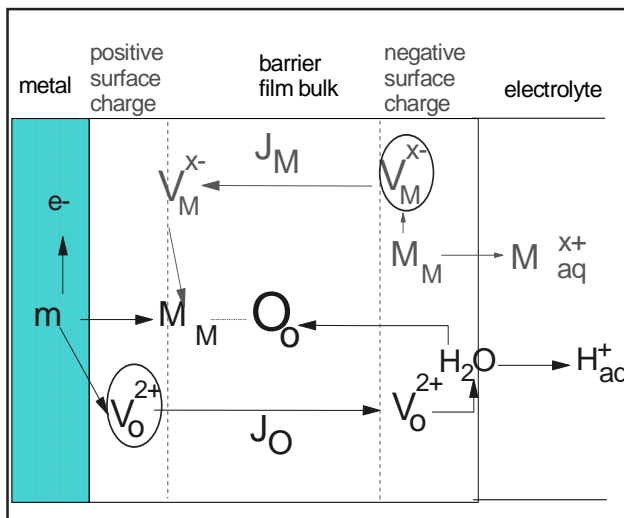

Fig. 13. *A scheme of the barrier film according to the surface charge assisted high field migration model [146].*
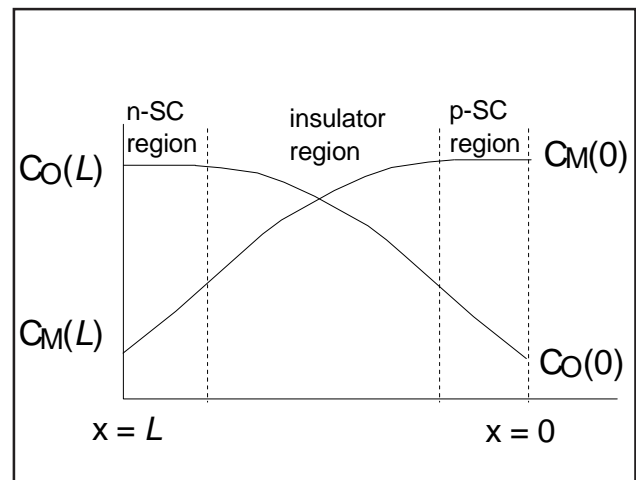

Fig. 14. *Concentration profiles of oxygen vacancies and metal vacancies in a barrier film according to the surface charge assisted high field migration approach [146].*

whereas an acceleration of the transport of oxygen vacancies in the transient regime is expected to be caused by the finite rate (i.e. delayed) accumulation of negative interface charge, resulting in:

$$i = A \exp \left\{ \left(\frac{B}{L} \right) \left[(1-\alpha)E + \frac{zeN_{AC}}{\varepsilon \varepsilon_0 L_{M|F}^2} \right] \right\} \qquad \text{(5-48 b)}$$

So far, the surface charge assisted high-field migration model is the only model for anodic oxide films capable of predicting and explaining also the EIS response of several metal/film/solution systems.

5.5 Correlations between growth laws and growth models

On the basis of many of the models discussed in chapter 5.4, expressions for the dependence of the oxide film thickness on time can be derived. The aim of this chapter is to explain, how the different experimental growth laws (see chapter 5.1) can result from the mechanistic models for oxide growth.

A linear growth law is observed, if the rate of a reaction at one of the interfaces is controlling the growth process, or if a protective film is converted to a non-protective one.

A logarithmic law requires that the rate determining step is determined by film thickness [117]. According to Chao et al. [116], the logarithmic law could be obtained by assuming any mechanism whose activation energy increases with film thickness. Examples of models leading to logarithmic growth are the place-exchange mechanism under potentiostatic conditions, the Fehlner and Mott's model based on anion transport controlled by anion emission from the environment and postulating an increasing order of the film, and the Point Defect Model for the transport of point defects developed by Macdonald et al. [116,117]. According to Bardwell et al. [61], the growth of an anodic film on iron can be modelled by means of direct logarithmic growth kinetics at times t > 30 s. This is in agreement with the observations and predictions of Moore and Jones [149].

An inverse logarithmic growth requires a field-assisted transport [117] or the emission of cations from metal into the film (Mott-Cabrera model)

[116]. According to Lister et al. [118], the inverse logarithmic law is a limiting case for thin films of the general sinh law for oxidation, derived by considering the migration of ions and vacancies in the lattice (see chapter 5.2).

Parabolic behaviour is observed when the growth of the film is controlled by diffusion of a species through the film [115]. According to Lister et al. [118], the parabolic law is a limiting case for thick films of the general sinh law for oxidation (see chapter 5.2). The early results of Bignold et al. [150] for film growth on iron in high-temperature sodium hydroxide solutions were found to be consistent with a parabolic growth mechanism.

Finally, cubic kinetics results from intermediate behaviour between parabolic and inverse logarithmic growth [118]. Lister et al. [118] stated that in general cubic kinetics is followed by metals on which the oxide supports inward movement of oxygen rather than outward movement of cations.

Mixed control is also possible, or transitions from growth obeying one law to growth obeying another kinetic law may occur during different stages of growth. For instance, a combination of field controlled and thickness controlled logarithmic behaviours was discussed by König and Schultze [117] for the case in which the regions with and without electric field were taken into account [117]. Assuming an exponential gradient of the chemical potential in the space charge region where the field is compensated, a generalised expression for the film growth current was derived. It represents the inverse logarithmic law if the film thickness is smaller than the space charge width, and the direct logarithmic law if the opposite is valid. This proposed generalised equation predicts a transition from the field assisted transport to a mechanism controlled by diffusion within the dielectric part when the film becomes thicker than the space charge region. Experimental evidence was given by the transition from the inverse logarithmic law at short periods of time to the direct law at long periods of time in an investigation of the anodic film growth on iron in borate buffer solution [117].

According to Lister [151], parabolic behaviour resulting from diffusion through pores in the oxide film may change to logarithmic behaviour because of mutual blocking of pores in the film.

5.6 Comments on modelling film growth on iron- and nickel-based materials

In spite of the great amount of experimental and theoretical work performed to understand the oxidation behaviour of iron- and nickel-based materials in ambient conditions, some fundamental questions have remained unanswered. At the moment it is still uncertain which species are responsible for film growth on iron- and nickel-based alloys. SIMS profiles measured for pre-grown passive films on iron immersed subsequently in an ^{18}O enriched solution have indicated that ^{18}O is at a maximum at the outer interface and then decreases throughout the entire thickness of the film [75]. This result suggests that the further growth of the oxide occurs by inward transport of oxygen through the film, which is kinetically equivalent to the motion of oxygen vacancies from the metal/film interface to the film/solution interface. Also the studies of Lister et al. (ref. 9 in [118]) using radioactive tracers have confirmed that the inner, protective oxide layer on stainless steel grows at the metal/oxide interface by inward movement of oxygen ions (in high temperature water).

However, several approaches used to explain the concentration profiles in oxide films on iron- and nickel-based materials are based on selective dissolution of cation species through the film. This is in turn related to the motion of metal vacancies from the film/solution interface to the metal/film interface. Because changes in the composition of the alloy immediately beneath the film have not been observed, the possibility of selective oxidation can normally be ruled out in low (ambient) temperature aqueous conditions. The higher mobility of iron cations has been explained to result in their depletion in the inner part of the film, and finally to the formation of Cr_2O_3 based films [9,17].

It has been shown and/or assumed that both cations and anions (or corresponding vacancies) can move in the oxides on iron and its alloys as well as on nickel-based alloys. A careful investigation of their mobilities seems to be missing, although it would be essential in order to improve the models presented for the growth of the films on these materials.

Another uncertainty is whether the transport phenomena leading to film growth occur totally in the solid state or if any transport in micropores filled with water is included. The approach based on transport in micropores has been used e.g. by Hashimoto et al. (refs. 8 and 9 in [152]) and it is commonly applied in modelling film growth in high-temperature aqueous environments (see chapter 7). However, a good discussion on surface diffusion on oxide surfaces within the pores does not seem to be available.

6 STRUCTURE AND PROPERTIES OF OXIDE FILMS ON METALS AT HIGH TEMPERATURES

6.1 General

Increase of temperature influences the thermodynamic stability of oxide phases, and it also affects the rates of chemical and electrochemical reactions as well as transport phenomena in oxide films on metals. In addition, the properties of aqueous solutions change markedly with increasing temperature. These factors cause pronounced changes in the structure and properties of oxide films.

The films formed at ambient temperatures (below about 100 °C) are typically only a few nm thick, and the initial composition is greatly influenced by previous surface treatment procedures and by the bulk composition of the alloy. Only relatively small enrichments of the different alloying constituents have been observed in the passive potential range. However, at temperatures 150...200 °C, noticeable changes in oxide films take place. Above 150 °C, rather thick oxide layers are formed, and a more or less pronounced enrichment or depletion of constituents can be found. The enrichment or depletion is mainly controlled by the electrode potential of the alloy and the pH of the environment. It has been observed that differences between the compositions of surface layers formed on different Fe-Cr-Ni materials tend to decrease as the temperature increases. This suggests that the composition is mainly controlled by various selective dissolution reactions of individual alloying constituents [95,153,154,155].

There are indications that the temperature region close to 200 °C is critical regarding the properties and protectiveness of surface oxide films. For instance, it has been observed that the pitting potential of stainless steel has a minimum at 200 °C [153] and that of Incoloy 800 in chloride solutions decreases with increasing temperature only at T < 200 °C. The pitting morphology has also been reported to depend on temperature [156]. Stellwag [95] has commented that the passive film formed on Incoloy 800 loses its protective nature at temperatures of 150…190 °C, and a film with a thickness of several hundred nanometers may result. These observations show that any extrapolation of the oxide film properties to higher temperatures is not acceptable without experimental proof.

Increase in porosity is one of the main changes in film properties with increasing temperature. Porosity is a potential factor leading to poorer protectiveness of the film, and it may also lead to exposure of products with different solubilities (e.g. due to gradually varying stoichiometry) to the solution. This in turn results in the establishment of concentration profiles in the pores, which has an influence on transport of species through the film. Compared to thin, dense oxide films, the prevailing situation may be drastically different.

Chapter 6 focuses on the properties of surface oxide films on iron- and nickel-based materials in high-temperature aqueous environments. To begin with, a short overview on the properties of water at high temperatures is given in chapter 6.2. The properties of oxide films on pure metals are discussed in chapter 6.3 and those of steels in chapter 6.4, while the properties of films on nickel-based alloys is the topic for chapter 6.5. The growth mechanisms of high-temperature films are discussed in chapter 7.

6.2 Properties of water at high temperatures

Increase of temperature has a strong influence on the physical and chemical properties of water. These in turn affect the electrochemical processes occurring on metal and metal oxide surfaces at high temperatures. An excellent overview of the

properties of water at ambient and at high temperatures can be found in [157]. A brief summary is given below:

The dissociation constant of pure water increases from about 10^{-14} at 25 °C up to about 10^{-11} at around 300 °C (see also [158]). This has important implications: the thermodynamic pH (defined as pH = $-\log a_{H_+}$) of neutral water is lower at 300 °C (about 5.5) than at 25 °C (pH = 7). This contributes to changes in the thermodynamic stability regions of various oxidation products. Also, the conductivity of pure water increases with temperature, exhibiting a maximum at around 240 °C. This, in turn, has important implications when determining the rates of transport in the water and of any electrochemical reactions in which an aqueous solution is involved.

When dilute aqueous solutions are considered, the temperature dependence of the solubility or dissociation of added substance has to be determined or evaluated separately for each specific case. Accordingly, prediction of the pH or the conductivity of an aqueous solution on the basis of the values determined at room temperature is not very straightforward. Generally, it can be commented that the thermodynamic pH of weakly acid solutions increases and that of weakly alkaline solutions decreases with increasing temperature.

The density of water decreases from 997 kg/m³ to about 710 kg/m³ and the viscosity of water from about $9 \cdot 10^{-4}$ to $9 \cdot 10^{-5}$ kg/ms with a temperature increase from 25 to 300 °C. The corresponding change in the dielectric constant is from 78 to 20. The latter has an influence on the capacitive behaviour of water and affects the electric properties of the whole metal/oxide film/solution system. This is essential to take into account e.g. when oxide films are studied by electrochemical a.c. techniques.

As the temperature is raised, the solubility of most inert gases decreases to a minimum at about 120 °C, and then again increases with increasing temperature. The solubility of gases has an influence on the oxidising or reducing character of the electrolyte, and therefore it greatly influences the composition of the oxide films. In contrast to gases, the solubility of most salts (NaCl, KCl, NaOH, KOH) increases over the whole temperature range from 25 to 300 °C. LiOH and Na_2SO_4

exhibit a solubility maximum at intermediate temperatures (100 and 225 °C respectively).

6.3 Films on pure metals

Although understanding the behaviour of oxides formed on pure metals is of paramount importance when modelling the behaviour of oxides formed on metal alloys, investigations on pure metals in high-temperature environments are relatively rare.

According to Bignold et al. [150], the oxidation of iron in high-temperature sodium hydroxide solutions leads to the growth of a porous duplex film consisting mainly of magnetite, with a thin hydroxide layer.

Studies during the early stages of film growth on iron in borate buffer solutions at 200 °C have shown that the oxide film is a good electronic conductor in the potential region of the stability of divalent iron, while the formation of trivalent iron leads to a considerable increase of the film resistance [159].

The anodic films formed on pure nickel in tetraborate buffer solutions during short polarisation times at 200 and 300 °C have been found to exhibit p-type semiconductor properties [160]. On the other hand, n-type behaviour has been measured for chromium in the same conditions at low potentials, while at higher potentials p-type behaviour was observed also for chromium [160].

6.4 Films on steels

Broomfield et al. [161] have summarised the possible oxide structures which can be formed on steels in high-temperature ($\cong$ 300 °C) aqueous environments as follows (see also Fig. 15):

a) A duplex oxide, which—when formed on stainless steels—characteristically has an outer layer of magnetite and an inner layer of iron-chromium spinel growing at a slowly decreasing rate. This oxide is observed in a wide pH range (room temperature pH: 4...12), i.e. in acid, neutral and alkaline conditions.

b) A non-protective powdery film, which can be formed on low-chromium steels in highly alkaline solutions (> 30% NaOH).

c) Laminated oxide consisting of many repeated layers of oxide, which is mainly found in acidic conditions.

d) The so-called Bloom oxide, which is a very thin oxide growing at a rapidly decreasing rate. This can be found in strongly alkaline conditions.

Also, the formation of a fast linear growth denting type oxide has been mentioned as an alternative. It is characteristically a thick oxide growing at a constant rate, and it can be found in acid conditions in the presence of chloride or bromide [161].

The main focus of this report is in duplex oxides (type a), and their structure on different types of steels is discussed below. The duplex oxide film has also been called the Potter-Mann film [11,163].

6.4.1 Structure of oxide films on carbon steels

The review and results of Robertson [9,11] support the duplex nature of the Fe_3O_4 film formed on carbon steel exposed to high-temperature (300 °C), de-oxygenated neutral and alkaline aqueous solutions. Although the duplex-film concept is certainly a simplification, it has proven to be useful in the modelling of the behaviour of the film. The inner layer consists of fine-grained oxide because

Fig. 15. *Scheme of possible morphologies of oxide films formed on iron and iron-chromium alloys in high temperature water [161].*

it grows in a confined space, while the outer layer consists of loosely packed, larger grains, because it grows without volume constraint. The boundary between the layers has been found to lie at the position of the original metal surface, which indicates that the inner layer grows at the metal/oxide interface and that the outer layer grows at the oxide/solution interface. The presence of γ-FeOOH overlayers on the Fe_3O_4 film has been observed also for passive films formed at high-temperature by Mössbauer spectroscopy [ref. 55 in 11].

The views presented by Robertson are in agreement with several earlier ideas and results presented e.g. by Potter and Mann [163] for unstressed carbon steel in static aqueous solutions containing 5…20% NaOH at 250…355 °C, and also with those presented by Castle and Mann [162], by Tomlinson [15] and Moore and Jones [149]. Moore and Jones have reported that in the early stages of iron oxide growth on carbon steel in pH 11 LiOH solution at 300 °C, the oxide is largely oriented and grows with a morphology dependent on the substrate grain orientation. After a certain film thickness is attained, however, the epitaxial oxide degenerates, leaving in its place a much thinner, fine-grained, randomly oriented inner layer partially covered by large solution-grown Fe_3O_4 crystals.

The structure of the film formed on carbon steel may be greatly influenced by the presence of oxidising or reducing compounds and by temperature and pressure. The effect of the environment is likely to be seen mainly in the outer part of the film, which became evident in the study of Allsop et al. [164]. They reported that magnetite was the predominant inner phase component under both reducing and oxidising conditions in lithiated coolant (pH about 10.5), while the major component of the outer oxide was of the hematite structure under oxidising conditions and of the magnetite structure under reducing conditions. De Bakker et al. [165] found out that low temperature and low pressure in simulated pressurised water reactor (PWR) coolant, which corresponds to reducing conditions, led to the formation of partially oxidised-and-substituted magnetite on carbon steel. This was stated to be associated with severe corrosion. At high temperature and high pressure, small-particle partially oxidised-and-substituted magnetite with less severe corrosion problems
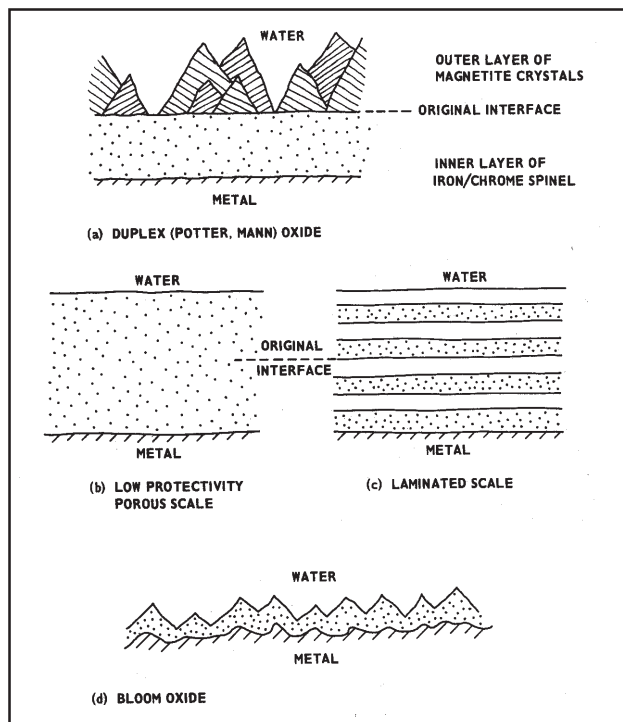
was detected. Oxide films formed under oxidising conditions on carbon steels were observed to be thinner than those formed under reducing conditions.

6.4.2 Structure of oxide films on stainless steels

The corrosion rate of stainless steel in high temperature aqueous solutions is at least ten times lower than that of carbon steels. Also, the corrosion films on Cr-containing steels are generally believed to be less porous that on carbon steels [9].

A general view of the oxide film formed on stainless steels at high temperatures in various kinds of environments is that the film consists of an inner Cr-rich layer and a more porous outer layer enriched in iron but depleted in chromium. This means that the duplex film concept can be used as a simplified model for the oxide films on stainless steels as well. This kind of films have been found also in flowing water conditions [9,166,95].

As discussed in chapter 3, stainless steels owe their superior corrosion resistance at ambient temperatures to the formation of Cr_2O_3 based layers in the inner part of the film. However, at higher temperatures, diffraction data and also IR data have indicated the predominance of spinel oxides on different stainless steels and on Incoloy 800 [9,167]. The formation of a uniform, probably even amorphous [168] layer of Cr-containing spinels in the inner part of the film has been commented to be responsible for the low corrosion rate of stainless steel. The formation of Cr-containing spinels instead of Cr_2O_3 based layers was thought to be supported by the fact that the corrosion rate of stainless steels is much larger than that possible for the film growth of Cr_2O_3 [9]. Although the fact that corrosion of stainless steel is related to the release of Fe species and the growth of a Cr_2O_3 layer is caused by other phenomena makes this way of reasoning seem a bit uncertain, the formation of spinels such as $FeCr_2O_4$, and $NiCr_2O_4$ is very likely and also generally accepted [118]. However, the composition of the inner layer may be influenced also by the surface treatment of the alloy, and in some cases also a composition close to Fe_3O_4 has been reported [15,169].

The outer oxide forms a porous layer consisting of non-uniform crystallite agglomerates. These crystallites can form as thick layers or as single crystallites at scattered sites depending whether mass transport in the system favours re-precipitation. As in the case of carbon steels (see chapter 6.4.1), the composition of this outer oxide is clearly influenced by the composition and properties of the aqueous environment: a different type of layer is formed under reducing conditions than under oxidising conditions. This can be seen e.g. on the basis of the scheme reported by Lin [170] for films formed in BWR nuclear power plants and shown in Fig. 16: normal water chemistry (NWC) in BWR conditions refers to an oxidising environment (see also [1]) and it leads to the formation of γ-Fe_2O_3, α-Fe_2O_3 and $NiFe_2O_4$ (or $Ni_xFe_{3-x}O_4$) in the outer layer on stainless steel, while hydrogen water chemistry (HWC) corresponds to reducing conditions (see also [1]) and results in the formation of Fe_3O_4 and $NiFe_2O_4$ (or $Ni_xFe_{3-x}O_4$). This scheme agrees with the composition suggested by several other authors for films formed on AISI 304 and/or AISI 316 stainless steels [171 and references therein, ref. 14 in 170,118]. According to Haginuma et al. [172] and the SIMS data of Bennett et al. [173], an oxygen content of 200 ppb (correspond-
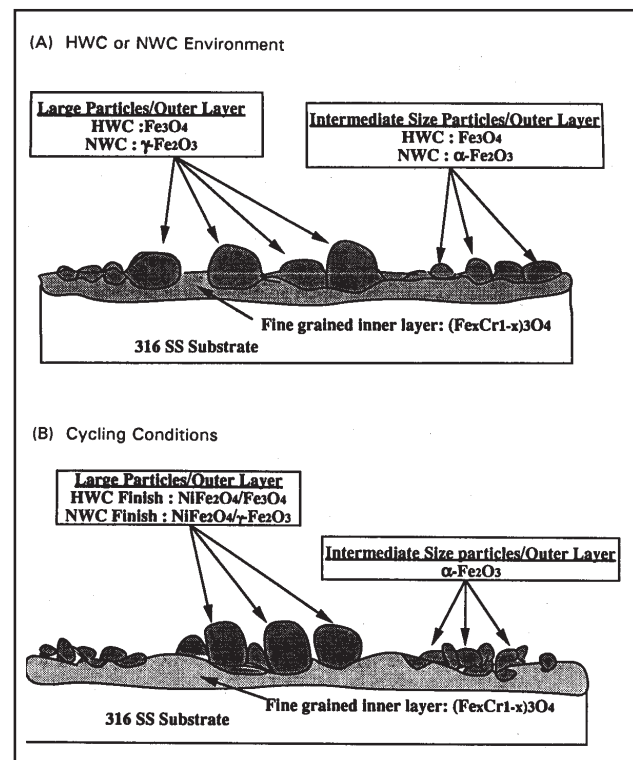

Fig. 16. *A schematic diagram of the oxide films formed on AISI 316 stainless steel in BWR water under different conditions [170].*

ing to normal water chemistry, NWC) results in a less pronounced duplex nature of the film, while in the presence of 1 ppm dissolved hydrogen a duplex film is clearly seen. Bogaerts and Bettendorf [153] have reported that the films on Fe-Cr-Ni alloys in pH range from neutral to 10.5 become depleted in chromium above a certain potential (i.e. above a certain high oxygen content), the value of which decreases with increasing pH and temperature. This behaviour is due to the transpassive dissolution of chromium. When this happens, passivity can only be maintained due to an elevated nickel content [153].

Concerning PWR conditions, in which the environment is reducing, a duplex film in PWR conditions has been stated to be formed on AISI 304 stainless steel, if released corrosion products are present in the coolant [174]. The steam generator corrosion films in the reducing PWR environment are primarily Fe-Ni chromites, with up to 30% Cr, and they are difficult to dissolve with any chemical decontamination reagents. This is a clear difference when compared e.g. to oxidising conditions e.g. in BWR coolant, in which the Cr content of the film can be much lower due to the oxidation of Cr(III) to soluble Cr species [153,175]. It has also been suggested that the oxide film on AISI 321 stainless steel in PWR coolant consists mainly of $FeCr_2O_4$, and that nickel possesses the oxidation state Ni^0 in the layer except for a few nanometers at the film/solution interface [176]. Allsop et al. [164] have reported that in lithiated coolant (pH about 10.5) the major component of the outer oxide was of the hematite structure under oxidising conditions and of the magnetite structure under reducing conditions on AISI 403 stainless steel, and that oxide films formed under oxidising conditions were thinner.

Besides the duplex-film model, a more detailed description of the film structure on stainless steels has also been given: Asakura et al. [59] studied the structure of films formed on AISI 304 stainless steel in boiling water reactor (BWR) coolant (κ = 0.08...0.3 μS/cm). Based on SEM and SIMS results, they divided the passive films formed on AISI 304 stainless steel into outer (characterised by a decrease of Cr content towards the outer surface of the oxide film) and inner (defined as a residual oxide in which no decrease of Cr content occurred) layers. The interface could be defined as

the maximum plane in Cr content. The outer layer was described to consist of two sublayers, a porous precipitation sublayer and a cracked inner sublayer which was hypothesised to be formed by the breakdown of the inner layer, occurring at oxygen concentrations > 100 ppb. This view agrees well with the description given by Castle and Masterson [177] for a typical oxide film formed on the surface of the primary circuit tubing in a PWR type plant. It also agrees well with the scheme presented by Hermansson [167] for films grown on stainless steel in BWR coolant under normal water chemistry (NWC) conditions. According to Hermansson, the inner part of the outer layer consists of $NiFe_2O_4$ (trevorite). The total thickness of this part was stated to vary from 0.02 μm to a few hundred μm. The composition of the deposited layer on top of trevorite was not discussed by Hermansson. Pores were likely to be present in the trevorite layer, but to a lesser extent in the inner chromite layer. The film structure described by Asakura et al. [59], Castle and Masterson [177] and Hermansson [167] should perhaps be called a triplex structure.

The formation of a hydrated iron oxide has been suggested also in the case of stainless steels (AISI 304 stainless steel at 300 and 350 °C; neutral and alkaline conditions, [178]), as in the case of carbon steels (see also ref. 55 in [11]).

The data on the electronic properties of films formed on stainless steels in high-temperature environments are rare. According to Carranza and Alvarez [156], the passive film formed on Incoloy 800 in chloride solutions is a p-type semiconductor. This conclusion was based on the measured difference in the magnitude of the anodic and cathodic charge transfer coefficients for a redox reaction occurring on the film.

6.5 Films on nickel-based alloys

Unlike for stainless steels, the oxide films on Inconel 600 cannot consist of solely spinels [9, ref. 87 in [9],179]. Due to their fixed valences, Ni and Cr can only form a spinel of fixed composition $NiCr_2O_4$, whereas the II and III valences of Fe allow it to form a continuous series of spinels. Accordingly, it has been predicted that an inner layer on Inconel 600 would consist of 48% $NiCr_2O_4$ and 52% NiO, while the outer layer would consist

of 27% $NiFe_2O_4$ and 73% NiO [9,ref. 87 in [9],179]. The higher Cr content of Inconel 690 results in a predicted inner layer of 90% $NiCr_2O_4$ and 10% NiO, and an outer layer of mainly NiO [9].

The predicted composition for the oxide film on Inconel 600 is supported by XPS investigations of films formed in a wide pH range (7–14) in solutions with different oxygen and hydrogen contents at 285 °C [179,180]. A thin (< 10...20 nm) chromium-based oxide layer was found to grow in a solid state process on Inconel 600 in hydrogen-saturated water and also in water containing higher concentrations of dissolved oxygen. In the latter case, however, this layer was rapidly overgrown by a deposited non-passivating layer of metal hydroxides whose composition and rate of growth varied with the oxygen concentration in the solution [179].

Depletion of nickel (i.e. enrichment of chromium) in the inner layer has been reported by Kang and Sejvar [45], Rosenberg [18] and in lithiated and deoxygenated conditions by Lister et al. [180]. Schuster et al. [176] have suggested the presence of $FeCr_2O_4$ in the oxide films formed in PWR plants (steam generator tubes), which agrees with the view on Cr depletion. Except for a few nanometers at the oxide/solution interface, the prevailing oxidation state of nickel was found to be Ni^0 [176].

The deposited outer layer on Inconel 600 in oxidising BWR environments has been observed to consist mainly of irregular loosely packed crystallites [181]. Iron enrichment towards the surface was found to be marked at the expense of nickel and chromium. Compared to stainless steels, the deposit on the Inconel was substantially thicker and less structured. The outer layer was reported to consist largely of Fe_2O_3 with Ni and Cr inclusions as a spinel structure. This is equivalent to the presence of $NiCr_2O_4$, which has been suggested e.g. by Kang and Sejvar [45] and Rosenberg [18], together with the presence of NiO.

The dependence of the film composition on the environment and also on irradiation is reflected in the observation that the films formed in oxidising in-core conditions on Inconel 600 in a nuclear power plant have been reported to consist of $Ni_xFe_{3-x}O_4$, and probably also NiO, while oxides formed in less oxidising out-of-core environment were at least partly in the form of $Ni_xCr_yM_zFe_{3-x-y-z}O_4$ (ferrite) and $Ni_xFe_yM_zCr_{3-x-y-z}O_4$ (chromite) in which M can be Co [45]. The more oxidising environment of the in-core conditions probably leads to strong transpassive dissolution of chromium from the film.

7 GROWTH OF OXIDE FILMS AT HIGH TEMPERATURES

This chapter summarises the state-of-art of the growth mechanisms and kinetics for oxide films on iron- and nickel-based materials in high-temperature aqueous environments. The corresponding summary for ambient-temperature films (chapters 5.4...5.6) and the review of the structure of high-temperature films (chapter 6) form a basis for the contents of this chapter.

7.1 Films on pure metals

The mechanism of film growth on pure iron in high temperature water has been studied by Bignold et al. [150]. Carbon steel was included in their investigations as well. Because of the similarity of the results between iron and carbon steel, the results for both are discussed in connection with the results on carbon steel in chapter 7.2.1.

Film growth data on pure chromium and nickel at high temperatures are currently being produced, and the first results and interpretations have been recently reported [160].

7.2 Films on steels

As discussed in chapter 6.4, the types of oxides formed on steels in high-temperature (about 300 °C) aqueous environment can be classified in four groups [161]. The duplex films are the prototypes of the protective films that form on structural steels in most high-temperature processes. This film is also called the Potter-Mann film (which in fact may consist of at least three different layers), and it grows according to a parabolic growth law. Chapter 7.2 is focused almost entirely on the growth mechanism of duplex films. Film growth on carbon steels and stainless steels is discussed separately in chapters 7.2.1 and 7.2.2.

Another oxide film type of some interest is the so-called Bloom oxide, which grows according to a logarithmic law [11]. This thin single oxide growing at a rapidly decreasing rate has been suggested to be formed on steels when no concentration gradients of hydrogen exist inside the film or when the dissolution during the early stages of oxidation is hampered [11,41,42,33,161,162,182]. The fact that stagnant conditions of water flow (i.e. experiments carried out in closed ampoules) seem to favour the formation of a Bloom-type film may in fact be caused by the fast saturation of the solution close to the film/solution interface. The possible direct or indirect effect of flow conditions is of great importance when carrying out characterisation of oxide films in simulated conditions and comparing e.g. results obtained in recirculation loops and static autoclaves.

The oxide types b) and c) mentioned in the beginning of chapter 6.4, as well as the fast linear growth denting type oxide, grow according to a linear law [11,161].

7.2.1 Films on carbon steels

The formation of a duplex oxide (Potter-Mann oxide) has been ascribed to the partial dissolution of the corroding surface [162], resulting in porosity during the early stages of oxidation. It has also been postulated that the transformation of a first grown epitaxial oxide to a duplex-film is induced by stress generated within the film as the film thickens [149].

Castle and Masterson presented in the 1960's one of the pioneering models, the solution-pores model, concerning the growth of a duplex oxide film on carbon steel [177]. In this model, formation of a duplex film of magnetite on carbon steel corroding in high-temperature neutral or mildly

alkaline deoxygenated solutions was used as a starting point. The magnetite was described as protective, and diffusion control was postulated to give an oxide film whose thickness varies parabolically with time, as already indicated above for duplex films.

The inner layer was described to consist of small, equiaxed grains, and it was said to grow in the space originally occupied by the metal at the metal/oxide interface. The oxide volume is roughly twice that of the metal it replaces (i.e. the Pilling-Bedworth ratio of Fe_3O_4 is 2.1). The outer layer grows at the oxide/solution interface, and its morphology was said to suggest that it has precipitated from the solution. The growth of the inner layer requires—as indicated in chapter 4—that oxygen in some form must cross the oxide film. Based on the slow transport rate of O^{2-} ions in magnetite, Castle and Masterson [177] suggested that water has continuous access to the metal/oxide interface through pores in the oxide. This was said to be consistent with earlier observations about the presence of pores in the magnetite film. It was also proposed that the outer layer grows by iron dissolving in water in the pores, diffusing along a pore and precipitating out at the outer oxide surface. The corrosion rate was postulated to be limited by the diffusion rate of dissolved iron in the pores.

The corrosion rates estimated on the basis of the Castle-Masterson model were in fair agreement with the experimentally observed rates [177]. The model was also able to account for the pH dependence of corrosion rates on the basis of its influence on the solubility of divalent iron ions. However, Robertson [9,11] and Tomlinson [15] have pointed out that the model was not able to explain:

- that a much larger volume of connected porosity is needed to account for the necessary Fe diffusion flux (only pores with a diameter less than 1 nm had been observed).
- that the corrosion rates in water and steam are approximately similar.
- that the activation energy observed for the corrosion is high (120 kJ/mol), while common activation energies for aqueous diffusion are about 15 kJ/mol.
- why iron in the solution does not precipitate on the pore walls but only outside the layer.

The recognition of these weak points led to the modification [15,9 and references therein] of the earlier ideas and, finally, to the development of the widely appreciated grain boundary- pores model (see Fig. 17 in chapter 7.2.2) for aqueous corrosion of carbon steels by Robertson [9]. This model is formally identical to that suggested for the gaseous oxidation of carbon steel.

The grain boundary-pores model for a duplex oxide film describes the situation when a coherent inner layer has already been developed. According to the model, the film grows by ingress of water along micropores (transport of O^{2-} ions in the solid state was considered to be too slow) to the metal/film interface and by the rate-limiting outward diffusion of iron ions along oxide grain boundaries. The ingress of water leads to the oxidation of approximately half of the metal in situ to form the inner layer at the metal/film interface. Part of the metal, which cannot be accommodated in the space vacated at the inner interface, was explained to contribute to film growth at the outer interface via deposition after arriving through the oxide. The formation of larger crystallites in the outer layer is a result of growth without volume constraint. The model assumes that micropores are created in the oxide as a result of growth stresses due to the mismatch of the oxide and metal volumes. The diameter of the pores is small, and they do not necessarily all extend across the sample. Accordingly, the open porosity is too small to provide adequate egress for relatively scarcely soluble iron ions. Therefore, faster transport of iron species along grain boundaries in the oxide under conditions of local equilibrium and charge neutrality was considered a more likely alternative. The external solution was stated to cause a concentration gradient of Fe^{2+} ions across the oxide [9]. If the diffusion of iron ions occurred in the solution, the establishment of this concentration gradient could be due to a thin ferrous hydroxide layer at the metal-oxide interface [162] or to variable stoichiometry in the inner oxide layer [41,42], or due to the influence of a pH or concentration gradient of hydrogen, as discussed by several authors [15,33,41,42,150,182,183]:

$$Fe_3O_4 + 3(2{-}b)\,H^+ + H_2 = 3Fe(OH)_b{}^{(2-b)} + (4{-}3b)\,H_2O$$

$$(7\text{-}1)$$
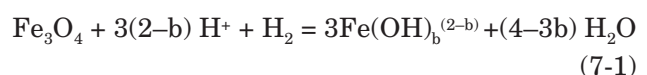
The establishment of this kind of gradient has even been stated to be the prerequisite for the growth of a porous film [41,42]. This seems to be slightly confusing, because in the model of Robertson it was on the other hand postulated that the transport of metal ions takes place along grain boundaries. This would require the establishment a concentration gradient in the solid state but not in the solution in the pores.

In addition to transport of water and iron ions, also transport of protons, electrons and H species through the film needs to be accounted for [11, 15,183]. According to Robertson [11] almost 90% of the hydrogen evolution may take place at the metal/film interface as a result of proton transport through the film, and a great part of this evolved hydrogen may be transported away through the metal [15,183]. The following reactions were suggested to dominate at the interfaces:

- inner interface:
  $(1 − 1/\nu)$ {Fe + 2H$^+$ = Fe^{2+} + H$_2$}
  (ν = the Pilling-Bedworth ratio)   (7-2)
- outer interface:
  $(1 − 1/\nu)$ {Fe^{2+} +4/3 H$_2$O
  = 1/3 Fe$_3$O$_4$ + 2H$^+$ + 1/3 H$_2$}   (7-3)
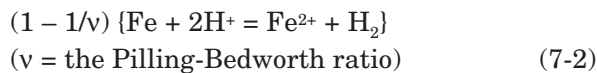
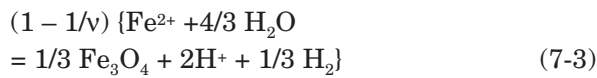The grain boundary-pores model explains the growth of oxide films on carbon steels in a very illustrative way. It is able to account for the observed temperature and pH dependencies of the corrosion, for the morphology of the inner and outer layers and the location of hydrogen evolution. However, the driving forces for the transport of species through the film have not been defined exactly. Also, there is still some uncertainty about which species are mobile and what the preferential short circuit paths are. Although the model seems to predict the behaviour of carbon steel well, the high value of the activation energy for corrosion seems to be the only direct experimental proof for the validity of the model in favour of models proposed earlier.

Park and Macdonald [184] have presented—according to our knowledge—the only EIS study on the formation of porous films on carbon steel in high-temperature aqueous environments. Their results were successfully accounted for by a one-dimensional finite transmission line electrical model. Park and Macdonald determined the polarisation resistance of corroding carbon steel in a variety of chloride containing solutions at 200…250 °C and found out that the resulting spectra were characteristic of a system that can be represented by a transport process in a porous film. They also found out that the reciprocal of the polarisation resistance, which is proportional to the instantaneous corrosion rate, at first (t < 300 h) increases with exposure time, but eventually (t ≅1000 h) tends to a constant value. At long exposure times the corrosion became also relatively insensitive to applied potential, which indicates that the increased thickness of the film results in loss of overpotential as IR drop. Accordingly, the early stages of corrosion were concluded to be autocatalytic, but at longer times a linear growth prevailed. The autocatalytic behaviour was attributed to the fact that the release of Fe^{2+} ions will lead to lower pH due to ion hydrolysis. In addition, electroneutrality demands transport of chloride ions from the bulk solution to compensate for the positive charge resulting from dissolution within the pores. The build-up of chloride ions occurs if the anodic reaction (iron dissolution) and the cathodic reaction (hydrogen evolution or oxygen reduction) are spatially separated, i.e. if the latter occurs on surfaces external to the pores. Enrichment of chlorides and lower pH together create an aggressive environment accelerating the corrosion rate. The work of Park and Macdonald demonstrates that EIS is well suited to study growth and behaviour of porous oxide films on metals in high-temperature aqueous environments [184].

7.2.2 Films on stainless steels

An early survey written by Berry and Diegle in 1979 [33] summarises older views on the oxide film growth on stainless steels in high temperature aqueous environments. According to it, the corrosion of stainless steel had been suggested to occur by two diffusion processes. The first one was anion (oxygen ion) diffusion through a thin adherent oxide film to react at the metal/oxide interface, while the second one was soluble metal ion diffusion via pores in the thin film to precipitate as oxide crystals at the oxide/water interface. The mechanism had been postulated to be influenced by the composition of the aqueous environment, i.e. on whether the environment was oxidising or

reducing. Under low oxygen or high hydrogen conditions (e.g. PWR coolant), diffusion of metal ion species via pores in the inner layer to form the outer layer was said to be rate controlling, while under oxidising conditions (e.g. BWR coolant) oxygen ion diffusion through the Fe_2O_3 film was stated to control the rate of oxidation.

The ideas reviewed by Berry and Diegle [33] partly suffered from uncertainties or unlikely assumptions. Similar problems had earlier led to the development of the grain boundary-pores model for carbon steels. Consequently, the grain boundary-pores model was extended to describe the non-localised corrosion of stainless steels and related alloys as well [9] (Fig. 17). Because the corrosion films on Cr steels are generally believed to be less porous that on carbon steels, the solid state diffusion concept was considered likely to be valid also for stainless steels.

Robertson explained that contrary to migration control in low-temperature conditions, film growth becomes diffusion-controlled at temperatures above 100...150 °C. In accordance with the model proposed for carbon steels, the corrosion rate of stainless steels was postulated to be controlled by the solid state transport of metal ions along grain boundaries in the oxide film. The inner layer of the duplex film was stated to grow by the ingress of water through the micropores, and the outer layer via deposition of metal ions transported through the film. The iron ion flux through the film was suggested to be carried as vacancies under alkaline conditions and as interstitials under acid conditions. The experimentally observed increase of corrosion at low and high pH values could be explained in terms of the pH dependence of the point defect concentration in the film. The growth of the outer layer via deposition results in a porous structure, in analogy with the structure of the films formed on carbon steels. For the deposition to occur, the solubility product of a relevant compound in the solution adjacent to the oxide surface must be exceeded. This may be a result of a high concentration of dissolved species in the bulk solution and—even more likely—a flux of cation species through the oxide film to the solution [9,11].

According to the model, the overall corrosion rate is controlled totally by transport in the inner layer [9] in agreement e.g. with the conclusions of Mann and Teare [186]. This means that the total rate of corrosion is not influenced by fluid flow conditions, by the presence or absence of the outer layer, nor by the saturation degree of the solution [8,9]. On the other hand, the release of the dissolved corrosion products to the solution is influenced by the composition of the precipitated outer oxide layer, flow velocity, pH, temperature, water saturation and presence of reducing or oxidising agents [9,32,33,168,186]. Low pH and high H_2 content generally favour high solubilities [33]. Accordingly, the release of soluble corrosion products is a function of the individual process parameters [188]. In practice, release has also been found to be highly time dependent [9].

With increasing temperature (at about 150...200 °C) the film growth rate on stainless steels in an aqueous environment exceeds the dissolution
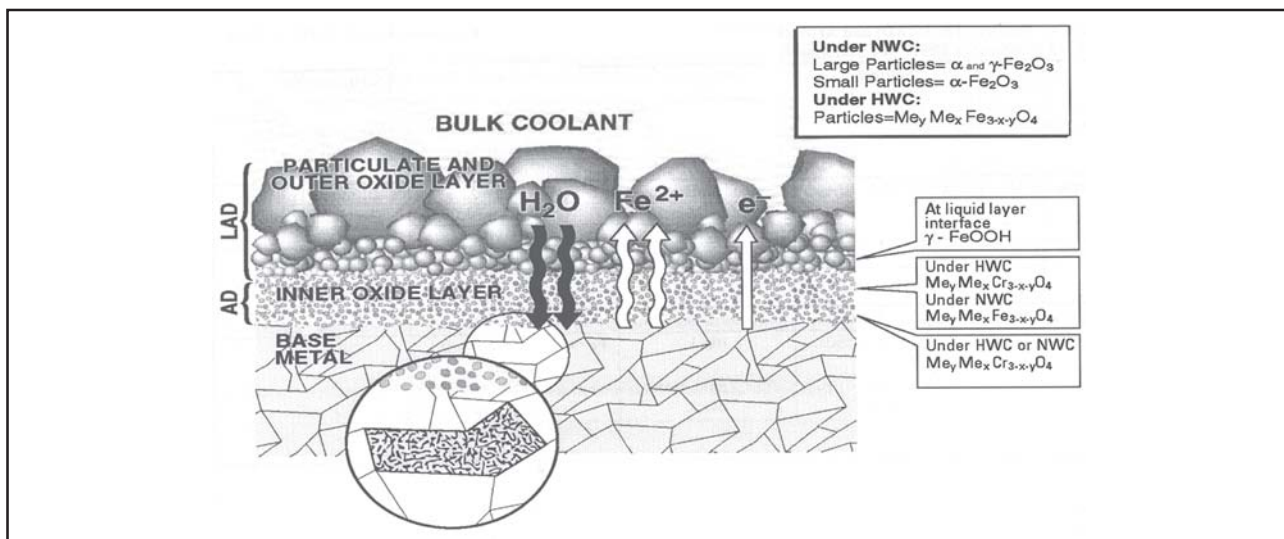

Fig. 17. Grain boundary-pores model for the high-temperature aqueous oxidation of stainless steels [9,185].

rate of iron ions, i.e. iron is not transported fast enough to be totally absent from the inner oxide layers. Neither is the rate for the lateral spreading of the less noble constituent chromium sufficient to form a continuous chromium oxide layer on the metal surface. Accordingly, oxidation of stainless steels proceeds in a non-selective way, while the depth distribution of different elements in the film is determined by their rates of selective dissolution through the film [9]. The transport rates of several metal ions in the oxides have been measured and found to follow a well defined order [9,189], which is probably due to increasing octahedral site preference energies (CFSE) along the series [ref. 66 in 9]:

$$Mn^{2+} > Fe^{2+} > Co^{2+} > Ni^{2+} >> Cr^{3+}$$
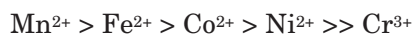
Consequently, the outer layer is expected to contain the Fe as magnetite and the inner layer to contain the balance of the Fe plus the Cr and the Ni as a Fe-Cr-Ni spinel. This is supported by experiments. If the potential is not high enough, Ni and Co may remain unoxidised and form metallic particles in the inner layer when the oxidation front passes. Cr in the inner layer tends to slow the diffusion rates of the surrounding ions, so that the spinel grows more slowly than the magnetite. This is a good explanation for the fact that the rate control resides always in the inner oxide layer.

The possible presence and role of a hydrated outermost layer has been discussed for instance by Francis and Whitlow [178] in the case of AISI 304 stainless steel at pH 7 and 12. This concept is included in the model of Robertson as well [9].

The model of Robertson is of great value in explaining film growth on stainless steels, as was the case also for carbon steels. However, it still needs more experimental support, concerning especially the preferential paths and driving forces for ion transport as well as the nature of mobile species/defects. Even the specific question about the egress of cations from the metal/film interface probably needs further confirmation: if micropores extend to the metal, as Robertson seems to assume, it is not justified to exclude the transport of metal ions also via the solution route. This statement is supported by the remarkably higher diffusion coefficient for pore diffusion (D = 4·10⁻⁴

cm²s⁻¹ [167]) than that reported for longitudinal grain-boundary diffusion (D = 2·10⁻¹³ cm²s⁻¹ [167]).

An even more comprehensive view can be obtained, if the concept of a three-layer film is applied. This concept was used by Asakura et al. [59] and H-P. Hermansson et al. [167], and it is discussed in chapter 6.4. The inner layer is again controlling the oxidation rate, while the inner part of the outer layer grows as a result of the breakdown of the inner layer.

7.3 Films on nickel-based alloys

The formation of an oxide film on nickel-based alloys has also been explained by means of a solid state oxidation mechanism [179]. Robertson [9] has applied the grain boundary-pores model to nickel-base alloys and proposed that these alloys oxidise non-selectively to form duplex layer oxides, the inner layer growing by ingress of water along oxide micropores and the outer layer growing by the outward diffusion of metal ions along oxide grain boundaries. This is in agreement with the ideas presented for stainless steels. The location of each alloy constituent in either the inner or the outer oxide is determined by the usual ranking of diffusion coefficients in cubic oxides, $Mn^{2+} > Fe^{2+} > Co^{2+} > Ni^{2+} >> Cr^{3+}$, with the faster diffusing elements entering the outer layer.

The presence of a substantial proportion of NiO in each layer (see chapter 6.5) allows the oxidation rate to be determined by the faster growth rate of NiO, rather than the slower rate of the Ni-Cr spinel. The model predicts that Cr will not lower the non-selective oxidation rate of Ni-Cr alloys until the Cr content exceeds 33%, because at lower Cr contents there will always be some NiO phase present to short-circuit the Cr spinel [9]. The corrosion rate of Inconel 690 is considerably lower than that of Inconel 600 because of the lower fraction of NiO in the film [9].

The formation and growth of an outer non-passivating precipitated layer on Ni-based alloys in alkaline solutions (pH 7...14) has been observed to depend on the hydrogen and oxygen contents of the water [179]. As in the case of stainless steels, this outer layer together with the water chemistry parameters and flow conditions influences the release of corrosion products to the solution [187].

8 BREAKDOWN OF OXIDE FILMS AND LOCALISED CORROSION

The breakdown of oxide films can be defined as a mechanical rupture leading to the exposure of the underlying surface to the environment. The breakdown can usually be explained to be induced by chemical reactions or changes, and these changes may be influenced e.g. by an electric field or by fluid flow conditions. The rupture may occur in the upper layer(s) of the oxide film, which results in the formation of a more porous film. This is the case in the model proposed e.g. by Asakura et al. [59]: breakdown of the dense oxide film on stainless steel induced by mechanical stresses due to volume changes leads to the formation of a cracked layer between the dense layer and the outer deposited layer.

Another possibility is that the rupture leads to the detachment of the film from the metal and thus to the exposure of metallic surface to the solution. A repeated breakdown–self-repair process may follow. This situation is likely to lead to localised corrosion such as pitting and, together with other mechanical stresses, also to stress corrosion cracking (SCC).

The initiation of localised corrosion sites requires breakdown of the passive oxide film and has generally been attributed to chemical and structural heterogeneity of the metal surface, i.e. existence of sulphide, oxide or silicate inclusions, segregated grain boundaries or segregated dislocation sites. Thus the mechanism of localised corrosion site formation has often been related to the galvanic effect of inclusions. However, localised corrosion sites have been observed to initiate on the surface of high-purity metals as well, if a sufficient amount of aggressive anions are present and the environment is oxidising enough. Accordingly, it seems likely that flaws may inherently exist in passive films and act as initiation sites [190]. Pitting has also been associated with a particular stage in the development of the passive film, corresponding to a specific film thickness, which depends on the composition of the solution but not on the potential [75].

Chapters 8.1 and 8.2 focus on the breakdown phenomena of passive films with comments on their significance to pit initiation. The role of oxide films in stress corrosion cracking is discussed in chapter 9.

8.1 Oxide film breakdown

As mentioned above, pit initiation is closely connected to the properties and breakdown of passive films. The pitting corrosion has been modelled using several different assumptions and mechanisms [190,191 and references therein]. A comprehensive review of pitting corrosion is beyond the scope of this report. However, the phenomena connected with changes in the oxide films and influencing pitting behaviour are discussed below. The discussion is mainly based on the recent work by Pickering and co-workers [190,191], who included the important role of IR drop in their model, and on the report of Sato [113]. Also the important conclusions based on the point defect model (PDM) of Macdonald (see chapter 5.4.8) are included.

Pickering and co-workers explained the local mechanical breakdown of passive films on the basis of microscopic roughness of even the smoothest metal surface. Because the electric field strength is not uniformly distributed over a thin oxide film, but it may be several times larger at the concave than at the flat regions, a larger electrostatic pressure (a concept introduced by Sato, ref. 18 in [190]) is applied at the concave sites. The breakdown of the film was explained to occur at the potential at which the electrostatic pressure at the concave site exceeds the compressive strength of the film. Sato [113] suggested that

above this critical potential pore nuclei with a radius larger than a critical value are formed, i.e. the film loses its electrocapillary stability. In addition to increasing the electrostatic pressure, the higher electric field increases also the rate of transport of defects through the concave regions of the film [190].

The role of the aggressive anions in oxide film breakdown was interpreted to be based on the fact that their adsorption at the film/solution interface reduces the surface energy (surface tension) at that interface, leading again to higher electrostatic pressure. Thus at high concentrations of the aggressive ion the electrostatic pressure will more

easily reach the value required for local breakdown. It was also suggested that the adsorbed aggressive anions lower the threshold value of electrostatic pressure needed for the occurrence of the breakdown, probably because of local thinning of the film. Thus aggressive anions were assumed to be required for the localised corrosion site initiation, although not for its growth [113,190].

Macdonald [120] has presented a mechanistic description of the influence of aggressive anions on the breakdown of oxide films (Figs 18 and 19). By means of applying the PDM model for passive films, it was explained that aggressive anions from the solution can occupy oxygen vacancies in
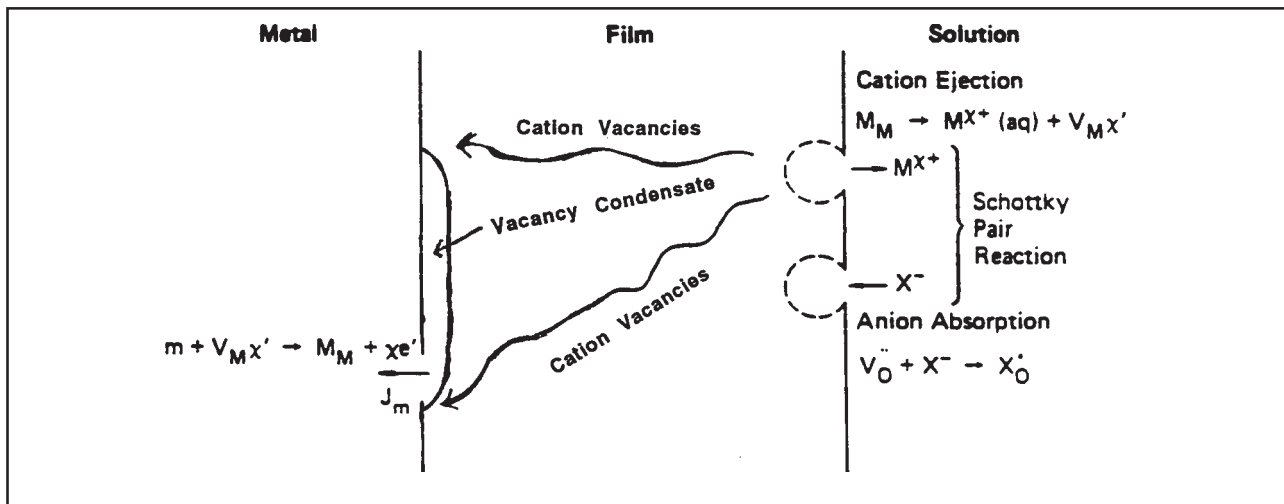

Fig. 18. Breakdown of a passive film according to the Point Defect Model (PDM) [120].
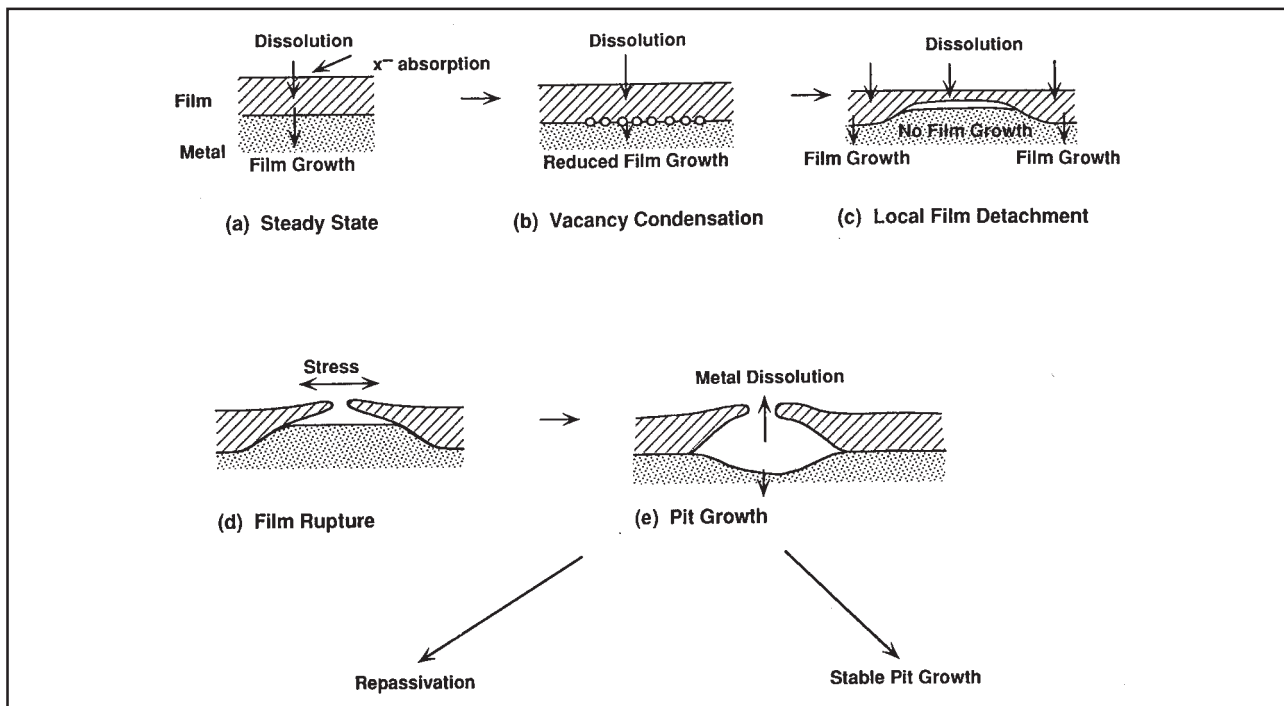

Fig. 19. Various stages of pit nucleation according to the Point Defect Model (PDM) [120].

the film at the film/solution interface. This leads to a change in the equilibrium of the Schottky reaction (see chapter 2.2) and increased production of cation vacancies. The cation vacancies are transported towards the metal/film interface, where an annihilation normally takes place. However, if the annihilation reaction is incapable of compensating for the increased amount of cation vacancies arriving at that interface, the excess vacancies will condense and lead to local detachment of the film from the underlying metal. Provided that the local tensile stresses are sufficiently high and/or the film dissolves locally, the barrier layer will rupture marking the initiation of a localised corrosion site. If, on the other hand, the mobility of cation vacancies in the film is low, the generation of excess vacancies is not compensated for by their transport towards the inner film. In this case a destruction of the barrier film at the film/solution interface is likely to occur, and it will soon be balanced by additional film growth over the localised area. This leads to porous film formation instead of oxide breakdown, as already indicated in chapter 2.5. The explanations based on the PDM model do not require that chloride ions are transported to the metal/film interface. Thus it agrees with the experimental observations which show that oxide films formed on Fe [75], on Fe-Cr-Ni and Ni-based alloys [153,154] at ambient temperatures contain little or no chloride. However, contradictory result have also been obtained for Ni and Fe-Cr alloys, but this may partly be due to different surface treatment [75]. At high temperatures, increasing amount of chlorides can be detected in the films [153,154].

A surface complexation effect has also been suggested as an explanation to the detrimental role of chloride ions on the stability of iron oxides [58].

Immediately after the exposure of the metal surface to the solution as a result of local breakdown of the oxide, a macrocell (i.e. well separated anode and cathode) forms. In the natural environment, the passive film surrounding the breakdown site acts as a cathode where the oxygen reduction occurs. Due to high potential differences, the breakdown site can be assumed to repassivate. However, because of the rugged nature of the new film, it is vulnerable to breakdown again under high electrostatic pressure. A succession of

breakdown/repassivation events follows, leading to deepening of the micropit. Further growth of the pit and its stabilisation can be explained to be controlled by the IR drops and their influence on local potential differences. These may even result in cathodic reactions such as hydrogen evolution in the pit [190].

Experimental results on the effect of temperature on pitting corrosion have shown that the pitting potential of AISI 304 stainless steel in buffered alkaline solutions has a minimum at 200 °C [153]. Also, the pitting potential of Incoloy 800 in chloride solutions has been found to decrease with increasing temperature up to 200 °C, but at higher temperatures it remains almost constant. The pitting morphology has been found to depend on temperature. This was not the case for the defect structure of the surface oxide, since the passive film formed on Incoloy 800 in chloride solutions was found to be a p-type semiconductor in the whole temperature range from 65...310 °C. Instead, the change in the pitting behaviour was said to be most probably connected with changes in the porosity of the film [156].

8.2 Role of Cr and Mo in suppressing localised corrosion

Chromium and molybdenum have been found to improve the stability of oxide films on iron- and nickel-based materials against breakdown and thus also against localised corrosion. The influence of chromium on the structure of the oxide films on stainless steels has been discussed above in chapters 3.2, 4.2, 6.4 and 7.2. Breakdown of films on stainless steels has been mainly attributed to the oxidation and dissolution of Cr(III) from the film [153,154] while molybdenum has been found to suppress the dissolution of chromium from the films in high temperature water [154]. Thus it seems very likely that the influences of chromium and molybdenum are to some extent interrelated. Some possible explanations for the effect of molybdenum are briefly summarised in this chapter.

According to Olefjord et al. [152], the stability of oxide films on Mo-containing steels in acid chloride solutions has been attributed in the literature to the formation of Mo(VI) oxide at the surface. The influence of molybdenum has been

explained using a non-homogenous film approach discussed for instance by Hashimoto et al. (refs. 8 and 9 in [152]). According to it, the film contains a high density of microcracks (or nanometer conducting channels) through which the current can leak. The microcracks are considered to be filled with water. In the case of Mo-alloyed steels, Mo(VI) ions have been suggested to form in the cracks and decrease the size of active sites. However, this explanation based on the existence of microcracks does not seem likely. A similar concept was disproved for instance by Robertson [9,11] in his model for high-temperature aqueous corrosion because of the insufficient rate of transport along such cracks.

These earlier ideas were in slight contradiction to the own results of Olefjord et al [152], who found that the concentration and the valence state of Mo in the film are potential dependent. At low potentials in the passive range, Mo(IV) was found to be predominant, while at higher potentials molybdenum was observed to exist mainly as Mo(VI). Olefjord et al. suggested that the role of Mo in the passive film was to stabilise the oxide products. Mainly the outer hydroxide layer was thought to be influenced, because Mo, Cr and Ni are enriched in it as a result of selective dissolution of Fe. This agrees well with the AES, XPS and SIMS results reported by Mischler et al. [193], according to which molybdenum (and also chloride) are concentrated in the outer part of the film on Fe-24%Cr alloys at 65 °C, but the thickness of the film is not influenced to a significant degree. Olefjord et al. [152] suggested that the defects created by Fe^{2+} are cancelled by the defects created by Mo^{4+} or Mo^{6+}. Thus an almost defect-free oxide is formed in which ionic conductivity is extremely low, leading to improved passivity.

Similar ideas, based the results from capacitance and photoelectrochemical measurements, were presented by Hakiki and Da Cunha Belo [98]. They described a mechanism whereby chromium affects the defect structure of the passive film and the properties of the film in terms of occupation of octahedral and tetrahedral positions in a unit cell of spinel structure. Molybdenum was suggested to cause a change in the distribution of the cationic species in the crystallographic lattice of the oxide, i.e. to decrease the content of Fe^{2+} donor species in the octahedral positions leading

to decreased conductivity—in agreement with the suggestions of Olefjord et al. [152].

Clayton and Lu [124] used the bipolar duplex membrane model described in chapter 5.4.4 to illustrate the influence of molybdenum. They proposed that increased pH in the film would lead to the formation of MoO_4^{2-} species most likely in the outer region of the film, which together with the formation of CrO_4^{2-} would contribute to the conversion of the anion selective oxides to cation selective phases. This facilitates the transport of protons towards the solution, and consequently the oxidation of the substrate metal by the remaining O^{2-} ions to form a barrier layer suggested to consist of X Cr_2O_3 · Y CrO_3. The increased proportion of this oxide product at the cost of hydrated $Cr(OH)_3$ was explained to lead to more protective nature of the passive films [124]. In addition to the effect on the composition of the film, molybdenum was suggested to improve the overall protective nature of the film also towards attack by aggressive anions [124]. This was attributed to the strong fixed negative charge of molybdate ions, which plays and important role in preventing e.g. the ingress of chloride ions especially in rapid diffusion paths such as atomic channels. The view of Clayton and Lu agrees well with the overall connection between semiconductor properties and susceptibility to localised corrosion suggested by Schmuki and Böhni [192]. It is also supported by the AES, XPS and SIMS results by Mischler et al. [193], which show that molybdenum influences the depth distribution of Cl^- in the films formed on Fe-24%Cr alloys at 65 °C; i.e. chloride is concentrated in the outer part of the film in the presence of molybdenum. To summarise the ideas of Clayton and Lu, molybdate anions support the lesser abundant chromate in increasing the cation selective efficiency of the outer oxide layers hence reducing the degree of hydration and chlorination of the film as well as enhancing the development of the chromium oxide barrier layer.

Macdonald [120] explained the influence of molybdenum using concepts based on his Point Defect Model (PDM) discussed already in chapters 5.3 and 5.4.8. According to his ideas, the diffusion of cation vacancies plays a central role in the behaviour of anodic films. A specific model, the solute/vacancy interaction model (SVIM), was de-

rived, suggesting that the film properties are modified by substitutionally present solute ions (i.e. alloying element ions) in the oxide film. The molybdenum segregated in the barrier layer was presumed to be present as Mo^{4+}_M (i.e. a Mo(VI) ion substituted into an Fe^{2+} or Ni^{2+} position) which appears formally as a centre of four positive charges. The interaction between the immobile Mo^{4+}_M defects and the mobile cation vacancies was described in terms of a chemical equilibrium. Due to the high charge of the Mo^{4+}_M defects, their interaction with the cation vacancies was suggested to be strong, and the number of vacancies with which they are complexed was explained to be large. Thus it can be assumed that their presence leads to the decrease of both concentration and diffusivity of the mobile cation vacancies in the film. The major impact is then considered to be a

great increase of the induction time for oxide film breakdown (i.e. the time required to accumulate a critical concentration of cation vacancies at the metal/film interface). The approach of Macdonald requires the presence of molybdenum in the inner part of the film. However, molybdenum has mainly been reported to be found in the outer region of the film. This casts a doubt on the applicability of the SVIM to model the influence of molybdenum to the breakdown of oxide films on stainless steels.

In spite of the great amount of research carried out, there does not seem to exist any generally accepted view on the mechanism how molybdenum improves the passive properties of oxide films on stainless steels. Accordingly, clarifying its influence is one of the most important future tasks in attempts to model the oxidation of engineering alloys.

9 OXIDE FILMS AND STRESS CORROSION CRACKING

9.1 Introduction to environmentally assisted cracking (EAC)

Environmentally assisted cracking (EAC) can be understood as a localised corrosion process caused or accelerated by mechanical stresses. The occurrence of EAC in iron- and nickel-based materials can most probably be correlated with the properties of oxide films formed due to exposure to the environment [154,194]. This kind of approach requires that the mechanical stresses are present, and this is assumed during the whole chapter 9. The different modes of mechanical stresses and their origins are not considered in more detail in this report.

The cracking itself may proceed along grain boundaries (intergranularly, IGSCC) or through the grains (transgranularly, TGSCC). The two most studied occurrences of cracking have been that of sensitised stainless steel in BWRs and that of nickel-base alloys (especially Inconel 600) in PWRs.

Cracking of stainless steels in BWR environment has been found to occur exclusively above a critical potential which is about –0.23 V vs. SHE at 288 °C. The critical potential has been found to be almost independent of other variables than temperature [195]. Cracking of stainless steel in BWRs is a form of IGSCC considered to be mainly influenced by Cr depletion associated with carbide precipitation at the grain boundaries, i.e. sensitisation. In addition, segregation of atoms to the grain boundary interface, extending only over several tens of Angstroms but providing an additional path for preferential reactivity at grain boundaries even in the absence of sensitisation, may contribute [194]. Non-equilibrium segregation is thought to play an important role especially in the mechanism of irradiation assisted stress

corrosion cracking (IASCC).

In BWRs where the bulk environment is oxidising, a crack is normally characterised by a gradient in the composition of the solution (pH etc.) and the potential in the solution inside the crack, as well as by a gradient in the composition of the oxide film on its walls. Both the pH, oxygen content and the potential difference between the metal and the solution at the crack tip are normally lower than those of the bulk environment. This points to the so-called occluded chemistry, which results from restrictions of mass transport into and from the crack. The occluded chemistry and the potential concepts have been recently discussed e.g. by Andresen [204] and Ferreira and Li [205]. One important feature of the occluded water chemistry is that even small concentrations of impurities such as SO_4^{2-} and NO_3^- ions in otherwise pure water may influence strongly the conditions inside the crack and thus lead to large changes in the cracking behaviour in e.g. BWR conditions. A more comprehensive discussion on this feature has been given e.g. by Ljungberg and Hallden and can be found in [197].

Based on the ideas presented by Segal et al. [206], it can be concluded that also the oxidation state and chromium content of the oxide film inside the crack change gradually with the distance from the crack mouth. The gradual change in the structure of the oxide film in stress corrosion cracks formed in AISI 304 stainless steel exposed to BWR coolant has been described as follows [171 and references therein]: The film near the crack opening was similar to that on the bulk surface exposed to oxidising coolant. As the crack tip was approached, the Fe_2O_3 particles decreased in density from multilayer coverage on the barrier film to monolayer coverage and to only partial coverage. Very few Fe_2O_3 particles were found near or at the crack tip. Deeper inside the

crack, a single layer compact film was present with large ferrite crystals (10–50 μm across). This inner film was an Fe-Ni oxide with varying amount of Cr, depending on the distance away from the crack opening. The crack opening region was depleted of chromium, whereas the crack tip region contained up to 15% chromium. Accordingly, also the formation of Cr_2O_3 close to the crack tip is possible.

In PWRs the bulk environment is always reducing even in-core under irradiation. Cracking of nickel-base alloys (especially that of Inconel 600) occurs then at low potentials close to the equilibrium potential of the H^+/H_2 redox reaction. The mechanism(s) of such cracking are less well understood than that of stainless steels in BWRs. There seem to be several factors affecting the cracking rate, e.g. heat treatment, carbide distribution, grain boundary segregation, surface finish etc.

Because of the large amount of available literature on this subject, the following discussion is limited to some observations and comments on the role of oxide films in the EAC of different materials. In addition, some of the existing models are commented with regard to the relevance of oxide film properties.

9.2   Stainless steels

Staehle et al. [194] have commented that stress corrosion cracking of stainless steels occurs in such ranges of potential in which the protective film is still protective but marginally unstable.

Cubicciotti and Ljungberg [48] have reported on the basis of a calculated potential-pH diagram for the $Cr-H_2O$ system with Fe that there is a correlation between the critical potential for IGSCC (for sensitised AISI 304 stainless steel) and the stable phase containing Cr: above the critical potential where IGSCC can occur, the stable phase is Cr_2O_3, while below the critical potential the stable phase is $FeCr_2O_4$. This suggests that Cr_2O_3 is not protective against IGSCC. In a more recent paper Cubicciotti [47] reported calculations which showed that a $FeCr_2O_4$ spinel is formed in BWRs under HWC but not under NWC conditions. In the latter case Fe_2O_3 is formed. The change of stability from Fe_2O_3 to $FeCr_2O_4$ occurs at the same potential (about –0.2 V vs. SHE) as that for which

intergranular stress corrosion cracking rates decrease rapidly. Accordingly, the mitigation of IGSCC risks in plant applying HWC was attributed to the presence of the $FeCr_2O_4$ spinel. Possible explanations for this were greater mechanical resistance to cracking, greater electric resistance decreasing electrochemical reaction rates, or inhibition of the cathodic half reaction. However, it has to be borne in mind that thermodynamic calculations are not capable of taking into account what happens in the inner part of the film, although the inner part is likely to control the whole oxidation process.

Congleton and Yang [196] have performed a comprehensive study on the cracking behaviour of sensitised AISI 316 stainless steel in high temperature low oxygen (below 5 ppb) water containing 5 ppm chloride over a temperature range 100...300 °C using SSRT tests, polarisation curves and AES. Cracking was found to occur at potentials more positive than the open circuit potential (zero current potential), suggesting that cracking was driven by an anodic dissolution controlled mechanism. At lower potentials, cracking was transgranular, while intergranular or mixed cracking became predominant at higher potentials. The onset of more rapid cracking corresponded approximately to the active-passive transition peaks. Transition from predominantly transgranular to predominantly intergranular cracking for the sensitised AISI 316 stainless steel occurred at potentials corresponding approximately to the position where the anodic current densities for the material simulating grain boundaries became appreciably higher than those for AISI 316 stainless steel. It seemed that higher susceptibility to SCC correlates with higher thickness of the oxide. The authors concluded from their work that the mechanical properties of the surface oxide films are likely to be more important than their chemical properties for crack initiation and propagation during SSRTs. However, higher susceptibility to SCC was also found to correlate inversely with the increasing concentration of Ni in the surface film, i.e. the chemical composition of the film.

9.3   Inconel 600

Rebak and Szklarska-Smialowska [209] have pointed out that IGSCC of Inconel 600 in PWR

water occurs only when a NiO film is formed during a corrosion process and exists on the metal surface. A high hydrogen content may reduce NiO to Ni and thus decrease the risk for IGSCC. This agrees well with the observations made by Lagerström et al. [210], according to which the crack growth rate of Inconel 600 seems to increase with increasing resistance of the surface film formed on the metal. The increase of the resistance can be attributed to a greater amount of NiO at the cost of metallic nickel. The observations of Staehle et al. [194] give further support to the important role of NiO in the IGSCC behaviour of Inconel 600: they found out that pure nickel is a good model material for studying the SCC of this alloy. The kinetics, extent, and aggravation of grain boundary reactivity related to the sulphur segregation was observed to be the same for pure Ni as for Inconel 600.

9.4 Role of oxide films in models for stress corrosion cracking

The models developed to explain EAC are to a great extent based directly or indirectly on anodic reaction processes. Once initiated, the SCC of iron- and nickel-based alloys has been suggested to proceed in increments (the so-called slip-dissolution model). Each increment consists of the following steps at the crack tip [refs. 11 and 12 in [170],197,198]:

a) activation, i.e. exposure of new metal surface by mechanical fracture

b) dissolution of the active surface

c) repassivation.

The coupled environment fracture model (CEFM) formulated by Macdonald and Urquidi-Macdonald [199] also assumes crack advance to occur via the slip-dissolution-repassivation mechanism, but charge conservation is required and used as a starting point for the derivations. The main difference between the basic slip-dissolution model and the CEFM is that the latter assumes the cathodic reaction to take place mainly at the bulk external surfaces while the former claims that the cathodic reaction mainly occurs at surfaces inside the crack. This difference has relevance to the application of novel cracking mitigation technologies. Other competing SCC mechanisms are based on the combination of selective dissolution and vacancy creep [200], internal oxidation [201], cleavage and surface-mobility [202,203]. Another approach in modelling SCC is based on the effect of hydrogen atoms [203].

Several excellent reviews on the alternative mechanisms of EAC have been published. These include the surveys by Galvele [202], Hänninen et al. [207], Turnbull and Psaila-Dombrowski [208], Turnbull [203] and Rebak and Szklarska-Smialowska [201].

The surface mobility SCC mechanism [202] and the recently introduced selective dissolution - vacancy creep (SDVC) model for SCC [200] include the postulate that SCC takes place by capture of vacancies in the metal close to the crack tip. Because vacancies in the metal lattice can be generated as a result of oxidation of the metal and dissolution of the metal from the oxide film (see chapter 5.3), the crack growth rate may be controlled by the growth of the oxide, i.e. the transport rate of species through the oxide film. Both models require a supply of metal vacancies for SCC to occur.

Also the slip-dissolution model and the CEFM model assume that the anodic and corresponding cathodic reactions contributing to crack growth occur partly on or in the oxide films. Thus the rates of these reactions may control the crack propagation rate, in which case the properties of the oxide films play a crucial role in determining the susceptibility of the material to SCC.

10 SUMMARY AND CONCLUSIONS

The construction materials used in coolant systems in power plants and in process industry are covered with oxide films as a result of exposure to the aqueous environment. The susceptibility of the materials to different forms of corrosion, as well as the extent of the incorporation of radioactive species on the surfaces of the primary circuit in nuclear power plants, are greatly influenced by the physical and chemical properties of these oxide films. The composition and characteristics of the oxide films are in turn dependent on the applied water chemistry. A comprehensive understanding of the correlations between applied water chemistry, the behaviour of oxide films, localised corrosion and other phenomena related to the optimum performance of the plant is lacking. Accordingly, this work was undertaken to give an introduction to the fundamental concepts and present views concerning the properties and structures of oxide films formed on metals in aqueous environments, as well as the transport phenomena leading to the growth of the films and incorporation of foreign species into the film. The most important observations and conclusions are summarised below. The results of this work will be utilised in future projects, the goals of which include the recognition of the rate-limiting steps in corrosion and activity incorporation.

10.1 Structures of oxide films formed on metal surfaces

Understanding the correlations of the structure of oxide films on metal surface with the performance of the corresponding material is essential when predicting possible material-related risks.

The most recent structural investigations point to a nano-crystalline structure of the oxide films formed on iron, nickel, and possibly also on chromium at ambient temperature. These oxide films have been characterised as mixed valence compounds. Their stoichiometry has been suggested to vary with potential within the limits of disorder corresponding to a few basic crystal structures. The water and hydroxyl content of the films, and even the formation of an outer disordered hydroxide layer have remained uncertain because of the lack of in situ experimental data.

The films formed on stainless steels appear to be nano-crystalline as well. These films are generally considered to consist of two sublayers with different compositions because of the selective dissolution of some of the constituent elements. The inner sublayer is enriched in Cr, while the outer layer is Fe-rich. This outer Fe-rich layer is more influenced by the external conditions both in thickness and stoichiometry. It is still uncertain, whether the possible oxidation products are present as separate phases or whether the films on stainless steel have a gradually changing in-depth composition.

10.2 Electronic properties of oxide films

The electronic properties of metal oxide films have a great influence on the corrosion and other electrochemical phenomena occurring on metal surfaces in aqueous environments.

In spite of the great number of publications on the subject, it is still controversial, whether the oxide films formed on metal surfaces in aqueous solutions should be treated as electronic conductors, semiconductors or insulators. The small thickness of the oxide films formed in aqueous environments, as well as the disordered structure of metal oxide films when compared to bulk crystalline phases, makes the application of classical semiconductor concepts rather difficult. Also, the insulating behaviour is usually complicated by direct and resonance tunnelling processes through the thin film.

One very important observation concerning the investigations reported in the literature is that the electronic properties of the films have been

seldom correlated with the oxide structures. The former have usually been measured with in-situ electrochemical techniques, while the structures are more commonly determined by ex-situ methods. Moreover, data on ionic and electronic conductivities of the films are also treated separately. Thus no comprehensive view on the charge distribution within the films formed especially on stainless steels and nickel-based alloys exists. In addition, connections of the charge distribution to the crystallographic defect structure is yet to be established.

10.3 Kinetics of oxide film growth on metals

A kinetic model for the growth and dissolution of oxide films on metals, including transport of species through the film, leads to the recognition of the rate-limiting steps of different processes in different conditions. This in turn makes it possible to influence the factors which determine the overall rate of corrosion phenomena and of activity incorporation.

The following main and side reaction steps have to be accounted for by a kinetic model for the oxidation of a metal covered by an oxide film in an aqueous environment:

a) *An electrochemical charge transfer reaction leading to the generation of point defects, the transport of which is responsible for film growth.*
For films in which oxygen vacancies or metal interstitials are the defects responsible for growth, this reaction will take place at the metal/film interface. Thus the film grows at that interface. Conversely, for films in which metal vacancy motion leads to film growth, this reaction is located at the film/solution interface. The formation of point defects in an electrochemical reaction results in the generation of both ionic and electronic charges at the interfaces.

b) *The transport of point defects through the film.*
This process is influenced greatly by the defect structure and the charge distribution of mobile and immobile species in the film.

c) *Charge transfer reactions at one interface, leading to the annihilation of the point defects, the transport of which is responsible for film growth at the opposite interface.*
If the film grows at the metal /film interface, the annihilation reaction at the film / solution interface competes with reactions involving the interaction of the film with the electrolyte, e.g. the incorporation of cationic and anionic species from the solution. On the other hand, if the film grows at the film/solution interface, the rate of consumption of vacancies in the underlying metal substrate is of importance for the total charge and material balance in the system. Thus both the structure of the underlying metal and the electrolyte composition have to be taken into account.

d) The generation, transport and annihilation of point defects, the motion of which leads to metal dissolution through the film.
These reactions are influenced by the same factors as cited in points a), b) and c) above.

e) *Important side reactions such as electron transfer from redox couples in the solution and changes in the valence of cations in the film.*
These reactions can greatly influence the susceptibility of the underlying metal to different types of corrosion.

Unfortunately, no general model capable to meet all (or even a considerable part) of the above mentioned requirements has appeared. A rather good agreement on the chemistry of the reactions of defect generation and annihilation, as well as on the effect of film structure on the transport of defects, already exists. Some attempts have also been made to correlate the ionic transport and electronic properties of the oxide films formed on metals. The main gap in the understanding is the lack of correlation between the kinetic approaches to film growth and the physical approaches to the crystal structure of oxide films formed on metals. In our opinion, this explains why the film growth models proposed so far in the literature cannot be regarded as satisfactory or sufficient.

10.4 Structure, properties and growth kinetics of films on metals in high-temperature aqueous environments

An extension of the concepts and models discussed above to cover metal oxide films on Fe and Ni based alloys in high-temperature aqueous environments is essential with regard to questions related to coolant systems in nuclear power plants and other high-temperature processes.

The metal oxide films formed on Fe and Ni based materials at ambient temperatures (below about 100 °C) are typically only a few nm thick. Their initial composition is greatly influenced by the previous surface treatment procedures and by the bulk composition of the alloy. Only relatively small enrichment of the different alloying constituents in different parts of the film have been observed in the passive potential range. On the other hand, rather thick oxide layers are formed above 150 °C, and a more or less pronounced enrichment or depletion of constituents can be found. The enrichment or depletion is mainly controlled by the electrode potential of the alloy and the pH of the environment. It has been observed that differences between the compositions of surface layers formed on different Fe-Cr-Ni materials tend to decrease as the temperature increases.

Increase in porosity is one of the main changes in film properties with increasing temperature. Porosity can eventually lead to decreased protectiveness of the film, and it may also lead to exposure of products with different solubilities (e.g. due to gradually varying stoichiometry) to the solution. This in turn results in the establishment of concentration profiles in the pores, which has an influence on transport of species through the film. Compared to thin, compact oxide films, the prevailing situation may be drastically different.

The duplex-film concept has proven to be useful in the modelling of the behaviour of oxide films on Fe and Ni based materials at high temperature. The duplex film was defined in this survey to refer to a film consisting of two different parts (layers), the physical properties of which are different. According to the reviewed literature, the inner layer of a duplex film consists of fine-grained oxide because it grows in a confined space. On the other hand, the outer layer consists of loosely packed, larger grains, because it grows without volume constraint. The boundary between the layers has been found to lie at the position of the original metal surface, which indicates that the inner layer grows at the metal/oxide interface and that the outer layer grows at the oxide/solution interface. The outer layer has been described to consist of two sublayers: a porous precipitated sublayer and a cracked inner sublayer which has been hypothesised to be formed by the breakdown of the inner layer.

The models for the growth of oxide films in high-temperature aqueous electrolytes can be stated to be in a childhood stage compared to those for growth at ambient temperature. The prevailing view for the growth of duplex films at high temperature is that the inner layer grows with the ingress of water along nanometer scale pores, while the outer layer forms via transport of metal ions along the grain boundaries. The only proof for such a view seems to be the high activation energy for corrosion. However, no electrochemical experiments to prove or disprove this view have been reported in the literature. One of the major arguments against the prevailing view is based on the fact that transport of metal ions in the nanometer pores is much more favourable than the longitudinal grain boundary diffusion proposed in the model. In addition, the role of electrolyte species in the formation of the outer layer by reprecipitation was not taken into account.

An electrochemical approach to the growth of oxide films on metals in high-temperature electrolytes emphasising the mechanism of generation and transport of species responsible for the growth process is still lacking. This approach should include a thorough understanding of the processes taking place in both the dense part and the porous part of the film. This should lead to better understanding of phenomena related to the incorporation of active species and e.g. Zn ions in nuclear power plant, and to different corrosion phenomena.

10.5 Role of oxide films in localised corrosion and stress corrosion cracking

The properties of oxide films on metal surfaces have a special role in such corrosion phenomena which are believed to be connected with the breakdown or rupture of oxide films.

The initiation of localised corrosion, requiring breakdown of the passive oxide film, has generally been attributed to the chemical and structural heterogeneity of the surface of the underlying alloy. Thus the mechanism of localised corrosion site formation has often been related to the galvanic effect of inclusions. However, localised corrosion sites have been observed to initiate on the surface of high-purity metals as well, if a sufficient amount of aggressive anions are present and the environment is oxidising enough. In such cases the local mechanical breakdown of passive films has been explained to be due to microscopic concavities, in which a higher electric field strength and hence a larger electrostatic pressure can be assumed to prevail. The breakdown of the film was suggested to occur at the potential at which the electrostatic pressure at the concave site exceeds the compressive strength of the film.

More recent modelling approaches attribute the passive film breakdown to the inability of the annihilation rate of metal vacancies at the metal/film interface to account for the high transport rate of such vacancies from the film/solution interface. The high transport rate of cation vacancies may in turn be attributed to the complex pair formation of oxygen vacancies with some species from the electrolyte, which influences the transport phenomena in the whole film. The fact that this view is generally accepted is a proof for the paramount role of oxide films in localised corrosion processes. The role of minor alloying elements such as Mo in the oxide film breakdown on stainless steels and nickel-based alloys has been explained in a satisfactory way on the basis of the concepts of charge distribution within the oxide film.

However, a sound correlation between the electric and electrochemical properties of the oxide film/electrolyte interface and the crystal structure of the film does not exist in this case, either. There is certainly a gap between concepts of film breakdown based on enhanced ionic motion in the film and the approaches attributing the localised corrosive attack to the electronic (semiconductive) properties of the oxide layer.

Studies on the role of oxide films in stress induced corrosion damage are also in their very beginning. Such studies are particularly important because several modern approaches to stress corrosion cracking attribute the crack formation and growth to an enhanced flow of vacancies in the metal substrate. As the engineering materials are covered with oxide films in most of the important industrial environments, these oxide films can serve as a source of the enhanced flow of vacancies in the metal. Thus the electric and electrochemical properties of oxide films must play a role in the stress corrosion crack initiation and crack growth process. Future studies on the subject will certainly help to resolve some controversial issues on the influence of the chemical environment on fracture of metallic materials.

10.6 Concluding remark

This survey contains an introduction to the basic concepts and a description of the state-of-the-art of the modelling related to oxidation of metal surfaces in aqueous environments. As a general conclusion it can be stated that the models presented for both ambient and high-temperature aqueous oxidation of metals lack correlations between electronic and ionic properties and structure of the oxide films, quantitative treatment and thus also capability to predict material behaviour in varying conditions. The situation calls for more experimental work combined with comprehensive modelling of the behaviour of both the compact and the porous part of the oxide film formed on a metal surface.

REFERENCES

1 Mäkelä K, Laitinen T, Bojinov M. The influence of modified water chemistries on metal oxide films, activity build-up and stress corrosion cracking of structural materials in nuclear power plants. Literature survey. Espoo: VTT Manufacturing Technology, 1998.

2 Cotton FA, Wilkinson, G. Basic Inorganic Chemistry, New York: John Wiley & Sons, Inc., 1976.

3 Douglas B, McDaniel DH, Alexander JJ. Concepts and models of inorganic chemistry, 2nd ed., New York: John Wiley & Sons, Inc., 1983.

4 Tarasevich MR, Efremov BN. Properties of spinel-type oxide electrodes. In: Trasatti, editor. Electrodes of conductive metallic oxides, Part 1. Amsterdam: Elsevier Scientific Publishing Company, 1980:221–259.

5 Gerischer H. Remarks on the electronic structure of the oxide film on passive iron and the consequences for its electrode behaviour. Corrosion Science 1989;29(2/3):191–195.

6 Sala B, Combrade P, Erre R, Benoit R, Le Calvar M. Chemistry of sulfur in high temperature water – Reduction of sulfates. Proc. Fifth Int. Symp. on Environmental Degradation of Materials in Nuclear Power Systems - Water Reactors. Monterey, California: NACE, 1991: 502–510.

7 Harding JH. Modelling the effect of zinc addition on the uptake of cobalt by oxide films in PWRs. Water chemistry of nuclear reactor systems 7, Vol. 1. London: British Nuclear Energy Society, 1996:309–316.

8 Lister DH. Activity transport and corrosion processes in PWRs. Water chemistry of nuclear reactor systems 6. London: British Nuclear Energy Society, 1992:49–60.

9 Robertson J. The mechanism of high temperature aqueous corrosion of stainless steels. Corrosion Science 1991;32:443–465.

10 Davenport AJ, Sansone M. High resolution in situ XANES investigation of the nature of the passive film on iron in a pH 8.4 borate buffer. Journal of the Electrochemical Society 1995; 142:725–730.

11 Robertson J. The mechanism of high temperature aqueous corrosion of steel. Corrosion Science 1989;29:1275–1291.

12 Kofstad P. High temperature corrosion. London, New York: Elsevier Applied Science, 1988.

13 Searson PC, Latanision RM, Stimming U. Analysis of the photoelectrochemical response of the passive film on iron in neutral solutions. Journal of the Electrochemical Society 1988;135:1358–1363.

14 Keddam M, Pallotta C. Electrochemical behaviour of passive iron in acid medium. Journal of the Electrochemical Society 1985;132: 781–787.

15 Tomlinson L. Mechanism of corrosion of carbon and low alloy ferritic steels by high temperature water. Corrosion (NACE) 1981;37 (10):591–596.

16 Maurice V, Yang WP, Marcus P. XPS and STM investigation of the passive film formed on Cr(110) single-crystal surfaces. Journal of the Electrochemical Society 1994;141:3016–3027.

17 Lorang G, Da Cunha Belo M, Simoes AMP, Ferreira MGS. Chemical composition of passive films on AISI 304 stainless steel. Journal of the Electrochemical Society 1994;141:3347–3356.

18 Rosenberg R. Loviisa 2:n primääripiirin dekontaminoinnin jälkiseuranta kokeellisin ja laskennallisin menetelmin. Osa 1 – Kirjallisuustutkimus. Espoo: VTT Kemiantekniikka, 1995.

19 Allen GC, Hallam KR. Characterisation of the spinels $M_xCo_{1-x}Fe_2O_4$ (M=Mn, Fe or Ni) using X-ray photoelectron spectroscopy. Applied Surface Science 1996;93:25–30.

20 Rosenberg HM. The solid state. 3rd ed. Oxford: Oxford Science Publications, 1988.

21 Rudden MN, Wilson J. Elements of solid state physics. Chichester: John Wiley & Sons Ltd., 1984.

22 Atkinson A. Diffusion in ceramics. In: Swain MV. editor. Materials Science and Engineering, Vol. 11. New York: VHC Publishers Inc., 1994:295-337.

23 Heslop RB, Jones K. Inorganic chemistry; a guide to advanced studies, Amsterdam: Elsevier Scientific Publ. Comp., 1976.

24 Palombari R, Pierri F. Ni(III) doped NiO as the electrode material for electrochemical devices employing protonic conductors. Journal of Electroanalytical Chemistry 1997;433:213–217.

25 Young EWA, Gerretsen JH, de Wit JHW. The oxygen partial pressure dependence of the defect structure of chromium (III) oxide. Journal of the Electrochemical Society 1987;134:2257–2260.

26 Schultze JW, Mohr S. Halbleiterverhalten technischer Elektroden. Dechema Monographie 90, Elektrochemie und Elektronik. Weinheim: Verlag Chemia, 1981:231–257.

27 Morrison SR. Electrochemistry at semiconductor and oxidized metal electrodes. New York: Plenum Press, 1980.

28 Schmuki P. Halbleitereigenschaften von Passivfilmen. Ph.D.Thesis, ETH Zürich, 1992.

29 Schmuki P, Büchler M, Virtanen S, Böhni H, Müller R, Gauckler LJ. Bulk metal oxides as a model for the electronic properties of passive films. Journal of the Electrochemical Society 1995;142:3336–3342.

30 Virtanen S, Schmuki P, Böhni H, Vuoristo P, Mäntylä T. Artificial Cr^- and Fe-oxide passive layers prepared by sputter deposition. Journal of the Electrochemical Society 1995;142:3067–3072.

31 Kennedy JH, Frese Jr. KW. Flatband potentials and donor densities of polycrystalline a-Fe_2O_3 determined from Mott-Schottky plots. Journal of the Electrochemical Society 1978;125:723–726.

32 Smith-Magowan D. Evaluation of the applicability of colloid studies to Cobalt-60 deposition in LWRs. Palo Alto, CA: Electric Power Research Institute, 1984. Report No.: EPRI NP-3773.

33 Berry WE, Diegle RB. Survey of corrosion product generation, transport, and deposition in light water nuclear reactors. Palo Alto, CA: Electric Power Research Institute, 1979. Report No.: EPRI NP-522.

34 Sweeton FH, Baes Jr. CF. The solubility of magnetite and hydrolysis of ferrous ion in aqueous solutions at elevated temperatures. Journal of Chemical Thermodynamics 1979;2:479–500.

35 Rosenberg R. Ydinvoimalaitosveden korroo-siotuotteiden alkuaineanalytiikka. Helsinki: Säteilyturvakeskus, 1994. Report No.: STUK-YTO-TR 79.

36 Rosenberg R, Tanner V. PWR-ydinvoimalai-toksen primääripiirin aktiivisuuskulkeutu-mismallit. Helsinki: Säteilyturvakeskus; 1995. Report No.: STUK-YTO-TR 80.

37 Kunig RH, Sandler YL. The solubility of sim-ulated PWR primary circuit corrosion prod-ucts. Palo Alto, CA: Electric Power Research Institute, 1986. Report No.: EPRI NP-4248.

38 Kang S, Solomon Y, Troy M. Reactor coolant high-temperature filtration. Vol. 2. Evalua-tion of effectiveness in reducing occupational radiation exposure. Palo Alto, CA: Electric Power Research Institute, 1984. Report No.: EPRI NP-3372 Vol. 2.

39 Bergmann CA, Durkosh, DE, Lindsay WT, Roesmer J. The role of coolant chemistry in PWR radiation-field buildup. Palo Alto, CA: Electric Power Research Institute, 1985. Re-port No.: EPRI NP-4247.

40 Polley MV, Garbett K, Pick ME. A survey of the effect of primary coolant pH on Westing-house PWR plant radiation fields. Palo Alto, CA: Electric Power Research Institute, 1994. Report No.: EPRI TR-104180.

41 Berge P, Ribon C, Saint Paul P. Effect of hydrogen on the corrosion of steels in high-temperature water. Corrosion/74, Paper 50.

42 Berge P, Ribon C, Saint Paul P. Effect of hydrogen on the corrosion of steels in high temperature water. Corrosion (NACE) 1977; 33:173–178.

43 Ashmore C B, Brown D J, Pritchard A M, Sims H E. Effects of HWC water chemistry on activity transport in BWRs. Water chemistry of nuclear reactor systems 7. London: British Nuclear Energy Society, 1996:222–229.

44 Lambert I, Lecomte J, Beslu P, Joyer F. Corrosion product solubility in the PWR pri-mary coolant. Water chemistry of nuclear reactor systems 4, London: British Nuclear Energy Society, 1986:105–106.

45 Kang S, Sejvar J. The CORA-II Model of PWR corrosion-product transport. Palo Alto, CA: Electric Power Research Institute, 1985. Report No.: EPRI NP-4246.

46 Chen CM, Aral K, Theus GJ. Computer-calcu-lated potential pH diagrams to 300 °C. Vol. 2: Handbook of diagrams. Palo Alto, CA: Elec-tric Power Research Institute, 1983. Report No.: EPRI NP-3137.

47 Cubicciotti D. Equilibrium chemistry of nitro-gen and potential-pH diagrams for the Fe-Cr-H_2O system in BWR water. Journal of Nucle-ar Materials 1989;167:241–248.

48 Cubicciotti D, Ljungberg, L. The Pourbaix diagram for Cr with Fe and the stress corro-sion cracking of stainless steel. Journal of Electrochemical Society 1985;132:987–988.

49 Cubicciotti D. Potential-pH diagrams for al-loy-water systems under LWR conditions. Journal of Nuclear Materials 1993;201:176–183.

50 Lee JB. Elevated temperature potential-pH diagrams for the Cr-H_2O, Ti-H_2O, Mo-H_2O, and Pt-H_2O systems. Corrosion (NACE) 1981; 37:467–481.

51 Beverskog B, Puigdomenech I. Revised Pour-baix diagrams for iron at 25–300 °C. Corro-sion Science 1996;38:2121–2135.

52 Beverskog B, Puigdomenech I. Revised Pour-baix diagrams for chromium at 25–300 °C. Corrosion Science 1997;39:43–57.

53 Beverskog B, Puigdomenech I. Revised Pour-baix diagrams for zinc at 25–300 °C. Corro-sion Science 1997;39:107–114.

54 Beverskog B, Puigdomenech I. Pourbaix diagrams for nickel at 25–300 °C. Corrosion Science 1997;39:969–980.

55 Koukkari P, Sippola H, Sundquist A. Multicomponent equilibrium calculations in process design: study of some acid digester reactors. Hydrometallurgy '94 (Proceedings) Cambridge, England, 11–15 July 1994.

56 Anderko A, Sanders SJ, Young RD. Real-solution stability diagrams: a thermodynamic tool for modeling corrosion in wide temperature and concentration ranges. Corrosion (NACE) 1997;53:43–53.

57 Sato N. The passivity of metals and passivating films. In: Frankenthal RP, Kruger J. editors. Passivity of Metals. Princeton, NJ: The Electrochemical Society Monograph Series, 1979:29–58.

58 Virtanen S, Schmuki P, Davenport AD, Vitus CM. Dissolution of thin iron oxide films used as models for iron passive films studied by in situ X-ray absorption near-edge spectroscopy. Journal of the Electrochemical Society 1997;144:198–204.

59 Asakura Y, Karasawa H, Sakagami M, Uchida S. Relationships between corrosion behaviour of AISI 304 stainless steel in high-temperature pure water and its oxide film structures. Corrosion (NACE) 1989;45:119–124.

60 Vetter KJ. General kinetics of passive layers on metals. Electrochimca Acta 1971;16:1923–1937.

61 Bardwell JA, MacDougall B, Graham MJ. Use of [18] O/SIMS and electrochemical techniques to study the reduction and breakdown of passive oxide films on iron. Journal of the Electrochemical Society 1988;135:413–418.

62 Cohen M. The passivity and breakdown of passivity on iron. In: Passivity of Metals, Frankenthal RP and Kruger J. editors. Princeton, NJ: The Electrochemical Society, 1978: 521–545.

63 Kruger J. Passivity of metals – a materials science perspective. International Materials Reviews 1988;33:113–130.

64 Rahner D. Fe_3O_4 as part of the passive layer on iron. Solid State Ionics 1996;86–88:865–871.

65 Nagayama M, Cohen M. The anodic oxidation of iron in a neutral solution. I. The nature and composition of the passive film. Journal of the Electrochemical Society 1962;109:781–790.

66 Nagayama M, Cohen M. The anodic oxidation of iron in a neutral solution. II. Effect of ferrous ion and pH on the behaviour of passive iron. Journal of the Electrochemical Society 1963;110:670–680.

67 Chen C-T, Cahan BD. The nature of the passive film on iron. I. Automatic ellipsometric spectroscopy studies. Journal of the Electrochemical Society 1982;129:17–26.

68 Cahan BD, Chen C-T. The nature of the passive film on iron. II. A-C impedance studies. Journal of the Electrochemical Society 1982;129:474–480.

69 Cahan BD, Chen C-T. The nature of the passive film on iron. III. The chemi-conductor model and further supporting evidence. Journal of the Electrochemical Society 1982;129: 921–925.

70 Kuroda K, Cahan BD, Nazri Gh, Yeager E, Mitchell TE. Electron diffraction study of the passive film on iron. Journal of the Electrochemical Society 1982;129:2163–2169.

71 Sato N, Noda T, Kudo K. Thickness and structure of passive films on iron in acidic and basic solution. Electrochimica Acta 1974; 19:471–475.

72 Sato N, Kudo K, Nishimura R. Depth analysis of passive films on iron in neutral borate solution. Journal of the Electrochemical Society 1976;123:1419–1423.

73 Schmuki P, Virtanen S, Davenport AD, Vitus CM. In situ X-ray absorption near-edge spectroscopic study of the cathodic reduction of artificial iron oxide passive films. Journal of the Electrochemical Society 1996;143(2):574–582.

74 Davenport A, Bardwell J, Vitus CM. In situ XANES study of galvanostatic reduction of the passive film on iron. Journal of the Electrochemical Society 1995;142:721–724.

75 Graham MJ. The application of surface techniques in understanding corrosion phenomena and mechanisms. Corrosion Science 1995; 37(9):1377–1397.

76 Hara N, Sugimoto K. The study of the passivation films on Fe-Cr alloys by modulation spectroscopy. Journal of the Electrochemical Society 1979;126:1328–1334.

77 Oblonsky LJ, Davenport AJ, Ryan MP, Isaacs HS, Newman RC. In situ x-ray absorption near edge structure study of the potential dependence of the formation of the passive film on iron in borate buffer. Journal of the Electrochemical Society 1997;144:2398–2404.

78 Oblonsky L, Devine T. A surface enhanced raman spectroscopic study of the passive films formed in borate buffer on iron, nickel, chromium and stainless steel. Corrosion Science 1995;37:17–41.

79 Ryan MP, Newman RC, Thompson GE. An STM study of the passive film formed on iron in borate buffer solution. Journal of the Electrochemical Society 1995;142(10):L177–L179

80 Toney MF, Davenport AJ, Oblonsky LJ, Ryan MP, Vitus CM. Atomic structure of the passive oxide film formed on iron. 1997 Joint International Meeting: 192nd Meeting of the Electrochemical Society, Inc. and 48th Annual Meeting of the International Society of Electrochemistry. Paris, France: 1997: Paper No. 322.

81 Itagaki M, Nakazawa K, Watanabe K, Noda K. Study of dissolution mechanisms of nickel in sulfuric acid solution by electrochemical quartz crystal microbalance. Corrosion Science 1997;39(5):901–911.

82 Bernard MC, Keddam M, Takenouti H, Bernard P, Sényarich S. Electrochemical behaviour of quasi-spherical b-Ni(OH)$_2$ particles studied by Raman spectroscopy. Journal of the Electrochemical Society 1996;143:2447–2451.

83 Oblonsky L, Devine T. Surface enhanced Raman spectra from the films formed on nickel in the passive and transpassive regions. Journal of the Electrochemical Society 1995;142 (11):3677–3682.

84 Melendres CA, Xu S. In situ laser raman spectroscopic study of anodic corrosion films on nickel and cobalt. Journal of the Electrochemical Society 1984;131:2239–2243.

85 Yau S-L, Fan F-R, Moffat TP, Bard AJ. In situ scanning tunneling microscopy of Ni(100) in 1 M NaOH. Journal of Physical Chemistry 1994 ;98:5493–5499.

86 Marcus P, Maurice V. STM and AFM studies of passive films. Materials Science Forum 1995;185–188:221–232.

87 Kowal A, Niewiara R, Peronczyk B, Haber J. In situ atomic force microscopy observation of change in thickness of nickel hydroxide layer on Ni electrode. Langmuir 1996;12:2332–2333.

88 Bojinov M, Fabricius G, Ihonen J, Laitinen T, Piippo J, Saario T, Sundholm G. Combination of Different Electrochemical Techniques to Characterize The Anodic Behaviour of Chromium. Materials Science Forum 1998;289–292:117–126.

89 Bojinov M, Fabricius G, Laitinen T, Saario T, Sundholm G. Conduction mechanism of the anodic film on chromium in acidic sulphate solutions. Electrochimica Acta.1998;44:247–261.

90 Yang WP, Costa D, Marcus P. Chemical composition, chemical states, and resistance to localized corrosion of passive films on an Fe-17%Cr alloy. Journal of the Electrochemical Society 1994;141:111–116.

91 Yang WP, Costa D, Marcus P. Resistance to pitting and chemical composition of passive films of a Fe-17%Cr alloy in chloride-containing acid solution. Journal of the Electrochemical Society 1994;141:2669–2676.

92 Sugimoto K, Matsuda S. Passive and transpassive films on Fe-Cr alloys in acid and neutral solutions. Materials Science and Engineering 1980;42:181–189.

93 Jacobs LC, De Vogel HP, Hemmes K, Wind MM, De Wit JH. Potential modulated ellipsometric measurements on an Fe-17Cr alloy in sulphuric acid. Corrosion Science 1995;37:1211–1233.

94 Jacobs LC, De Vogel HP, Hemmes K, Wind MM, De Wit JH. Potential modulated ellipsometric measurements on the Fe17Cr alloy in sulphuric acid. Materials Science Forum 1995;185-188:481–488.

95 Stellwag B, Lockorrosion in Dampferzeugerheizrohren aus CrNi-Stahl – Ursachen und Schutzmöglichkeiten. Habilitationsschrift. Friedrich-Alexander-Universität Erlangen-Nürnberg, 1991.

96 Bardwell JA, Sproule GI, MacDougall B, Graham MJ, Davenport AJ, Isaacs, HS. In situ XANES detection of Cr(VI) in the Passive film on Fe-26Cr. Journal of the Electrochemical Society 1992;139:371–373.

97 Hakiki NE, Boudin S, Rondot B, Da Cunha Belo M. The electronics structure of passive films formed on stainless steels. Corrosion Science 1995;37(11):1809–1822.

98 Hakiki NE, Da Cunha Belo M. Electronic structure of passive films formed on molybdenum-containing ferritic stainless steels. Journal of the Electrochemical Society 1996;143 (10):3088–3094.

99 Sieradzki K, Newman RC. A percolation model for passivation in stainless steels. Journal of the Electrochemical Society 1986;133: 1979–1980.

100 Calinski C, Strehblow H-H. ISS depth profiles of the passive layer on Fe/Cr alloys. Journal of the Electrochemical Society 1989; 136(5):1328–1331.

101 Ryan MP, Newman RC, Thompson GE. A scanning tunneling microscopy study of structure and structural relaxation in passive oxide films on Fe-Cr alloys. Philosophical Magazine B 1994;70(2):241–251.

102 Ryan MP, Newman RC, Thompson GE. Atomically resolved STM of oxide film structures on Fe-Cr alloys during passivation in sulfuric acid solution. Journal of the Electrochemical Society 1994;141(12):L164–L165.

103 Jabs T, Borthen P, Strehblow H-H. X-ray photoelectron spectroscopic examinations of electrochemically formed passive layers on Ni-Cr alloys. Journal of the Electrochemical Society 1997;144(4):1231–1243.

104 Schmuki P, Böhni H, Mansfeld F. A photoelectrochemical investigation of passive films formed by alternating voltage passivation. Journal of the Electrochemical Society 1993; 140(7):L119–L121.

105 Stimming U, Schultze JW. A semiconductor model of the passive layer on iron electrodes and its application to electrochemical reactions. Electrochimica Acta 1979;24:859–869.

106 Abrantes LM, Peter L. Transient photocurrents at passive iron electrodes. Journal Electroanalytical Chemistry 1983;150:593–601.

107 Delnick FM, Hackerman N. Passive iron. A semiconductor model for the oxide film. Journal of the Electrochemical Society 1979;126: 732–741.

108 Stimming U. Photoelectrochemical studies of passive films. Electrochimica Acta 1986;31: 415–429.

109 Burleigh TD. Anodic photocurrents and corrosion currents on passive and active-passive metals. Corrosion (NACE) 1989;45(6):464–472.

110 Trefz J, Schweinsberg M, Reier T, Schultze JW. Systematic investigation on the corrosion of iron under conditions relevant to storage of nuclear waste. Materials and Corrosion 1996; 47:475–485.

111 Azumi K, Ohtsuka T, Sato N. Spectroscopic photoresponse of the passive film formed on iron. Journal of the Electrochemical Society 1986;133:1326–1328.

112 Noda K, Tsuru T, Haruyama S. The impedance characteristics of passive films on iron. Corrosion Science 1990;31:673–678.

113 Sato N. Anodic breakdown of passive films on metals. Journal of the Electrochemical Society 1982;129:255–260.

114 Sunseri C, Piazza S, Di Quarto F. A photoelectrochemical study of passivating layers on nickel. Materials Science Forum 1995;185-188: 435–446.

115 Rickert H. Electrochemistry of solids, an introduction. Berlin-Heidelberg-New York: Springer-Verlag, 1982.

116 Chao CY, Lin LF, Macdonald DD. A point defect model for anodic passive films. I. Film growth kinetics.1981;128(6):1187–1194.

117 König U, Schultze JW. The examination of the influence of a space-charge layer on the formation kinetics of thin passive films by Schottky-Mott analysis. Solid State Ionics 1992;53–56:255–264.

118 Lister DH, Davidson RD, McAlpine E. The mechanism and kinetics of corrosion product release from stainless steel in lithiated high temperature water. Corrosion Science 1987; 27(2):113–140.

119 Fromhold Jr. AT. Space-charge effects on anodic film formation. In: Oxide and Oxide Films, Vol. 3, Diggle JW, Vijh AK. editors. New York: Marcel Dekker, 1976:1–271.

120 Macdonald DD. The point defect model for the passive state. Journal of the Electrochemical Society 1992;139:3434–3449.

121 Fromhold Jr. AT. Metal oxidation kinetics from the viewpoint of a physicist: The microscopic motion of charged defects through oxides. Langmuir 1987;3:886–896.

122 Peat R, Peter L. A study of the passive film on iron by intensity modulated photocurrent spectroscopy. Journal of Electroanalytical Chemistry 1987;228:351–364.

123 Keddam M, Lizee J-F, Pallotta C, Takenouti H. Electrochemical behaviour of passive iron in acidic medium. I. Impedance approach. Journal of the Electrochemical Society 1984; 131:2106–2024.

124 Clayton CR, Lu YC. A bipolar model of the passivity of stainless steel: The role of Mo addition. Journal of the Electrochemical Society 1986;133:2465–2473.

125 Vermilyea DA. Anodic films. In: Delahay P., editor. Advances in Electrochemistry and Electrochemical Engineering, Vol. 3. New York, London: Interscience Publishers, 1963: 211–286.

126 Battaglia V, Newman J. Modeling of a growing oxide film: The iron/iron oxide system. Journal of the Electrochemical Society 1995; 142:1423–1430.

127 Kirchheim R. Growth kinetics of passive films. Electrochimica Acta 1987;32(11):1619–1629.

128 Kirchheim R. The growth kinetics of passive films and the role of defects. Corrosion Science 1989;29(2/3):183–190.

129 Kirchheim R, Heine B, Hofmann S, Hofsäss H. Compositional changes of passive films due to different transport rates and preferential dissolution. Corrosion Science 1990;31: 573–578.

130 Vetter K, Gorn F. Kinetics of layer formation and corrosion processes of passive iron in acid solutions. Electrochimica Acta 1973;18:321–326.

131 Gabrielli C, Keddam M, Minouflet F, Perrot H. Investigations of the anodic behaviour of iron in sulfuric medium by the electrochemical quartz crystal microbalance under ac regime. Materials Science Forum 1995;185–188:631–640.

132 Gabrielli C, Keddam M, Minouflet F, Perrot H. Ac electrogravimetry contribution to the investigation of the anodic behaviour of iron in sulfuric medium. Electrochimica Acta 1996; 41:1217–1222.

133 Macdonald DD, Urquidi-Macdonald M. Theory of steady-state passive films. Journal of the Electrochemical Society 1990;137:2395–2402.

134 Macdonald DD, Biaggio SR, Song H. Steady-state passive films. Interfacial kinetic effects and diagnostic criteria. Journal of the Electrochemical Society 1992;139:170–177.

135 Urquidi M, Macdonald DD. Solute-vacancy interaction model and the effect of minor alloying elements on the initiation of pitting corrosion. Journal of the Electrochemical Society 1985;132(3):555–558.

136 Goossens A, Vazquez M, Macdonald DD. The nature of electronic states in anodic zirconium oxide films. Part 1: The potential distribution. Electrochimica Acta 1996;41:35–45.

137 Goossens A, Vazquez M, Macdonald DD. The nature of electronic states in anodic zirconium oxide films. Part 2: Photoelectrochemical characterization. Electrochimica Acta 1996; 41:47–55.

138 Dignam MJ. Mechanisms of ionic transport through oxide films. 91–286 In: Oxides and Oxide Films, Vol. 1. Diggle JW. editor. New York: Marcel Dekker, 1973: 91–286.

139 Dignam MJ. The kinetics of the growth of oxides. In: Comprehensive Treatise of Electrochemistry, Vol. 4. Bockris J, Conway B, Yeager A, White R. editors. New York: Plenum Press, 1981: 247–306.

140 Young L, Smith DJ. Models for ionic conduction in anodic oxide films. Journal of the Electrochemical Society 1979;126(5):765–769.

141 Greef R, Peat R, Peter LM, Pletcher D, Robinson J. Instrumental methods in electrochemistry. Chichester: John Wiley & Sons, 1985.

142 Lohrengel MM. Formation of ionic space charge layers in oxide films on valve metals. Electrochimica Acta 1994;39(8/9)1265–1271.

143 Lohrengel MM. Pulse measurements for the investigation of fast electronic and ionic processes at the electrode/electrolyte interface. Berichte der Bunsengesellschaft für Physikalische Chemie 1993;97:440–447.

144 Kanazirski I, Bojinov M, Girginov A. Kinetics of the anodic oxidation of bismuth in glycol-borate electrolyte – a space charge approach. Electrochimica Acta 1993;38(8):1061–1065.

145 de Wit HJ, Wijenberg C, Crevecouer C. Impedance measurements during anodization of aluminum. Journal of the Electrochemical Society 1979;126:779–785.

146 Bojinov M. The ability of a surface charge approach to describe barrier film growth on tungsten in acidic solutions. Electrochimica Acta 1997;42:3489–3498.

147 Bojinov M. Modelling the formation and growth of anodic passive films on metals in concentrated acid solutions. Journal of Solid State Electrochemistry 1997;1:161–171.

148 Bojinov M, Betova I, Raicheff R. Influence of molybdenum on the transpassivity of a Fe + 12%Cr alloy in H_2SO_4 solutions. Journal of Electroanalytical Chemistry 1997;430:169–178.

149 Moore Jr. JB, Jones RL. Growth characteristics of iron oxide films generated in dilute lithium hydroxide solution at 300 °C. Journal of the Electrochemical Society 1968;115:576–583.

150 Bignold GJ, Garnsey R, Mann GMW. High temp. aqueous corrosion of iron development of theories of equilibrium solution phase transport through a porous oxide. Corrosion Science 1972;12:325–332.

151 Lister DH. The transport of radioactive corrosion products in high-temperature water. II. The activation of isothermal steel surfaces. Nuclear Science and Engineering 1976;59: 406–426.

152 Olefjord I, Brox B, Jelvestam U. Surface composition of stainless steel during anodic dissolution and passivation studied by ESCA. Journal of the Electrochemical Society 1985; 132:2854–2861.

153 Bogaerts WF, Bettendorf C. Electrochemistry and corrosion of alloys in high-temperature water. Palo Alto, CA: Electric Power Research Institute, 1986. Report No.: EPRI NP-4705.

154 Bogaerts WF, Bettendorf C. High-temperature electrochemistry and corrosion. Palo Alto, CA: Electric Power Research Institute, 1988. Report No.: EPRI NP-5863.

155 Robertson J, Forrest JE. Corrosion of carbon steels in high temperature acid chloride solutions. Corrosion Science 1991;32(5/6):521–540.

156 Carranza RM, Alvarez MG. The effect of temperature on the passive film properties and pitting behaviour of a Fe-Cr-Ni alloy. Corrosion Science 1996;38(6):909–925.

157 Cohen P. (editor). The ASME handbook on water technology for thermal power systems. New York: The American Society of Mechanical Engineers, 1989: 1828 p.

158 Marshall WL, Franck EU. Ion product of water substance, 0–1000 °C, 1-10,000 bars. New international formulation and its background. Journal of Physical Chemistry Ref. Data 1981;10(2):295–304.

159 Saario T, Sirkiä P. Surface film characterisation of a copper alloy Cu-Zr-Cr (PH), austenitic stainless steel AISI 316, and ferritic satinless steel F82H (modified). Espoo: VTT, 1997. Report VALB218.

160 Bojinov M, Laitinen T, Saario T, Sirkiä P. Oxide Films in High Temperature Aqueous Environments: their role in the mechanisms of activity build-up and stress corrosion cracking in nuclear power plants. RATU2 research programme, RAVA5 project. Espoo: VTT, 1997. Interim report.

161 Broomfield JP, Forrest JE, Holmes DR, Manning MI. Oxide growth mechanisms on chromium alloy steels. Palo Alto, CA: Electric Power Research Institute, 1986. Report No.: EPRI NP-4647.

162 Castle JE, Mann GMW. The mechanism of formation of a porous oxide film on steel. Corrosion Science 1966;6:253–262.

163 Potter EC, Mann GMW. Oxidation of mild steel in high-temperature aqueous systems, 1st Int. Congr. Metallic Corros. London: Butterworths, 1961: 417–423.

164 Allsop HA, Sawicki JA, Godin MSL, Lister, DH. The effect of dissolved oxygen in lithiated coolant. Water chemistry of nuclear reactor systems 6. London: British Nuclear Energy Society, 1992: 25–32.

165 de Bakker PMA, Verwerft M, Wéber M, De Grave E. On the corrosion mechanisms in an experimental PWR irradiation facility. Water chemistry of nuclear reactor systems 7. London: British Nuclear Energy Society, 1996: 100–102.

166 Lister DH. The transport of radioactive corrosion products in high-temperature water - I. Recirculation loop experiments. Nuclear Science and Engineering 1975;58:239–251.

167 Hermansson H-P, Stigenberg M, Wikmark G. Kinetics in passivating oxide films. Water chemistry of nuclear reactor systems 7, London: British Nuclear Energy Society, 1992: 141–143.

168 Tapping RL, Davidson RD, McAlpine E, Lister DH. The composition and morphology of oxide films formed on type 304 stainless steel in lithiated high temperature water. Corrosion Science 1986;26(8):563–576.

169 Buckley D. Surface analysis of 316Ti steel exposed to simulated BWR conditions. Willigen: PSI, 1994. Report TM-43-93-16.

170 Lin CC. Hydrogen water chemistry effects on BWR radiation buildup. Vol. 1: Laboratory results and plant data. Palo Alto, CA: Electric Power Research Institute, 1994. Report No.: EPRI TR-104605-V1.

171 Lumsden JB. Characterization of surface films in BWR pipe cracks: a final report. Palo Alto, CA: Electric Power Research Institute. Report No.: EPRI NP-4055M

172 Haginuma M, Ono S, Takamori K, Takeda K, Tachibana K, Ishigure K. Effect of zinc addition on cobalt ion accumulation into the corroded surface of type 304 SS in high-temperature water. Water chemistry of nuclear reactor systems 7. London: British Nuclear Energy Society, 1992: 128–130.

173 Bennett PJ, Gunnerud P, Pettersen JK, Harper A. The effects of water chemistry on cobalt deposition in BWRs. Water chemistry of nuclear reactor systems 7. London: British Nuclear Energy Society, 1992: 189–195.

174 Ocken H. Surface treatments to reduce radiation fields. Test-loop studies and plant demonstrations. Palo Alto, CA: Electric Power Research Institute, 1988. Report No.: EPRI NP-5209-SR.

175 Wood CJ. Manual of recent techniques for LWR radiation-field control. Palo Alto, CA: Electric Power Research Institute, 1986. Report No.: EPRI NP-4505-SR.

176 Schuster E, Neeb KH, Ahlfänger W, Henkelmann R, Järnström RT. Analyses of primary side oxide layers on steam generator tubes from PWRs and radiochemical issues on the contamination of primary circuits. Journal of Nuclear Materials 1988;152:1–8.

177 Castle JE, Masterson HG. The role of diffusion in the oxidation of mild steel in high temperature aqueous solutions. Corrosion Science 1966;6:93–104.

178 Francis JM, Whitlow WH. The morphology of oxide film growth on AISI type 304 stainless steel in high temperature water at 300 °C and 350 °C. Journal of Nuclear Materials 1966;20:1–10.

179 McIntyre NS, Zetaruk DG, Owen D. X-ray photoelectron studies of the aqueous oxidation on Inconel-600 alloy. Journal of the Electrochemical Society 1979;126:750–760.

180 Lister DH, McAlpine E, Hocking WH, Tapping RL. Corrosion-product release in LWRs: 1983 progress report. Palo Alto, CA: Electric Power Research Institute, 1985. Report No.: EPRI NP-3888.

181 Bridle DA, Bird EJ, Mitchell CR. Cobalt deposition in oxide films on reactor pipework. Palo Alto, CA: Electric Power Research Institute, 1986. Report No.: EPRI NP-4499.

182 Lister DH, McAlpine E, Hocking WH. Corrosion-product release in light water reactors. Palo Alto, CA: Electric Power Research Institute, 1984. Report No.: EPRI NP-3460.

183 Tomlinson L, Hurdus MH, Silver PJB. The effect of hydrogen on the corrosion of a 2.25% Cr ferritic steel by high temperature water. Corrosion Science 1981;21:369–380.

184 Park J, Macdonald DD. Impedance studies of the growth of porous magnetite films on carbon steel in high temperature aqueous systems. Corrosion Science 1983;23:295–315.

185 Baston VF, Garbauskas MF, Ocken H. Material characterization of corrosion films on boiling water reactor components exposed to hydrogen water chemistry and zinc injection. Water chemistry of nuclear reactor systems 7, Vol. 1. London: British Nuclear Energy Society, 1996:558–565.

186 Mann GMW, Teare PW. The oxidation of iron-chromium alloys in ferrous chloride solution at 300 °C. Corrosion Science 1972;12:361–369.

187 Lister DH, McAlpine E, Tapping RL, Hocking WH. Corrosion-product release in LWRs: 1984–1985 progress report. Palo Alto, CA: Electric Power Research Institute, 1986. Report No.: EPRI NP-4741.

188 Lister DH, Davidson RD. Corrosion-product release in light water reactors. Palo Alto, CA: Electric Power Research Institute, 1989. Report No.: EPRI NP-6512.

189 Smith AF. The tracer diffusion of transition metals in duplex oxide grown on a T316 stainless steel. Corrosion Science 1981; 21(7):517–529.

190 Xu Y, Wang M, Pickering HW. On electric field induced breakdown of passive films and the mechanism of pitting corrosion. Journal of the Electrochemical Society 1993;140: 3448–3457.

191 Wang M, Pickering HW, Xu Y. Potential distribution, shape evolution, and modeling of pit growth for Ni in sulfuric acid. Journal of the Electrochemical Society 1995;142(9): 2986–2995.

192 Schmuki P, Böhni H. Semiconductive properties of passive films and susceptibility to localised corrosion. Werkstoffe und Korrosion 1991; 42:203–207.

193 Mischler S, Vogel A, Mathieu HJ, Landolt D. The chemical composition of the passive film on Fe-24Cr and Fe-24Cr-11Mo studied by AES- XPS and SIMS. Corrosion Science 1991; 32(9):925–944.

194 Staehle RW, Begley JA, Agrawal AK, Beck FH, Lumsden JB, Biggert AS, Davis CA. Corrosion and corrosion cracking of materials for water-cooled reactors. Palo Alto, CA: Electric Power Research Institute, 1981. Report No.: EPRI NP-1741.

195 BWR Water Chemistry Guidelines Revision Committee: CJ Wood et al. BWR water chemistry guidelines. Palo Alto, CA: Electric Power Research Institute, 1984. Report No.: EPRI TR-103515.

196 Congleton J, Yang W. The effect of applied potential on the stress corrosion cracking of sensitized type 316 stainless steel in high temperature water. Corrosion Science 1995; 37(3):429–444.

197 Ljungberg L, Halldén E. BWR water chemistry impurity studies: literature review of efefcts on stress corrosion cracking: interim report. Palo Alto, CA: Electric Power Research Institute. Report No.: EPRI NP-3663.

198 Ford FP, Taylor DF, Andresen PL, Ballinger RG. Corrosion-assisted cracking of stainless and low-alloy steels in LWR environments. Palo Alto, CA: Electric Power Research Institute, 1987. Report No.: EPRI NP-5064M.

199 Macdonald DD, Urquidi-Macdonald M. A coupled environment model for stress corrosion cracking in sensitized type 304 stainless steel in LWR environments. Corrosion Science 1991;32:51–81.

200 Aaltonen P, Saario T, Karjalainen-Roikonen P, Piippo J, Tähtinen S, Itäaho M, Hänninen H.. Vacancy-creep model for EAC of metallic materials in high temperature water. Corrosion '96. Denver, Colorado: NACE International, 1996: Paper No. 81, 12 p.

201 Rebak RB, Szklarska-Smialowska Z. The mechanism of stress corrosion cracking of alloy 600 in high temperature water. Corrosion Science 1996;38(6):971–988.

202 Galvele JR. Electrochemical aspects of stress corrosion cracking. In: White RE et al., editors. Modern Aspects of Electrochemistry, Number 27. New York: Plenum Press, 1995: 233–358.

203 Turnbull A. Modelling of environment assisted cracking. Corrosion Science 1993;34(6): 921–960.

204 Andresen PL. SCC growth rate behaviour in BWR water of increased purity. 8th Int. Symp. on Environmental Degradation of Materials in Nuclear Power Systems—Water Reactors, August 10–14, 1997, Amelia Island, USA.

205 Li R, Ferreira MGS. The thermodynamic conditions for hydrogen generation inside a stress corrosion crack. Corrosion Science 1996;38(2):317–327.

206 Segal MG, Swan T. Chemical considerations in the choice of decontamination reagents for water reactors. Water chemistry of nuclear reactor systems 3, Vol. 1. London: British Nuclear Energy Society, 1983:187–194.

207 Hänninen H, Aho-Mantila I, Törrönen K. Environment sensitive cracking in pressure boundary materials of light water reactors. International Journal of Pressure Vessel and Piping 1987;30:253–291.

208 Turnbull A, Psaila-Dombrowski M. A review of electrochemistry of relevance to environment-assisted cracking in light water reactors. Corrosion Science 1992;33:1925–1966.

209 Rebak RB, Szklarska-Smialowska Z. Effect of partial pressure of hydrogen on IGSCC of alloy 600 in PWR primary water. Corrosion (NACE) 1991;47(10):754–757.

210 Lagerström J, Ehrnstén U, Saario T, Laitinen T, Hänninen H. Model for environmentally assisted cracking of Alloy 600 in PWR primary water. Proceedings of the Eight International Symposium on Environmental Degradation of Materials in Nuclear Power Systems - Water Reactors. Florida, August 10–14, 1997: 349–356.

APPENDIX 1

A	constant in the high-field migration equation, $A\,cm^{-2}$
a	atomic jump distance, cm
B	field coefficient in the high-field equation, $V^{-1}\,cm$
B', B"	constants in the structural change model, $V^{-1}\,cm$
c_o	concentration of oxygen vacancies, $mol\,cm^{-3}$
$c_O(0)$	concentration of oxygen vacancies at the film|solution interface, $mol\,cm^{-3}$
$c_O(L)$	concentration of oxygen vacancies at the metal|film interface, $mol\,cm^{-3}$
D_O	diffusivity of oxygen vacancies, $cm^2\,s^{-1}$
d_2	constant in the local field model
E	applied potential, V
$\boldsymbol{E}$	electric field strength, $V\,cm^{-1}$
$\boldsymbol{E}_L$	total electric field strength in the metal|film|solution system, $V\,cm^{-1}$
$\boldsymbol{E}_{local}$	local electric field strength, $V\,cm^{-1}$
$\boldsymbol{E}^{\sim}_{ox}$	average field strength, $V\,cm^{-1}$
$\boldsymbol{E}(x)_{ox}$	position dependent field strength in the oxide film, $V\,cm^{-1}$
$\boldsymbol{E}(x)_{sc}$	position dependent space charge field strength in the oxide film, $V\,cm^{-1}$
$\boldsymbol{E}_{diel}$	electric field strength in the dielectric part of the film, $V\,cm^{-1}$
e	charge of the electron, 1.602×10^{-19} C
F	Faraday's number, 96487 C mol^{-1}
i	current density, $A\,cm^{-2}$
J_O	flux of oxygen vacancies in the film, $mol.cm^{-2}s^{-1}$
K	dimensional dielectric constant of the film, $F\,cm^{-1}$
K_{local}	local dimensional dielectric constant of the film, $F\,cm^{-1}$
K_1	dynamic dielectric constant of the film in the dielectric polarisation model, $F\,cm^{-1}$
k	rate constant, $mol\,cm^{-2}\,s^{-1}$
L	oxide film thickness, cm
$L_{M\|F}$	thickness of the oxygen vacancy accumulation layer, cm
$L_{F\|S}$	thickness of the metal vacancy accumulation layer, cm
m	metal atom in the metal phase
M_i^{x+}	metal interstitial in the oxide film lattice
M_M	metal position in the oxide film lattice
M^{x+}_{aq}	solvated metal ion in the electrolyte
N	concentration of mobile charge carriers, cm^{-3}

N_{AC}	concentration of electron acceptors (metal vacancies), cm^{-3}
N_D	concentration of electron donors (oxygen vacancies), cm^{-3}
n	number of electrons per oxide molecule
null	perfect lattice position
O_O	oxygen position in the oxide film lattice
P	dielectric polarisation, $V\ cm^{-1}$
Q	quantity of charge, $C\ cm^{-2}$
q	negative background space charge, $C\ cm^{-2}$
S	capture cross section, $cm^2\ C^{-1}$
V_O^{2+}	oxygen vacancy in the oxide film lattice
V_M^{x-}	metal vacancy in the oxide film lattice
V_m	molar volume of the phase in the oxide film, $cm^3\ mol^{-1}$
W	activation energy, $J\ mol^{-1}$
W_e	zero field activation energy, $J\ mol^{-1}$
w	proportionality factor in the dielectric polarisation model
x_{sc}	space charge screening parameter, cm^{-1}
z	charge of a moving defect in the oxide lattice
α	polarizability of the film|solution interface
γ_{local}	geometrical factor in the local field model
ε	dimensionless dielectric constant of the film
ε_o	dielectric permittivity of free space, $8.85 \times 10^{-14}\ F\ cm^{-1}$
η_e	electrochemical potential of the electron in the film, $J\ mol^{-1}$
$\mu^{\neq}$	activation dipole (product of charge and half-jump distance)
μ_e	chemical potential of the electron in the film, $J\ mol^{-1}$
ϕ	electrostatic potential, V
$\Delta\phi_{total}$	total potential drop in the metal|film|solution system, V
$\Delta\phi_F$	potential drop in the film, V
$\Delta\phi_{M\|F}$	local potential drop at the metal|film interface, V
$\Delta\phi_{M\|F,s}$	steady state local potential drop at the metal|film interface, V
$\Delta\phi_{F\|S}$	local potential drop at the film|solution interface, V
$\Delta\phi_{F\|S,\ s}$	steady state local potential drop at the metal|film interface, V
χ_s	steady state electric susceptibility

APPENDIX 2

AES	Auger electron spectroscopy
AFM	Atomic force microscopy
AISI	American iron and steel institute
BWR	Boiling water reactor
CEFM	Coupled environment fracture model
CFSE	Crystal field stabilisation energy
EAC	Environmentally assisted cracking
EELS	Electron energy loss spectroscopy
EIS	Electrochemical impedance spectroscopy
HWC	Hydrogen water chemistry
IGSCC	Intergranular stress corrosion cracking
IMPS	Intensity modulated photocurrent spectroscopy
ISS	Ion scattering spectroscopy
MSE	Mercurous sulphate electrode
NWC	Normal water chemistry
PDM	Point defect model
PWR	Pressurised water reactor
RHEED	Reflection high-energy electron diffraction
SCC	Stress corrosion cracking
SCE	Saturated calomel electrode
SDVC	Selective dissolution vacancy creep
SERS	Surface enhanced Raman spectroscopy
SHE	Standard hydrogen electrode
SIMS	Secondary ion mass spectrometry
SSRT	Slow strain rate test
SEM	Scanning electron microscopy
STM	Scanning tunnelling microscopy
SVIM	Solute-vacancy interaction model
TEM	Transmission electron microscopy
TGSCC	Transgranular stress corrosion cracking
XANES	X-ray absorption near-edge spectroscopy
XPS	X-ray photoelectron spectroscopy
XRD	X-ray diffraction

ELEMENTAL COMPOSITION OF IMPORTANT ALLOYS **APPENDIX 3**

	C	Cr	Cu	Fe	Mn	Ni	S	Si	Ti	Others
AISI 304 SS	0.08	19		remainder	2	9.3	0.03	1		N: 0.1
AISI 308 SS	0.08	20		remainder	2	11	0.03	1		
AISI 316 SS	0.08	17		remainder	1	12	0.03	1		Mo: 2.5 N: 0.1
AISI 316 L	0.03	17		remainder	2	12	0.03	1		Mo: 2.5 N: 0.1
AISI 321 SS	0.08	18		remainder	2	10.5	0.03	1	≤ 0.7	N: 0.1
AISI 403 SS	0.15	12.3		remainder	1	0.6	0.03	0.5		
Incoloy 800	0.05	21	0.38	46	0.75	32.5	0.008	0.5	0.38	Al: 0.38
Inconel 600	0.08	15.5	0.25	8	0.5	76	0.008	0.25	–	
Inconel 690	≤ 0.05	30	≤ 0.5	9	≤ 0.5	remainder		≤ 0.5		
Inconel 182	0.05	14	0.10	7.5	7.75	67	0.008	0.50	0.4	Nb 1.75